BREAST IMMOBILIZATION DEVICE OPTIMIZATION FOR DUAL MODALITY TOMOSYNTHESIS

A thesis
presented to
the faculty of the School of Engineering and Applied Science
University of Virginia

In partial fulfillment
of the requirements for the degree
Master of Science in Biomedical Engineering

By
Kelly Lynn Klanian
December 2012

APPROVAL SHEET

The thesis

is submitted in partial fulfillment of the requirements

for the degree of

Master of Science

AUTHOR

The thesis has been read and approved by the examining committee:

Dr. Mark Williams

Advisor

Dr. Jason Papin

Dr. Robert Ribando

Accepted for the School of Engineering and Applied Science:

Dean, School of Engineering and Applied Science

December

2012

ABSTRACT

Conventional x-ray mammography continues to be the mainstay for breast cancer screening. However, traditional mammography has a multitude of limitations, including low sensitivity for the detection of early malignancies and high false positive rates. Breast compression using a flat compression paddle is commonly used to immobilize the breast as 2-D x-ray images are acquired during a clinical scan. Although strong compression is used to flatten the breast and thus reduce the amount of superimposed tissue that can mask tumors in the two-dimensional image, small masses can still be occult, especially in radio-dense breasts.

These challenges have motivated researchers to explore other imaging modalities beyond conventional x-ray mammography to aid in the fight against breast cancer. For example, our dual modality tomosynthesis (DMT) scanner performs both x-ray breast tomosynthesis (XBT) and molecular imaging breast tomosynthesis (MBIT) with the breast in a single configuration in order to assure that accurate co-registration can be obtained between the two resulting 3-D image sets. Both XBT and MBIT use a tomosynthesis image acquisition approach, in which multiple views of the breast are obtained over a range of viewing angles. XBT provides anatomical information and can reliably resolve objects on a sub-millimeter scale. MBIT provides functional information through the use of an intravenously injected tracer tagged with a radioisotope and has a spatial resolution on the order of 2.5 to 5.0 mm. Standard, flat paddle compression has been used to immobilize the breast during pilot DMT studies. The 3-D nature of the tomosynthesis image reduces the problem of tumor masking since thin slices from the reconstructed volume can be displayed. Thus, some of the motivation for vigorous breast

compression is eliminated. This, in part, has motivated our investigation of alternative strategies for immobilizing the breast during DMT scanning.

The overall goal of this project was to develop an innovative breast immobilization device that can be integrated into the DMT scanner to improve image quality as well as patient comfort. Our hypothesis was that MBIT image quality could be improved by reducing the radial distance between the breast itself and the gamma camera at large viewing angles (away from the direction of compression). In addition, we hypothesized that compressing the breast in a more natural configuration would increase the level of patient comfort during a scan. Preliminary experimental studies showed that our optimized breast immobilization device is capable of improving both image contrast and signal-to-noise ratio (SNR) as compared to standard, flat paddle compression. Furthermore, qualitative assessments were made with respect to patient comfort and noticeable improvements were observed with one exception. The single exception was that when evaluating the prototype immobilization device, women with large breasts expressed discomfort because the prototype was not wide enough to fully contain all of their breast tissue. Accordingly, we are in the process of fabricating similar immobilization devices with a range of sizes to be evaluated for their ability to comfortably accommodate a broad range of breast sizes, while still providing improved image contrast and SNR.

ACKNOWLEDEGMENTS

First and foremost, I would like to acknowledge and thank all those who have supported me and offered constructive suggestions during the development of this research work. I am particularly grateful for the professional guidance extended to me by my advisor, Dr. Mark Williams. I wish to recognize the help provided by those who work tirelessly at the University of Virginia Breast Care Center and the Physics Machine Shop. In addition, assistance provided to me by my colleagues and friends was greatly appreciated. Lastly, I would like to thank my family for their love, support, patience and understanding throughout the duration of my studies.

TABLE OF CONTENTS

LIST OF FIGURES

LIST OF TABLES

LIST OF ABBREVIATIONS

^{99m}Tc = technetium 99m

Al = aluminum

ACR = American College of Radiology

ANOVA = analysis of variance

AOR = axis-of-rotation

Be = beryllium

Ci = curie

CMOS = complementary metal-oxide-semiconductor

CsI = cesium iodide

DCIS = ductal carcinoma in situ

DMT = dual-modality tomographic

DOI = diffuse optical imaging

FOV = field-of-view

FWHM = full-width-at-half-maximum

kVp = kilovolt peak

MBIT = molecular imaging breast tomosynthesis

ML = medial-lateral

MLO = medial-lateral oblique

MRI = magnetic resonance imaging

NIH = national institute of health

NM = nuclear medicine imaging

PC = polycarbonate

PMT = photomultiplier tube

PSPMT = position sensitive photomultiplier tube

QQ = quantile-quantile

Rh = rhodium

ROI = region of interest

SBI = Society of Breast Imaging

SNR = signal-to-noise ratio

US = ultrasound

W = tungsten

XBT = x-ray breast tomosynthesis

CHAPTER 1

INTRODUCTION

Apart from non-melanoma skin cancer, breast cancer is the most common cancer among women in the United States and is also one of the leading causes of cancer death among women of all races around the world [10]. Breast cancer incidence rates vary depending on a number of different factors including gender, age, race, and ethnicity [10]. The Susan G. Komen foundation recently estimated that the number of new cases of breast cancer (both invasive and non-invasive) among U.S. women in 2012 will total nearly 300,000, while approximately 40,000 deaths will be attributed to the disease [27]. Gender specific incidence and mortality rates in the United States are reported in Table 1-1. Risk factors abound for breast cancer, though the two most important are gender and age [27].

	Men	Women
Incidence (new cases)	1.2 per 100,000	125.7 per 100,000
Mortality (deaths)	0.3 per 100,000	22.2 per 100,000

Table 1-1: Incidence and Mortality Rates in the United States [10]

Most health care professionals would agree that the best defense against breast cancer is early detection. As such, the American College of Radiology (ACR) and the Society of Breast Imaging (SBI) recently released recommendations on breast cancer screening in *The Journal of the American College of Radiology*. These recommendations suggest that those women who are at average risk for breast cancer should start annual mammograms at age 40, while those who have a higher risk should start breast cancer screening at least by age 30 [5].

1.1 Current Practice: X-ray Mammography

X-ray mammography is the traditionally accepted modality for breast cancer screening. During a mammogram, a woman's breast is positioned by a radiation technologist and exposed to ionizing radiation to produce an image. The breast is immobilized with a flat compression paddle as illustrated in Figure 1-1. On average, twenty pounds force is typically applied to compress a woman's breast during a clinical exam. Most women who have experienced a clinical mammogram express angst and discomfort. In addition, mammography has reportedly missed 10-15% of breast cancers [11] and contributes to false positive readings. As a result, patients experience a sense of heightened anxiety and apprehension. Additional diagnostic tests are oftentimes required to definitively determine disease presence, which also augments inflationary health care costs. Consequently, researchers and clinicians alike are expressing interest in the use of alternative imaging modalities in conjunction with mammography to combat these ever persistent problems.

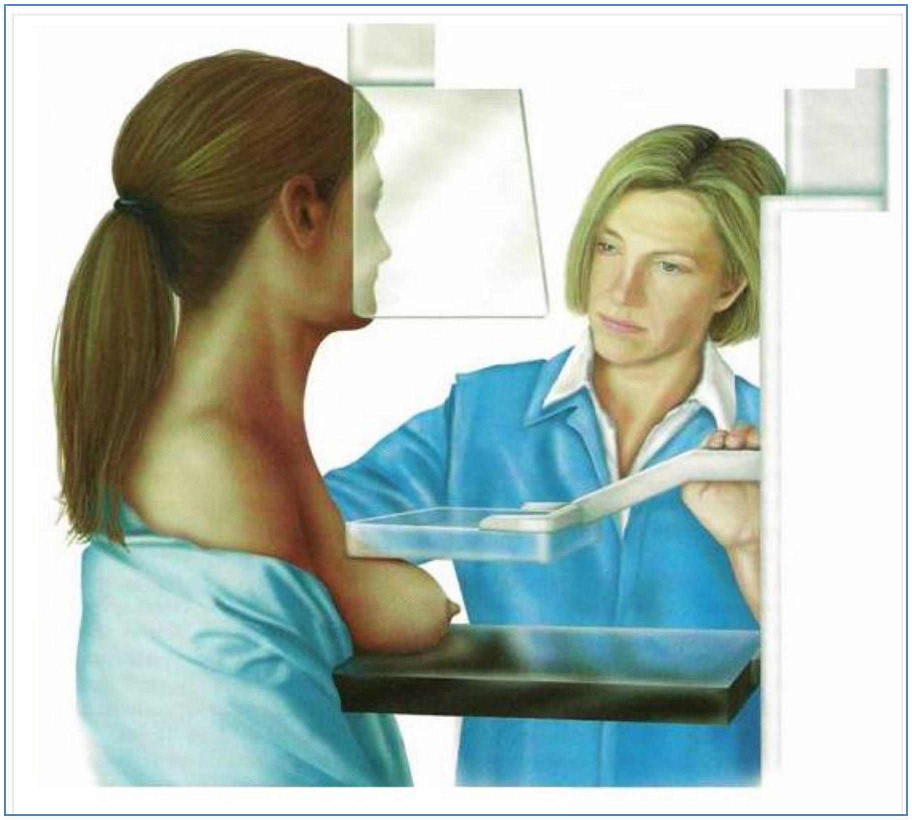

Figure 1-1: X-ray Mammogram: Standard Compression Illustration [14]

1.2 Alternative Approaches to X-ray Mammography

Alternative imaging modalities currently used in clinical practice include: Breast Ultrasound (US), Magnetic resonance imaging (MRI) of the breast, X-ray Breast tomosynthesis (XBT), and Nuclear Medicine Imaging (NM). Those alternatives currently under development include: Diffuse Optical Tomography (DOT) and Dual Modality Tomosynthesis (DMT). A brief description as well as the advantages and disadvantages of each of these alternatives will be discussed in the paragraphs that follow.

1.2.1 Breast Ultrasound (US)

Ultrasound imaging also referred to as ultrasound scanning or sonography, involves exposing the breast to high-frequency sound waves to produce a picture of the internal structure [9]. An ultrasound image is acquired by sweeping a transducer across the breast after a clear gel is applied to the skin [9]. Ultrasound imaging is oftentimes touted as an adjunct screening tool for women with very dense breasts or silicone breast implants [9]. It is also used to screen women who may be pregnant and do not want to be exposed to x-rays [9]. However, it has been reported that the sensitivity of ultrasound alone is 39.5%, while the sensitivity of mammography and ultrasound together is 48.8% [17]. Breast ultrasound screening has not been widely accepted because of issues related to reproducibility, high-false-positive rates, operator dependencies of the examination, and inability to image most DCIS cases [18].

1.2.2 Magnetic Resonance Imaging (MRI)

A powerful magnetic field, radio waves and a computer are used in MRI to produce detailed pictures of the breast [8]. Hundreds of images are generated during each exam and in most cases, the imaging physician requests a contrast agent (dye) to improve the quality of the images [8]. An image of the breast is acquired by having the patient lay in the prone position on a table with a special device called a coil which is also used to improve image quality [8]. MRI is performed, in addition to annual mammography, for "women with >20% lifetime risk for the development of breast cancer" [18]. It has been reported that the sensitivity of MRI is 90.7%, while the sensitivity of mammography and MRI together is 93% [17]. As emphasized by the

ACS, screening with MRI is “inappropriate for women at <15% lifetime risk for breast cancer” [18]. The ACS also suggests that breast MRI is not meant to replace mammography because there are cases, particularly of ductal carcinoma in situ (DCIS), which are only detectable by mammography alone [18]. Furthermore, the addition of breast MRI to the screening algorithm for women at greatest risk is considerably expensive [18]. As such, it is important to consider its use on a case-by-case basis.

1.2.3 X-ray Breast Tomosynthesis (XBT)

X-ray tomosynthesis acquisition is similar to conventional mammography with regard to breast positioning and compression, but differs in that the X-ray tube takes multiple low-dose exposures as it moves through a limited (e.g., 30°) arc of motion [23]. The resulting projection images are reconstructed into a 3D tomographic image of the breast, sectioned in the orientation of acquisition [23]. XBT is the most recent modality to be implemented in the clinical environment, and experts agree that it does provide some significant advantages over conventional mammography. These advantages include “permitted depth localization, improved conspicuity of structures by removing the visual clutter associated with overlying anatomy, and improved local structure contrast by restricting the overall image dynamic range to that of a single slice” [12]. It has been reported that the use of tomosynthesis as an adjunct to digital screening mammography leads to a decrease in the recall rate by nearly half [23]; however, these results must be validated as XBT becomes more widely accepted by clinicians and researchers alike.

1.2.4 Nuclear Medicine Imaging (NM)

Unlike traditional x-ray examinations, nuclear medicine uses radiation that is emitted from a patient's body after a radioactive material is introduced [15]. This radiation is in the form of gamma rays, which are a lot like x-rays, but have a shorter wavelength [15]. Gamma ray signals are measured by a gamma camera which consists of a crystal array (called scintillation crystals) [15]. The crystals detect the emitted photon and convert it into light, which is then transformed into an electric signal and digitized (converted into a computer signal) to reconstruct an image that can be easily interpreted [15]. One of the unique things that nuclear medicine tests add in terms of disease detection is extreme sensitivity to abnormalities in an organ's function [25]. However, nuclear medicine imaging cannot yet provide spatial resolution on the order of microns, as is commonly observed with conventional x-ray imaging techniques.

1.2.5 Diffuse Optical Tomography (DOT)

Diffuse optical tomography can be used to screen for breast cancer and should be able to provide quantitative images of tissue absorption and diffusion coefficient maps [22]. As suggested by its name, diffuse optical *tomography* uses multiple projection images in conjunction with a reconstruction algorithm to improve spatial resolution over conventional diaphanography [22]. The optical source of light for the imaging system is a diode laser [22]. The light signal is delivered to and from the tissue via fiber optic cables, and light detection is accomplished with a single photomultiplier tube (PMT) [22]. Both a change in blood volume and a change in blood oxygenation can alter the light amplitude signal [3]. This method is currently being explored as a breast screening tool because of its ability to reveal the aforementioned changes that are specific to early stage cancer [3]. DOT is an attractive imaging method because it is inexpensive, portable, and fast [3]. That being said, because it has low spatial resolution, DOT could benefit from structural guidance by combining it with other higher spatial resolution imaging tools [3].

1.2.6 Dual Modality Tomosynthesis (DMT)

Note: significant portions of Section 1.2.6 were taken with permission from reference [16]

Dual modality tomosynthesis differs significantly from the clinical and developmental imaging techniques mentioned herein. The Dual Modality Tomosynthesis Scanner, as depicted in Figures 1-2 and 1-3, acquires both x-ray and gamma-ray projection images across a limited angle range. The x-ray tube, x-ray detector, and gamma camera rotate around a central axis of rotation (AOR) to perform both XBT and MBIT with the breast in a single configuration. This ensures that the resulting 3-D image sets can be properly co-registered. The gantry itself was built by Dexela Ltd., a PerkinElmer Company (London, England). A Dexela 2923MAM flat panel complementary metal-oxide-semiconductor (CMOS) x-ray detector was mounted to the gantry arm, as was a gamma camera, provided by Jefferson Labs. Angular rotation of the gantry arm is controlled by a software program written by Dexela.

In addition to the CMOS detector, the x-ray system is comprised of a high output, oil-cooled tungsten (W) target x-ray tube (Varian model RAD 70) with a nominal focal spot size of 0.3 mm in the left-right direction and 0.43 mm in the anode-cathode direction. The system also contains a 0.76 mm beryllium (Be) window and 0.050 mm rhodium (Rh) filter. The array size of the x-ray detector is 3072 x 3888, with a pitch of 75μm in 1x1 binning mode. The active area of the detector is 230 x 290 mm. Its high frame rate (up to 26 frames/sec) and its low noise properties make it ideal for tomosynthesis applications.

The gamma camera consists of a 3 x 4 array of Hamamatsu H8500 position sensitive photomultiplier tubes (PSPMTs) that are optically coupled to a NaI(TI) crystal array with a crystal pitch of 2.2 mm and a crystal thickness of 6 mm. The camera is also equipped with a lead parallel hole collimator that has an associated efficiency of 2.34×10^{-4}, while the acquisition is controlled by software written in K-max (Sparrow Corporation, Port Orange, FL). The camera, as previously mentioned, is mounted to the gantry arm via a motor controlled Velmex bi-slide linear translation stage system which permits the gamma camera to move up and down using an analog joystick. The gamma camera is moved manually along two slider rails towards the patient in the posterior direction to acquire gamma images after x-ray image acquisition has been completed.

Though there are marked differences between this system and most of those previously mentioned one obvious similarity is worth noting. Flat paddle compression is the traditionally accepted format for rendering the breast immobile during image acquisition. Much like its clinical counterparts, the DMT breast immobilization device is comprised of a flat breast support and compression paddle, where the radial distance between the compression paddle and the AOR is adjustable. Polycarbonate (PC) is used to manufacture compression paddles because it exhibits both strength and ductility, important properties when considering patient safety. However, the flat nature of the current technology does present some significant limitations, especially for tomographic applications.

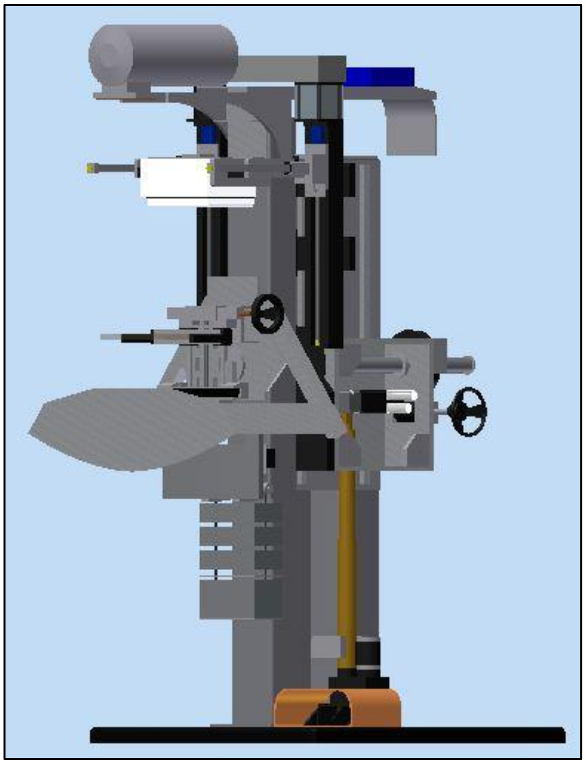

Figure 1-2: Drawing of the Dual Modality Tomosynthesis Scanner

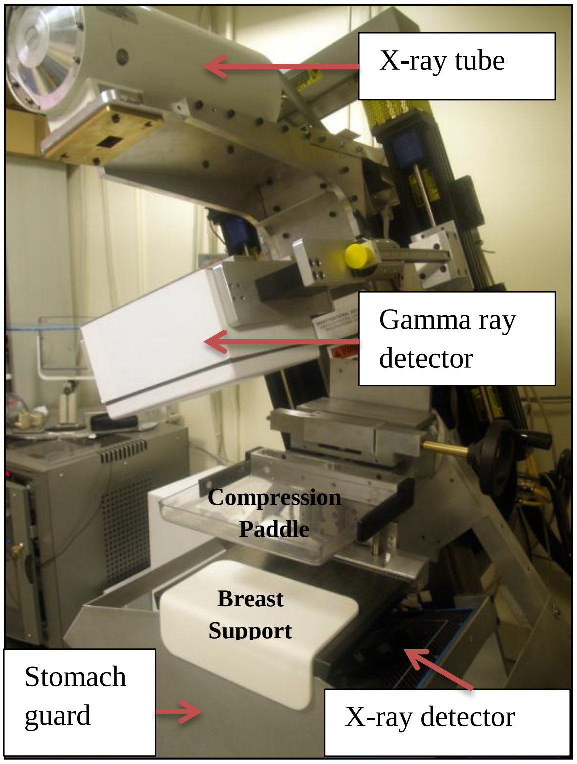

Figure 1-3: Photograph of the Dual Modality Tomosynthesis Scanner

1.3 Breast Immobilization Device Design Limitations

Flat paddle compression is primarily used to hold the breast firmly in place during image acquisition. During compression, superimposed normal breast tissue obscures malignancies, making them difficult to detect. This is especially true for women with radio dense breasts, as healthy dense tissue and diseased tissue have a similar appearance in the acquired structural image. Additionally, flat paddle compression restricts the viewing angle range for imaging system positioning. Acquiring images over a broader range of viewing angles would result in an image set that more accurately depicts the breast structure itself and any cancerous lesions that may be present. Most tomographic imaging systems operate within a very limited angular range due to the restrictive nature of the hardware and the associated risk of system component collisions. In addition, the flat nature of the compression paddle does not permit close proximity between the breast and the imaging system, particularly at large angles away from the zero degree view. As the radial distance between the breast and the imaging system increases, the quality of the image itself decreases and it becomes increasingly difficult to accurately resolve malignancies, especially those in the early stages of disease progression. All of these design limitations have motivated us to optimize the breast immobilization device to improve image quality and provide our patients with a more pleasant imaging experience.

CHAPTER 2

BREAST IMMOBILIZATION DEVICE OPTIMIZATION

Having investigated a number of different alternatives to flat paddle compression, including the use of flexible materials and breast suctioning, we believe that the best way to immobilize the breast and achieve our technical goals is to implement a design that consists of a rigid yet curved compression paddle and breast support. Both the compression paddle and support are mounted on a mechanical positioning system that permits their separation to be adjusted in order to accommodate a variety of breast thicknesses. The technical attributes associated with the breast immobilization device include secure breast placement, proper shape for imaging the full breast, and contoured design to permit close access to the breast by the imaging device, while simultaneously maximizing patient comfort. The evolution of the design was driven by the need to create enough compressive force to prevent the breast from moving during the scan and ensure that the resulting image contains all of the necessary breast tissue. In addition, both the compression paddle and breast support are crafted from a low-attenuation material (polycarbonate), thereby permitting minimal reduction in the signal intensity.

2.1 Design Evolution and Material Selection

Figure 2-1: Bolx I & II Bolus Material (JRT Associates)

A multitude of flexible materials were explored as the design process ensued, and of those considered, Bolx I and Bolx II (manufactured by JRT Associates) showed the most promise. Both are approved for patient use because they are non-toxic and non-allergenic. Bolx I, as seen on the right hand side of Figure 2-1, has a layer of thin, plastic "skin" such that it can be used repeatedly. Conversely, Bolx II as seen on the left hand side of Figure 2-1 is only meant for single patient use. Though the transparent nature of these flexible materials was initially encouraging, they were ultimately abandoned as realistic design alternatives because neither material provided enough downward force when applied to secure the breast or pectoral muscle in place and prevent patient movement. Multiple sources indicate that approximately 50% of breast cancers occur in the superior lateral (upper outer) quadrant of the breast as indicated in Figure 2-2 [26, 20]. Consequently, it is extremely important to ensure that the breast tissue in this quadrant is held securely in place by the immobilization device. Of equal importance, the breast immobilization device must also generate enough compressive force to secure the pectoral muscle in place so as to guarantee that the breast tissue lining the chest wall will be included in the resulting image. The anatomy of the breast is illustrated in Figure 2-3.

Providing adequate compressive force motivated us to explore other options above and beyond those discussed thus far.

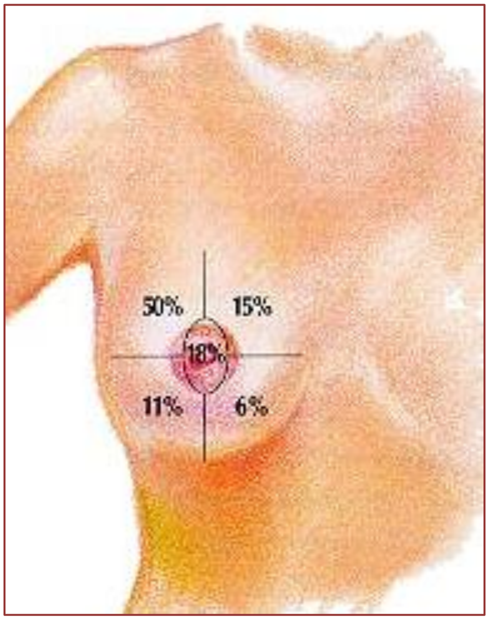

Figure 2-2: Breast Cancer Incidence [26]

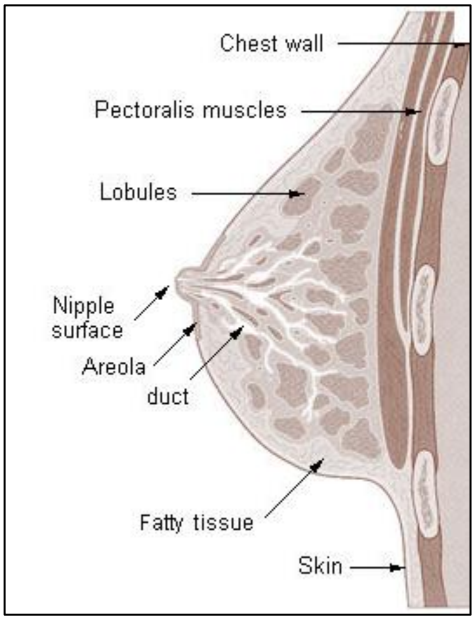

Figure 2-3: Breast Anatomy [21]

A rigid "tongue-and-groove" alternative flat paddle design was temporarily considered as shown in Figure 2-4. The design consisted of two-inch thick strips of plastic fastened together (much like the planks of a conventional hardwood floor) to form both the compression paddle and the breast support. The goal of this eccentric design was to compress the breast and have the ability to remove the plastic strips that were not above (or below) the breast tissue itself, so that close proximity between the breast and the gamma camera could be obtained at wide-angles. This design alternative was

Figure 2-4: Photograph of "tongue-and-groove" alternative design

eventually abandoned because it could prove unsafe and because the air gaps between the plastic strips were very apparent in the resulting reconstructed image (see Figure 2-5).

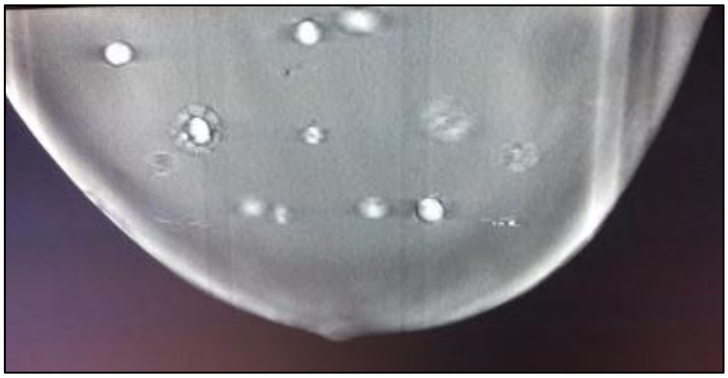

Figure 2-5: "Tongue-and-groove" tomographic image slice

Breast suctioning is oftentimes associated with obstetrics more so than radiology because it is used to pump milk from a woman's breast after she has given birth. A typical breast pump is shown in Figure 2-6. We briefly considered adapting the breast pump to suit our needs; however, two distinct design flaws prevented us from doing so. First, the suction cups themselves are not radio-translucent, meaning they would show up in the resulting image potentially hindering the radiologist's ability to read the image correctly. Second, the suctioning process does not provide the downward force necessary to include the pectoral muscle (and subsequently the breast tissue at the chest wall) in the acquired image. As a result, this design prospect was discarded in favor of a rigid, curved alternative.

Figure 2-6: Breast Pump [1]

Though the curved breast immobilization device differs in shape from its flat clinical counterparts, it is manufactured from the same material. Polycarbonate was chosen because of its high strength and ductility. The molecular structure of polycarbonate is fundamentally important to our understanding, characterization, and use of the polymer itself. From a structural standpoint, polycarbonate is comprised of a bisphenol A component and a carbonate group [6]. Figure 2-7 provides good insight into the molecular makeup of polycarbonate. The two hexagons commonly referred to as phenyl groups, play a significant role in polycarbonate's ability to deform and flex when subjugated to an applied load. It has been reported that the remarkable ductility of polycarbonate is attributed to a variety of "large-amplitude molecular motions" including a 180° phenyl ring flip [24]. The flexibility of polycarbonate is validated by the fact that it has a relatively low Young's modulus, in the vicinity of 2.6 GPa [28]. Young's modulus measures the resistance of a material to elastic (recoverable) deformation under load [7]. A stiff material has a relatively high Young's modulus and changes its shape only slightly when subjected to an elastic load, while a flexible material has a relatively low Young's modulus and changes shape significantly under elastic loads [7].

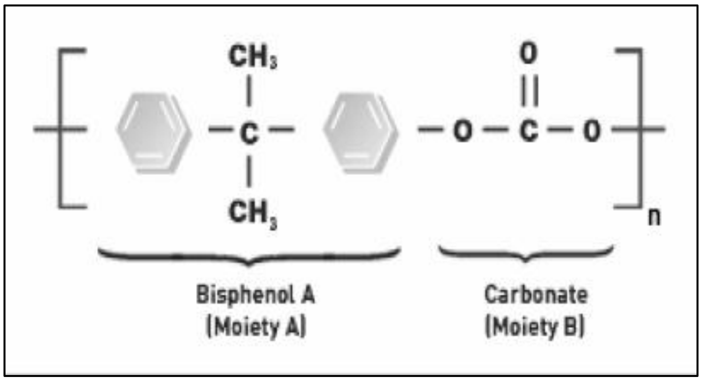

Figure 2-7: Molecular structure of polycarbonate [6]

Stiffness, however, should not be confused with strength. Stiff materials require higher loads to elastically deform, [7] where as strong materials require higher loads to deform permanently [7]. The room temperature compressive strength of polycarbonate is oftentimes reported on industrial websites to approximate 12,000 psi (~80 MPa) [4, 19]. One particular report suggests that the compressive strength of polycarbonate at room temperature is somewhat dependent upon strain rate until high strain rates are realized [2]. Figure 2-8 confirms these findings and validates the compressive strength of polycarbonate as advertised by most suppliers.

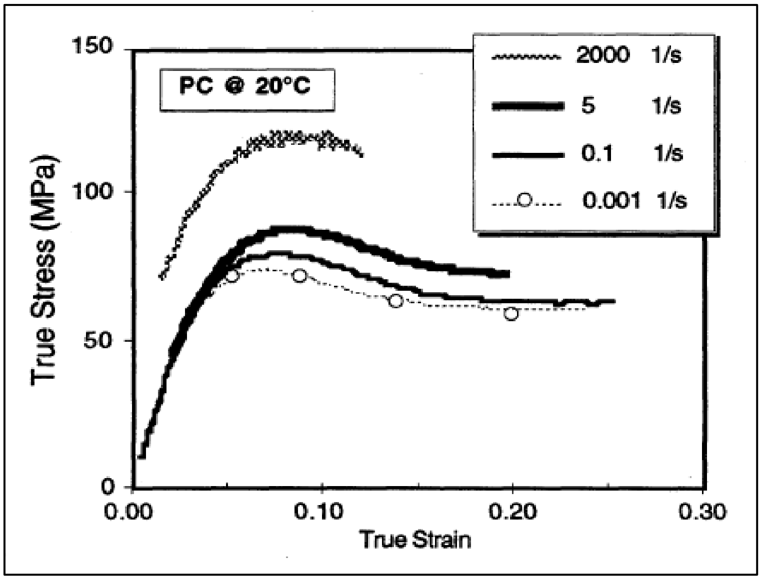

Figure 2-8: Compressive Strength of Polycarbonate [2]

2.2 Curvature Quantification

The curvature of the optimized breast immobilization device was empirically derived using an 1100 mL gelatin breast phantom, a twenty pound ankle weight, and a crudely fabricated curved segment of polycarbonate to quantify the area of an ellipse associated with the phantom breast. To date, our lab has accrued fifty-four human subjects to participate in clinical trial IRB-HSB #8825. The largest breast volume observed thus far is approximately 1100 mL. This volume was calculated as the product of the maximum compressed thickness of the breast observed in the DMT pilot study and an image-based assessment of the maximum projected breast area observed in that study. We chose to use 1100 mL to quantify the x- and y-coordinates of an ellipse because this value realistically defines the upper bound breast size realized in the pilot DMT study. In addition, we chose to use a twenty pound ankle weight for two main reasons. First, as previously suggested, the average compressive force generated during a clinical exam is twenty pounds. Second, it is important to simulate uniform force distribution to the best of our ability. Figure 2-9 demonstrates the experimental set-up that was used to determine the semi-major and semi-minor axes of an ellipse, ultimately quantifying the x- and y-coordinates of both the breast support and the compression paddle. An elliptical shape was chosen because it naturally follows the contours of a breast, more so than other geometries.

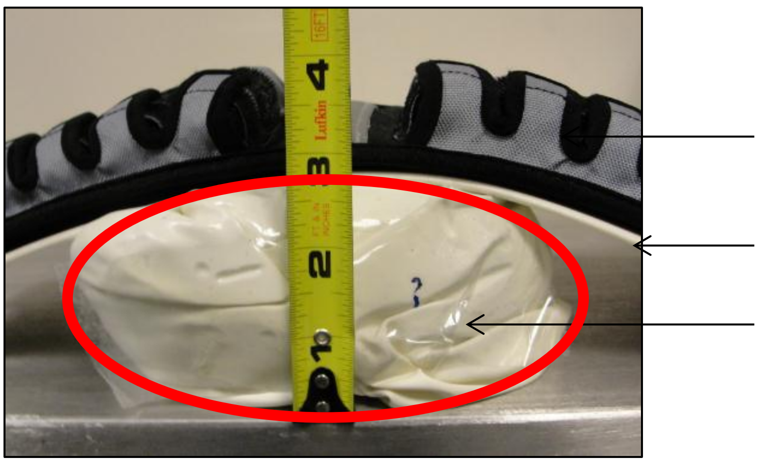

Figure 2-9: Photograph of experimental set-up to determine semi-major and semi-minor axis of an ellipse defining the breast immobilization device

In polar coordinates relative to the center where the angular coordinate θ is measured from the major axis, the equation of an ellipse described by semi-major axis *a* and semi-minor axis *b* can be expressed as,

$$r(\theta) = \frac{a*b}{\sqrt{(b\cos\theta)^2+(a\sin\theta)^2}} \quad (1)$$

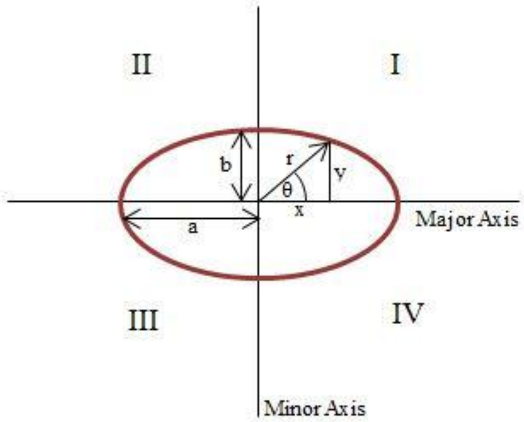

Figure 2-10: Schematic of an ellipse used to derive the x- and y-coordinates of the breast immobilization device

From geometry, the x- and y-coordinates are described as,

$$x(\theta) = r\cos\theta \tag{2}$$

$$y(\theta) = r\sin\theta \tag{3}$$

Substituting the value of r, equations (2) and (3) can be re-written as,

$$x(\theta) = \frac{a*b}{\sqrt{(bcos\theta)^2+(asin\theta)^2}}\cos\theta \tag{4}$$

$$y(\theta) = \frac{a*b}{\sqrt{(bcos\theta)^2+(asin\theta)^2}}\sin\theta \tag{5}$$

The semi-major axis measured during the experiment is 8.6 cm (3.39 inches), while the semi-minor axis is 4.4 cm (1.73 inches). Equations (4) and (5) are used in conjunction with parameters *a* and *b* to determine the x-and y-coordinates of an ellipse as reported in Appendix A. The coordinate values in quadrants I and II, as defined in Figure 2-10, correspond to points on the curved compression paddle, while those in quadrants III and IV correspond to points on the curved breast support, in effect dividing the ellipse into two equivalent halves down the major axis. These semi-elliptical constructs are truncated at either end to accommodate a variety of different breast sizes. Had we not chosen to truncate the optimized breast immobilization device, it would only compress a very limited range of breast sizes and could potentially cause discomfort due to tissue pinching.

2.3 Truncation Calculations

In order to truncate the breast immobilization device, the same methods described in Section 2.2 were employed to determine the semi-major and semi-minor axes of an 840 mL gelatin breast phantom. This value is the average breast volume observed during the pilot DMT study, and as such, it was used to determine the truncation points of the breast immobilization device. The semi-major axis associated with the 840 mL gelatin breast phantom was measured to be 8.1 cm, while the semi-minor axis was 4.25 cm. For the purposes of this calculation, we required elliptical area conservation, as the area (much like the volume) does not change when compressive force is applied, though the phantom breast will experience reshaping. As such, the semi-major and semi-minor axes of the 840 mL gelatin breast phantom were used to calculate the area (A_1) of the associated ellipse. In general, the area of an ellipse can be described as,

$$A = \pi * a * b \tag{6}$$

The area, A_1, of an ellipse with a semi-major axis equal to 8.1 cm and a semi-minor axis equal to 4.25 cm is 108 cm^2. The area within the truncated breast immobilization device, A_2, must be equal to the area, A_1, of the ellipse defined by the 840 mL gelatin breast phantom (see Figure 2-11). In other words, the truncation points along the major-axis are dictated by the calculated area under the curve, A_2, where the red line representing the breast immobilization device (defined by an 1100 mL gelatin breast phantom) is shifted down to the green line (defined by an 840 mL gelatin breast phantom) in quadrants I and II of Figure 2-11 and shifted up to the green line in quadrants III and IV. The goal of the calculation is to equate A_2 to the cross-sectional area of the green ellipse (A_1 = 108 cm^2), truncating the breast immobilization device such that the area of the average compressed breast is equal to the area of the optimized device.

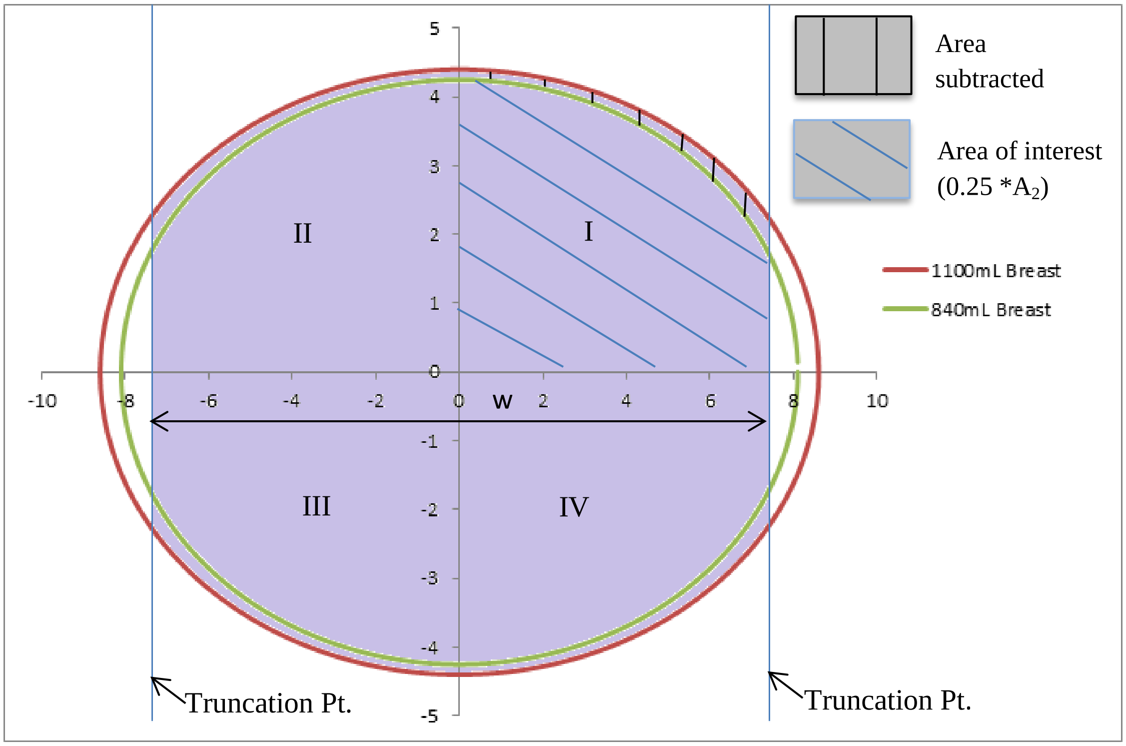

Figure 2-11: Illustration of truncation locations and area within the truncated breast immobilization device

As evident in Figure 2-11, the area under the curve is calculated in quadrant I and subsequently multiplied by four. The equation of an ellipse in Cartesian coordinates is used to calculate the area under the curve and is expressed as,

$$\left(\frac{x}{a}\right)^2 + \left(\frac{y}{b}\right)^2 = 1 \tag{7}$$

Isolating the variable y results in the following equation:

$$y = \sqrt{1 - \frac{x^2}{a^2}} * b \tag{8}$$

A delta (Δ = 0.15 cm), representing the difference between the semi-minor axis associated with the 1100 mL gelatin breast phantom and the 840 mL gelatin breast phantom, is incorporated into equation (8) as follows:

$$y = \left(\sqrt{1 - \frac{x^2}{a^2}} * b\right) - \Delta \tag{9}$$

Integrating equation (9) from 0 to w/2, where *w* is the width of the truncated breast immobilization device, we obtain

$$\int y\,dx = \int_0^{w/2} \left(\sqrt{1 - \frac{x^2}{a^2}} * b - \Delta\right) dx \tag{10}$$

Equation (10) can be re-written as

$$\int y\,dx = \int_0^{w/2} \left(\sqrt{1 - \frac{x^2}{a^2}} * b\right) dx - \int_0^{w/2} \Delta\,dx \tag{11}$$

Simplified further, equation (11) becomes

$$\int y\,dx = b\int_0^{w/2} \left(\sqrt{1 - \frac{x^2}{a^2}}\right) dx - \left(\Delta * \left(\frac{w}{2}\right)\right) \tag{12}$$

From algebra,

$$\sqrt{1 - \frac{x^2}{a^2}} = \frac{\sqrt{a^2 - x^2}}{a} \tag{13}$$

Equation (12) can then be expressed as

$$\int y\,dx = b\int_0^{w/2} \left(\frac{\sqrt{a^2 - x^2}}{a}\right) dx - \left(\Delta * \left(\frac{w}{2}\right)\right) \tag{14}$$

Using trigonometric substitution and considering the following triangle:

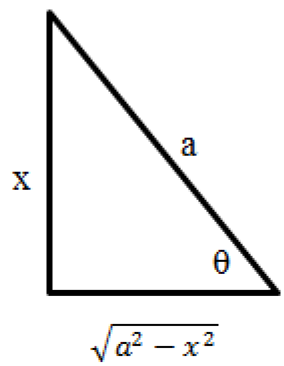

Figure 2-12: Trigonometric Substitution Triangle

Equation (14) can be re-written as

$$\int y\,dx = b \int \cos\theta a cos\theta d\theta - \left(\Delta * \left(\frac{w}{2}\right)\right) \tag{15}$$

Where $\cos\theta = \frac{\sqrt{a^2-x^2}}{a}$, $x = a\sin\theta$, $dx = a\cos\theta\, d\theta$, and $\theta = \sin^{-1}\left(\frac{x}{a}\right)$

Rearranging constants, equation (15) becomes

$$\int y\,dx = ab \int \cos^2\theta\, d\theta - \left(\Delta * \left(\frac{w}{2}\right)\right) \tag{16}$$

Where $\cos^2\theta = \frac{(1+\cos 2\theta)}{2}$ such that equation (16) is modified as follows:

$$\int y\,dx = ab \int \frac{(1+\cos 2\theta)}{2} d\theta - \left(\Delta * \left(\frac{w}{2}\right)\right) \tag{17}$$

Rearranging equation (17), we obtain

$$\int y\,dx = \frac{ab}{2}\int (1+\cos 2\theta)d\theta - \left(\Delta * \left(\frac{w}{2}\right)\right) \tag{18}$$

Equation (18) then becomes,

$$\int y\,dx = \frac{ab}{2}\left[\theta + \frac{1}{2}\sin 2\theta\right] - \left(\Delta * \left(\frac{w}{2}\right)\right) \tag{19}$$

Where $\sin 2\theta = 2\sin\theta cos\theta$, such that equation (19) can be re-written as,

$$\int y\,dx = \frac{ab}{2}\left[\theta + \frac{1}{2}(2)\sin\theta\cos\theta\right] - \left(\Delta * \left(\frac{w}{2}\right)\right) \tag{20}$$

Equation (20) can then be expressed in terms of *x* by,

$$\int y\,dx = \frac{ab}{2}\left[\sin^{-1}\left(\frac{x}{a}\right) + \frac{1}{2}(2)\left(\frac{x}{a}\right)\left(\frac{\sqrt{a^2-x^2}}{a}\right)\right]_0^{w/2} - \left(\Delta * \left(\frac{w}{2}\right)\right) \tag{21}$$

A_2 is finally expressed as,

$$A_2 = 4 * \left[\frac{ab}{2}\sin^{-1}\left(\frac{w}{2a}\right) + \frac{bw}{4}\left(\sqrt{1-\frac{w^2}{4a^2}}\right) - \left(\Delta * \left(\frac{w}{2}\right)\right)\right] \tag{22}$$

Where *w* is the truncated width of the breast immobilization device, a = 8.6 cm and b = 4.4 cm.

The points of truncation along the major axis of the ellipse at +/- *w/2* were calculated by setting A_2 equal to A_1. Appendix B clearly illustrates that $A_2 = A_1 = 108$ cm^2 when *w/2* = +/-7.5 cm. As such, the total width of the truncated breast immobilization device (*w*) is 15 cm. Referring to Appendix A, the theta values (θ) that correspond to *w/2* = +/- 7.5 cm are easily realized. These results suggest that the curved compression paddle should be truncated at θ=+16° and θ=+164° from the positive x-axis, while the curved breast support should be truncated at θ=+196° and θ=+344° from the positive x-axis.

2.4 Detailed Device Description and Fabrication

A prototype breast immobilization device was fabricated by Virginia Industrial Plastics Incorporated (Elkton, Virginia) and is shown in Figure 2-13. As previously described, the prototype is comprised of a curved compression paddle and a curved breast support, both of which are vacuum formed from 0.125 inch thick polycarbonate. The vacuum forming process involves the following steps. First, a mold is made for the component part [31]. Then, the mold is placed into a machine and the polycarbonate sheet clamped into the frame [31]. Heat is then applied to the polycarbonate until it becomes pliable [31]. Finally, the softened polycarbonate sheet is lowered onto the mold, at which time suction is applied [31]. Upon completion of the component part, it is dismounted from the machine and precision trimmed [31].

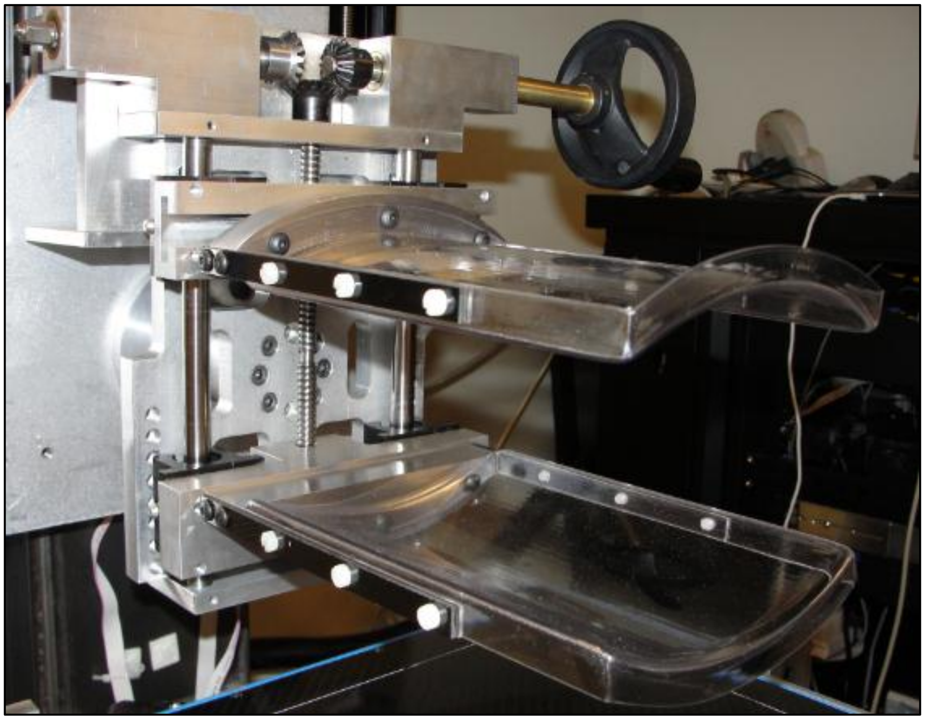

Figure 2-13: Photograph of Optimized Breast Immobilization Device

The overall dimensions of the curved compression paddle and the curved breast support are 7.75 inches long x 5.91 inches wide x 1.26 inches high. Though the width (x-dimension) of the device was dictated by the location of the truncation points and the height was dictated by both the semi-minor axis of the ellipse and the location of the truncation points, the length (y-dimension) of the device was chosen in keeping with the length of the standard flat paddle used to compress the breast during the pilot DMT study. To ensure that all parts of the breast anatomy are held securely in place during the scan, rigidity was added into the design by including a 0.375 inch high lip along the perimeter edge of both component parts. A detailed drawing of the breast immobilization device is included in Appendix C.

The curved compression paddle and curved breast support are mounted to the gantry by identical support mechanisms facing in opposite directions and centered on the axis of rotation (AOR) of the DMT scanner. The compression paddle is oriented such that it is concave downwards (in the negative z-direction), while the breast support is oriented such that it is concave upwards (in the positive z-direction). The support mechanisms are fabricated from aluminum and rigid carbon fiber components. The overall dimensions of the support pieces are dictated by the dimensions of the breast immobilization device itself and are disclosed in the support system drawings included in Appendix C. The curvature of the aluminum part is determined by the semi-major and semi-minor axes of the ellipse that defines the shape of the breast immobilization device. The truncation points for the aluminum part are the same as those outlined for the breast immobilization device.

The support mechanism that integrates the compression paddle into the gantry is mounted to a right handed ball lead screw, while the support mechanism that integrates the breast support into the gantry is mounted to a left handed ball lead screw whose pitch is the same as that of the right handed lead screw. The right handed ball lead screw is coaxial with and rigidly attached to the left handed ball lead screw. The lead screw axes intersect the AOR and are parallel to the z-axis. A single mechanical crank system translates the paddle in the negative z-direction while simultaneously translating the support in the positive z-direction. Thus, the paddle and the support move in opposite directions at equal speeds and by equal distances towards the AOR. The immobilized breast is centered on the AOR when fully immobilized.

CHAPTER 3

GELATIN BREAST PHANTOM AND GAMMA CAMERA TRAJECTORY STUDIES

Gelatin breast phantom and gamma camera trajectory studies were performed to evaluate the effectiveness of the prototype breast immobilization device by comparing the reconstructed MBIT images associated with a camera trajectory dictated by the optimized breast immobilization device with those of standard, flat paddle compression. At the time of the experiment, the gamma camera used in the pilot DMT study was not available, because it was being repaired by our collaborators at West Virginia University. Therefore, a similar camera was employed for the purposes of this study. Figure 3-1 illustrates the experimental set-up that was used to obtain projection data for each of the aforementioned trajectories. Of particular importance, the immobilization devices themselves were not used in the set-up because Virginia

Plastics Inc. was concurrently fabricating the optimized breast immobilization device. However, a thin-walled, low-attenuation acrylic box was used to simulate flat paddle compression.

3.1 Study Design

3.1.1 Experimental Set-Up

Note: significant portions of Section 3.1.1 were taken with permission from reference [13]

The gamma camera that was selected for use and built at Jefferson Labs (Newport News, VA), consists of a 3 x 4 array of Hamamatsu H8500 PSPMTs optically coupled to a NaI (TI) crystal array with a crystal pitch of 1.4 mm and a crystal thickness of 6 mm. The camera is also equipped with a lead parallel hole collimator that has an associated efficiency of 1.10 $x10^{-4}$, while the acquisition is controlled by software written in K-max (Sparrow Corporation, Port Orange, FL). The camera was positioned in front of a computer-controlled rotation stage mounted on a linear translation stage, which allowed us to vary both the viewing angle and the AOR-to-camera distance to simulate the motion of the gamma camera in the DMT system. COSMOS, a motor controller software program written by Velmex, was used to rotate as well as translate the gelatin breast phantom to specific locations so as to acquire the projection data needed to reconstruct the MBIT images. An 840 mL radioactive gelatin breast phantom was used in this experiment as illustrated in Figure 3-1. The phantom contained two plastic, thin-walled spherical lesions with an inside diameter of 15 mm.

Figure 3-1: Photograph of Experimental Set-up

3.1.2 Activity and Acquisition Time Calculations

During a two minute clinical scan, we typically see an activity concentration of 0.33 μCi/mL within the normal breast tissue. In the interest of efficiency, the desired background activity concentration was doubled (0.67 μCi/mL) for these experiments to reduce the acquisition time associated with each projection view. The lesion-to-background activity concentration ratio that was chosen for these experiments was 10:1. The total activity at the time of the experiment was determined by multiplying the desired concentrations by the appropriate

(orange)	Data as Input
(white)	Calculated Data
(blue)	Required Quantities for experiment

Breast tissue vol.		Lesion vol.		Desired Concentration			Total Act. @ time of exp.		Hours Before exp.		Total Act. to put in		Packets of jello Reqd.
[cups]	*[mL]*	*[cups]*	*[mL]*	*Bkg [µCi/mL]*	*Ratio (Lesion:Bkg)*	*Lesion[µCi/mL]*	*Bkg [µCi]*	*Lesion [µCi]*	*hrs*	*min*	*Bkg [µCi]*	*Lesion [µCi]*	*Bkg [#]*
3.5	840	0.5	120	0.67	10	6.7	563	804	5	0	1000.9	1429.8	5.25

Table 3-1: Spreadsheet calculating background and lesion activity

volume, as illustrated in Table 3-1. Since the activity is injected into gelatin that is initially in liquid form, the experiments were not conducted until a few hours later, after the gelatin had set. ^{99m}Tc-pertecnitate, the radioactive isotope used in these studies, has a half-life of approximately six hours. As such, we had to account for decay when calculating the *initial* amount of radioactivity required for both the lesions and the phantom itself by estimating the requisite gelatin set time based on our intuition and experience. The Beer-Lambert Law, which can be expressed as,

$$A(t) = A_0 e^{-\lambda t} \tag{23}$$

was used to compute the total *initial* activity needed by first rearranging the variables to obtain equation (24).

$$\lambda = -\frac{LN\left(\frac{A_{thalf}}{A_O}\right)}{t_{half}} = -\frac{LN\left(\frac{1}{2}\right)}{t_{half}} = \frac{LN(2)}{t_{half}} = \frac{LN(2)}{6.02} \tag{24}$$

Equation (24) is the half-life of ^{99m}Tc-pertecnitate and can be substituted back into equation (23) to subsequently solve for A_o, where t = 5 hours and A(t) is the total activity at the time of the experiment. The Beer-Lambert Law then becomes,

$$A_o = A(t)e^{\frac{LN(2)}{6.02}t} \tag{25}$$

Finally, the total number of gelatin packets needed to create the breast phantom was computed by multiplying 1.5 by the breast tissue volume (in cups). The lesions were filled with radioactive water rather than gelatin to facilitate easy cleanup at the end of the experiments.

After the gelatin phantom had set, the image acquisition time had to be calculated before beginning the experiments. Again, the Beer-Lambert Law was employed in Table 3-2 to determine the concentration of activity in the gelatin phantom at the start of the experiment.

Input:										
	* Format of input: TIME(hours, minutes,sec) with hours in military time									
Output:		Value to put into Kmax program for acquisition time for single projection								
							Concentration [μCi/mL]			
Phantom Vol.	**Syringe Act B4 added to jello [μCi]**	**Syringe Act after added to jello [μCi]**	**Total Added Activity [μCi]**	**Time Act Added***	**Time Exper. Started***	**Time Elapsed**	**When added to jello**	**Exper. Start**	Desired Concen. [μCi/ml]	Required Time [s]
840	1001	0	1001	0.392	0.583	4.600	1.1917	0.7017	0.33	56.43692

Table 3-2: Spreadsheet calculating image acquisition time

The two parameters that were needed to compute $A(t_{exp})$ included the concentration of activity in the gelatin phantom at the time that it was added and the time that had elapsed between the addition of activity and the commencement of the experiments themselves. Once $A(t_{exp})$ had been determined, the desired concentration dictated by clinical observation, 0.33 μCi/mL, and clinical scan time, 120 seconds per image acquired, were used to calculate the acquisition time for the very first image obtained during the experiment. In order to account for decay over the time course of the entire experiment, this acquisition time was entered into the K-max GUI, as illustrated in Figure 3-2, to determine the associated number of counts, or total events, in the first image. This number was subsequently held constant for all of the remaining acquisitions.

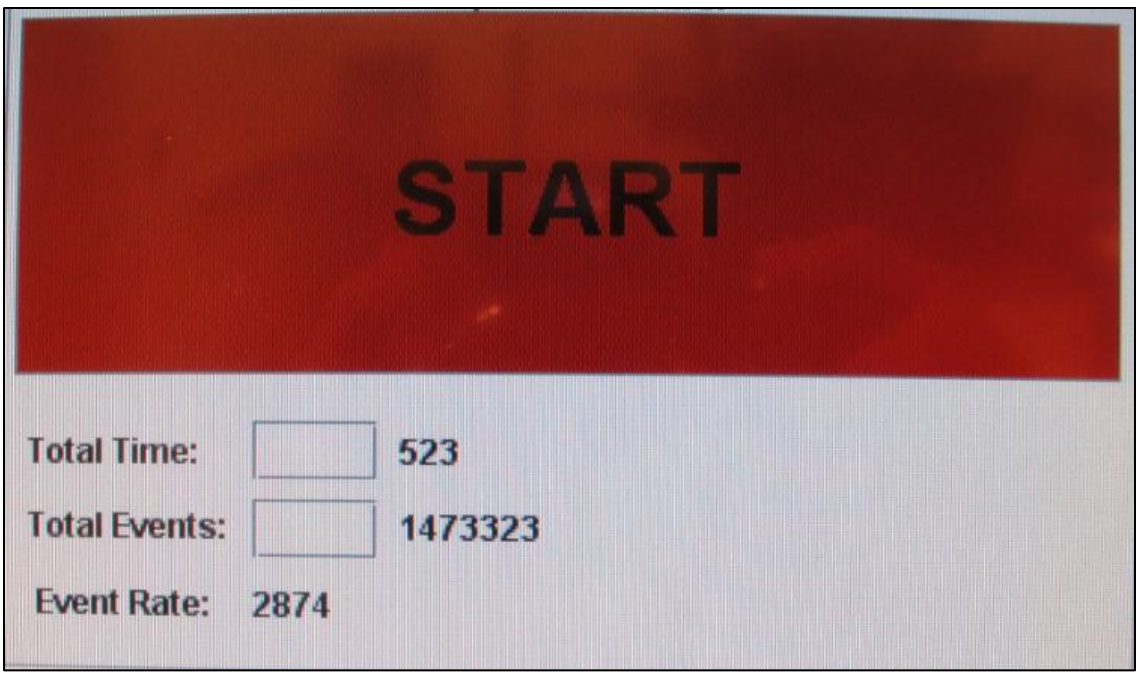

Figure 3-2: K-max GUI

3.1.3 Trajectory Calculations

As previously mentioned, two gamma camera trajectories were calculated to determine the relative position of the camera with respect to the gelatin breast phantom. The first trajectory was dictated by the flat compression paddle and breast support that were used in the pilot DMT study, while the second trajectory was dictated by the optimized breast immobilization device. Two assumptions were made with respect to these trajectories. We assumed that the center normal of the detector always intersected the AOR, and that the projection of the detector surface is tangent to the immobilization device at every projection angle. These trajectories were evaluated between -67.5° and 67.5° at angular increments of 5.625°. Twenty-five projection views were acquired during the scan, including a zero degree view, though only nine of these projection views were used to reconstruct the 3-D image. A series of Monte Carlo simulations were performed by Zongyi Gong, a friend and fellow colleague, to determine the optimal acquisition angle range (+/- 67.5°) and number of projection views (9), as he perfected the MBIT reconstruction algorithm that he wrote and developed. Considering Figure 3-3, the "flat paddle" trajectory was calculated as follows:

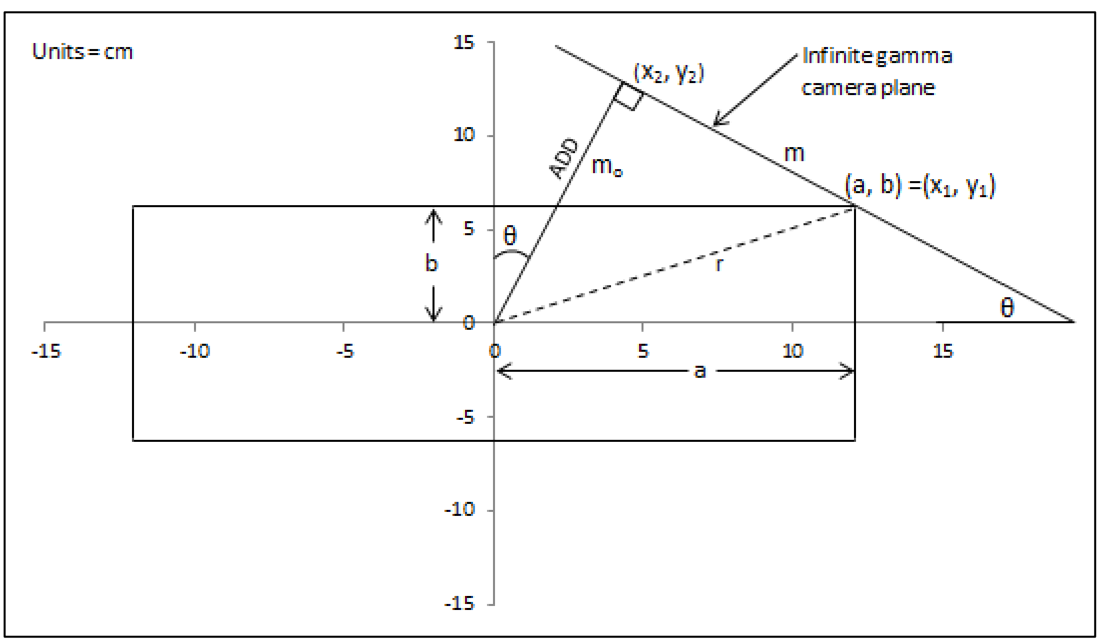

Figure 3-3: "Flat Paddle" Trajectory Schematic

By definition, the slope of the line defining the gamma camera plane is,

$$m = \tan(\theta) \tag{26}$$

Furthermore, because the line defining the AOR to detector distance (ADD) is perpendicular to the line defining the gamma camera plane, its slope can be defined as the negative reciprocal of m.

$$m_o = -\frac{1}{m} = -\frac{1}{\tan(\theta)} \tag{27}$$

The slope-intercept form of a line can be used to describe ADD because both the slope and y-intercept of the line are known.

$$y = m_o x = -\frac{1}{tan\theta} x \tag{28}$$

The point-slope form of a line can be used to describe the camera detector plane because both the slope and the point (a, b) are known. Point *a* is simply half of the width of the flat compression paddle, whereas point *b* is half of the average compressed breast thickness observed during the pilot DMT study plus half the thickness of the breast support and compression paddle combined.

$$y - b = m(x - a) \tag{29}$$

Equation (29) can be expressed as,

$$y = mx - ma + b \tag{30}$$

The location (x_2, y_2) on the camera can be found by setting equation (28) equal to (30).

$$m_0 x_2 = m x_2 - ma + b \tag{31}$$

Equation (31) can be rearranged to solve for x_2 as follows:

$$x_2 = \frac{-ma+b}{m_o-m} = \left(\frac{-((tan\theta * a)+b)}{-\frac{1}{tan\theta}-tan\theta}\right) \tag{32}$$

Substituting equation (32) into equation (28) yields

$$y_2 = m_o\left(\frac{-ma+b}{m_o-m}\right) = -\frac{1}{tan\theta}\left(\frac{-((tan\theta * a)+b)}{-\frac{1}{tan\theta}-tan\theta}\right) \tag{33}$$

Given θ, the gamma camera trajectory values associated with "flat paddle" compression (x_2, y_2) are presented in Appendix D. Similarly, the trajectory associated with the optimized breast immobilization device was computed by considering Figure 3-4.

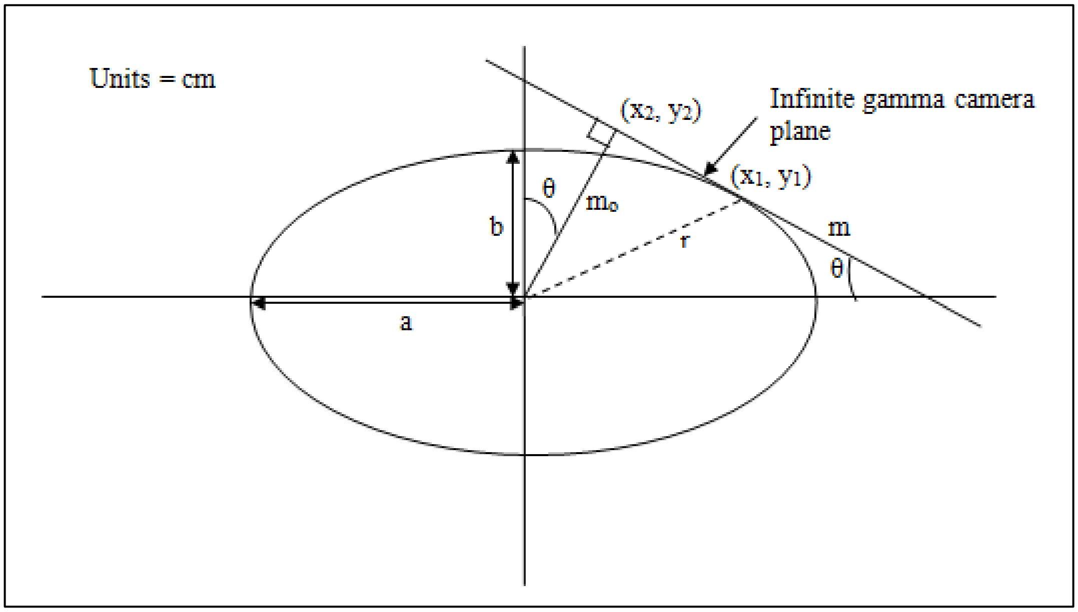

Figure 3-4: Optimized Breast Immobilization Device Trajectory Schematic

Again by definition, the slope of the line defining the camera detector plane is

$$m = \tan(\theta) \tag{34}$$

The slope of the line defining the AOR to detector distance (ADD) is once more,

$$m_o = -\frac{1}{m} = -\frac{1}{\tan(\theta)} \tag{35}$$

In order to calculate x_1, the equation of an ellipse in Cartesian coordinates is manipulated to yield equation (36) where *a* is half of the width of the 1100 mL gelatin breast phantom plus the height of the lip of the optimized breast immobilization device and *b* is half of the thickness of the 1100 mL gelatin breast phantom plus the height of the lip of the optimized breast immobilization device.

$$y = \sqrt{1 - \frac{x^2}{a^2}} * b \tag{36}$$

Taking the derivative of equation (36) with respect to the variable *x*, we obtain the following:

$$\frac{dy}{dx} = b\left(\frac{d}{dx}\left(\sqrt{1 - \frac{x^2}{a^2}}\right)\right) \tag{37}$$

Using the chain rule where $\frac{d\sqrt{u}}{du} * \frac{du}{dx}$,$u = 1 - \frac{x^2}{a^2}$ and $\frac{d\sqrt{u}}{du} = \frac{1}{2} * u^{-\frac{1}{2}} = \frac{1}{2\sqrt{u}}$, equation (37) can be expressed as,

$$\frac{dy}{dx} = \frac{b\left(\frac{d}{dx}\left(1 - \frac{x^2}{a^2}\right)\right)}{2\sqrt{1 - \frac{x^2}{a^2}}} \tag{38}$$

Therefore, the derivative can be re-written as,

$$\frac{dy}{dx} = \frac{-b(2x)}{2a^2\sqrt{1 - \frac{x^2}{a^2}}} \tag{39}$$

Finally, equation (39) becomes

$$\frac{dy}{dx} = \frac{-bx}{a^2\sqrt{1-\frac{x^2}{a^2}}} \qquad (39)$$

Equation (39) is the slope of the line defining the gamma camera plane and can be re-written as follows:

$$\frac{dy}{dx} = m = \tan(\theta) = \frac{-bx}{a^2\sqrt{1-\frac{x^2}{a^2}}} = \frac{-bx}{a\left[a^2\left(1-\frac{x^2}{a^2}\right)\right]^{\frac{1}{2}}} \qquad (40)$$

By squaring equation (40), we obtain

$$m^2 = \frac{b^2x^2}{a^2(a^2-x^2)} = \frac{b^2x^2}{a^4-a^2x^2} \qquad (41)$$

By rearranging the equation and isolating the variable *x*, equation (41) becomes

$$x^2 = \frac{m^2a^4}{m^2a^2+b^2} \qquad (42)$$

As a result, we obtain the following expression for x_1.

$$x_1 = \pm\sqrt{\frac{m^2a^4}{m^2a^2+b^2}} \qquad (43)$$

Equation (43) can then be substituted into equation (36) to solve for y_1. Subsequently, the parameters x_2 and y_2 can be computed as a function of x_1 and y_1, by setting the equation of a line describing ADD ($y_2=m_ox_2$) equal to the equation of a line describing the gamma camera plane $(y-y_1)=m(x_2-x_1)$.

$$m_0x_2 = mx_2 - mx_1 + y_1 \qquad (44)$$

Solving for x_2, we obtain

$$x_2 = \frac{-mx_1+y_1}{m_o-m} \tag{45}$$

Equation (45) can then be substituted into $y_2=m_o x_2$ to calculate y_2. The gamma camera trajectory values associated with the optimized breast immobilization device (x_2, y_2) are also presented in Appendix D.

3.2 Reconstruction Algorithm Description

Note: Significant portions of Section 3.2 were taken from a personal interview with Zongyi Gong (2012, June 19).

The reconstruction algorithm that was used to create the 3-D image from the projection data acquired during the experiment was written in Matlab by Zongyi Gong. The Maximum Likelihood Expectation Maximization (MLEM) algorithm is an iterative, statistics based approach to image reconstruction. This algorithm differs significantly from the popular analytical method called filter back projection. Filter back projection will not prevent the transfer of noise from the projection images into the 3-D volume. Because we deal with fairly noisy projection images, the MLEM method is preferred. Generally speaking, the algorithm iteratively finds the 3-D reconstructed volume that has the highest probability of returning the experimentally obtained projection images.

The MLEM approach involves three main steps. First, the algorithm calculates important geometries, such as phantom location, detector location, and AOR-to-detector distance. Second, it chooses an initial, uniform 3-D volume that will change with each successive iteration. Finally, it simulates forward projection by virtually rotating the detector to produce computer-generated projection images from the 3-D volume. These projection images may differ from those acquired during the experiment. These differences are incorporated into a “changing factor," which is then multiplied by the current 3-D volume to create a new 3-D volume. This iterative, forward projection approach is repeated until the "changing factor" is zero, in effect providing a true representation of the 3-D volume. Furthermore, the MLEM algorithm models the emitted photon as a Gaussian function instead of a delta function in the forward projection to provide attenuation correction and resolution recovery in the resulting 3-D image.

3.3 Results

A comparison study was conducted to evaluate the effectiveness of the optimized breast immobilization device once the MBIT images had been reconstructed using the MLEM algorithm. The image quality figures of merit included lesion contrast and signal-to-noise ratio (SNR). Lesion intensity and background intensity were measured in single slices of the 3-D reconstructed volume where the lesion intensity appeared brightest. Lesion intensity was defined as the average pixel value in a 4 x 4 pixel ROI centered on the lesion, while background intensity was defined as the average background pixel value in a 30 x 20 pixel ROI near the lesion of interest. Figures 3-5 and 3-6 respectively illustrate a lesion ROI and background ROI in a single slice image for the gamma camera trajectory defined by the optimized breast immobilization device. Similar images were acquired and analyzed for the gamma camera trajectory defined by the standard, flat compression paddle. A total of five trials were conducted for each trajectory.

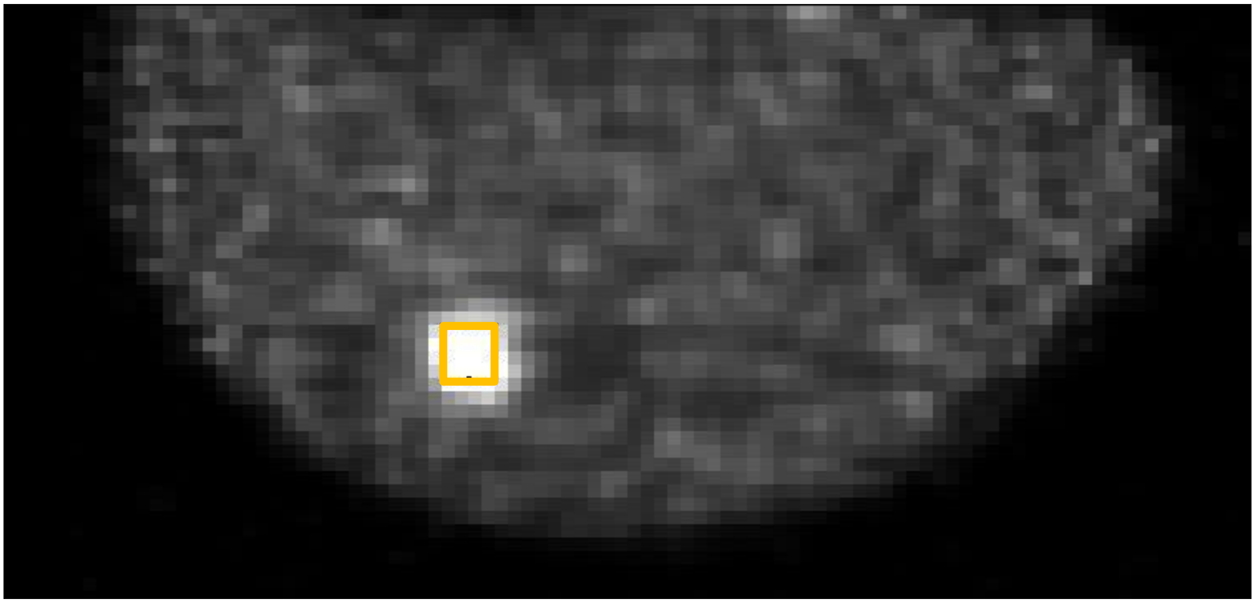

Figure 3-5: In-plane Slice Image Used to Determine Lesion Intensity (parallel to the x-y plane of the gelatin breast phantom)

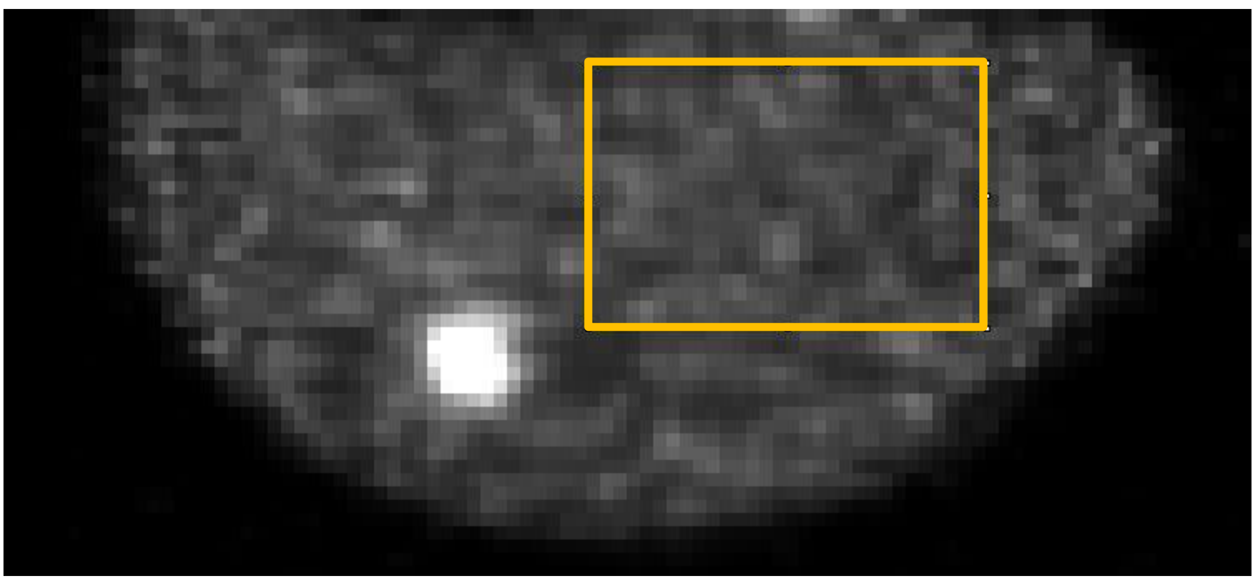

Figure 3-6: In-plane Slice Image Used to Determine Background Intensity (parallel to the x-y plane of the gelatin breast phantom)

Lesion contrast and SNR were subsequently calculated for each trial as follows:

$$Contrast = \frac{N_L - N_B}{N_B} \tag{46}$$

$$SNR = \frac{N_L - N_B}{\sigma_B} \tag{47}$$

where N_L is the average pixel value in the lesion ROI, N_B is the average pixel value in the background ROI, and σ_B is the standard deviation of the pixel values in the background ROI. Of particular importance, the lesion contrast and SNR were calculated for both a “shallow” lesion and a “deep” lesion, located at depths of approximately 20 mm and 50 mm below the surface of the phantom, respectively. Image J, a commonly used image processing program, was employed to determine the parameters necessary to evaluate both lesion contrast and SNR. Excel was used to calculate lesion contrast and SNR, and Matlab was used to plot the results which are presented in Figures 3-7 and 3-8. The Matlab source code and Excel files are included in Appendix E. In general, lesion contrast and SNR improvements were observed as graphically depicted below.

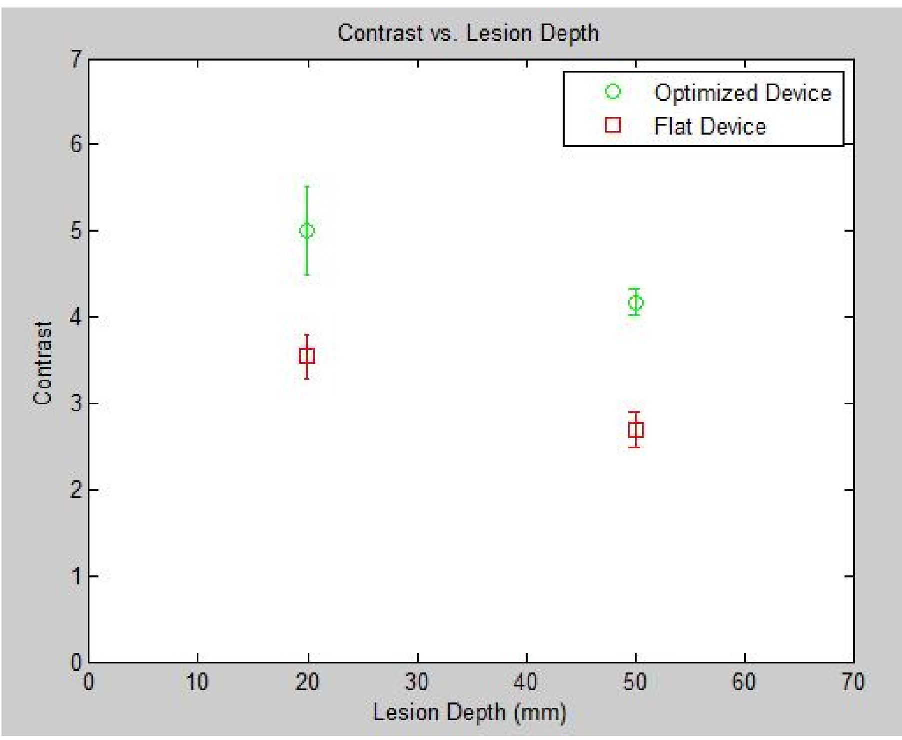

Figure 3-7: Lesion Contrast. Error Bars indicate standard deviation of 5 repeated trials of the experiment.

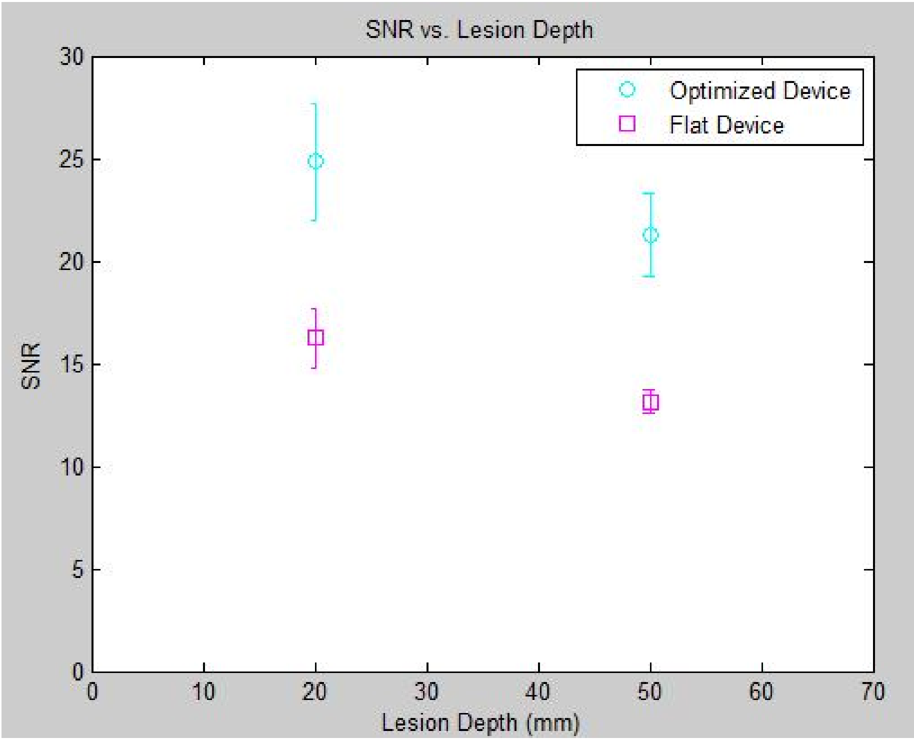

Figure 3-8: SNR. Error Bars indicate standard deviation of 5 repeated trials of the experiment.

3.4 Discussion

The “shallow” lesion contrast improved from 3.6 to 5.0, an increase of 41%, while the “deep” lesion contrast improved from 2.7 to 4.2, an increase of 35%. The “shallow” lesion SNR improved from 16.2 to 24.8, an increase of 53%, while the “deep” lesion SNR improved from 13.1 to 21.3, an increase of 38%. If our gamma system was in fact perfect, we would expect the lesion to convolve nicely with a delta function to produce an image that ideally represents the lesion with no additional object blurring or signal intensity reduction. That being said, our system is not perfect, and as such, we expect to see somewhat different results. In reality, the lesion is convolved with a Gaussian function, resulting in a larger, less intense representation of the lesion itself.

Intuitively, the lesion contrast and SNR improvements observed as a result of these studies are expected. Because the gamma camera detector surface is significantly closer to the lesion when the camera trajectory is dictated by the optimized breast immobilization device (as illustrated in Appendix D), the Gaussian function convolved with the lesion has a smaller standard deviation and full width at half maximum (FWHM). As such, the lesion should appear both brighter and less extensive in the resulting image. We hypothesized that the mean lesion contrast and mean SNR would improve with decreasing radial distance between the gamma camera detector surface and the object (lesion) of interest.

This hypothesis was substantiated by conducting a non-parametric Kruskal-Wallis statistical test to determine whether or not the mean lesion contrast and mean SNR values associated with each trajectory are equal. The Kruskal-Wallis test is merely an extension of the Wilcoxon rank sum test and is frequently used to compare the means between two or more distinct samples. Though our goal is simply to compare two samples, the Kruskal-Wallis test was preferred over the Wilcoxon rank sum test because the Kruskal-Wallis Matlab function outputs both the p-value and a corresponding box and whiskers plot, whereas the Wilcoxon rank sum function does not. The Kruskal-Wallis source code is included in Appendix E.

The Kruskal-Wallis test was chosen in lieu of a much more robust, parametric two-sample t-test, or by extension, analysis-of-variance (ANOVA) test, for two main reasons. First, both the two-sample t-test and the ANOVA test assume that “all sample populations are normally distributed” [29]. The Quantile-quantile (QQ) plots presented in Appendix E clearly illustrated that some of the sample data moderately deviates from a straight line, indicating that the data is not normally distributed. The occasional outliers that are observed at the tails of the QQ plots also suggest a deviation from normality. Second, the ANOVA test assumes that “all sample populations have equal variance" [29]. Having calculated the variance associated with each sample population as indicated in Appendix E, it is quite obvious that they differ significantly. Consequently, the Kruska-Wallis test was selected for use because it only assumes that all observations are mutually independent and that all samples come from populations with the same continuous distribution [30].

The small p-values presented in Table 3-3 prove that the data is statistically significant and that the null hypothesis can be rejected (p-value < 0.05 was considered statistically significant). In other words, the mean contrasts associated with both the "shallow" and "deep" lesion differ between the two trajectories, as do the mean SNRs. Furthermore, the box and whiskers plots generated in Matlab and displayed in Figures 3-9 through 3-12, prove not only a difference, but more importantly, an *improvement* in lesion contrast and SNR, as was expected. These results are encouraging and validate that the prototype design has the potential to help improve image quality as we move forward with our clinical trial studies.

	Lesion Depth	
Figure of Merit	**Shallow (20 mm)**	**Deep (50 mm)**
Contrast	0.009	0.009
SNR	0.009	0.009

Table 3-3: P-Values associated with contrast and SNR according to lesion depth.

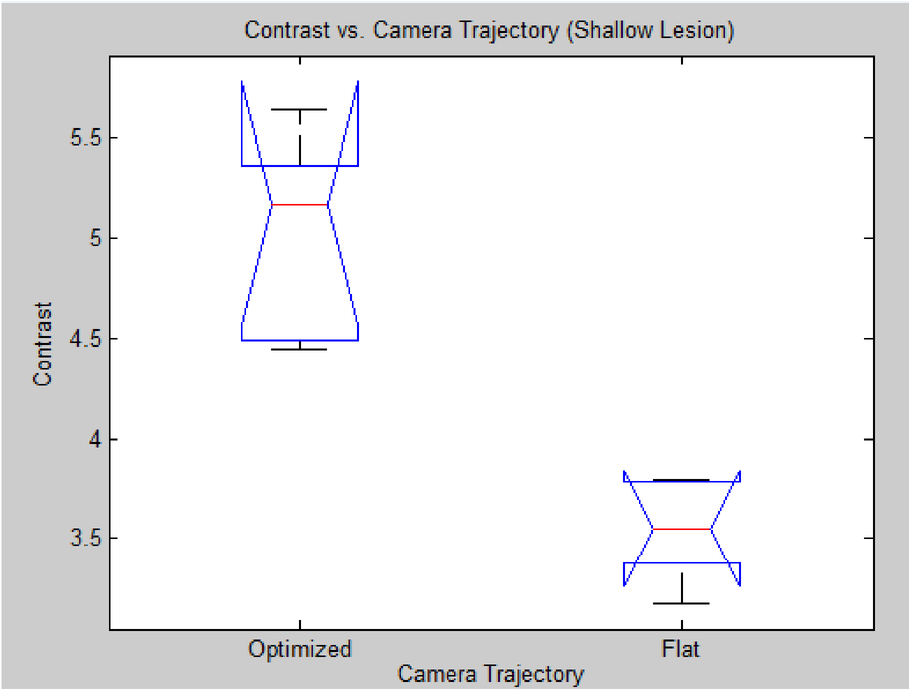

Figure 3-9: Box and whiskers plot comparing contrast (shallow lesion)

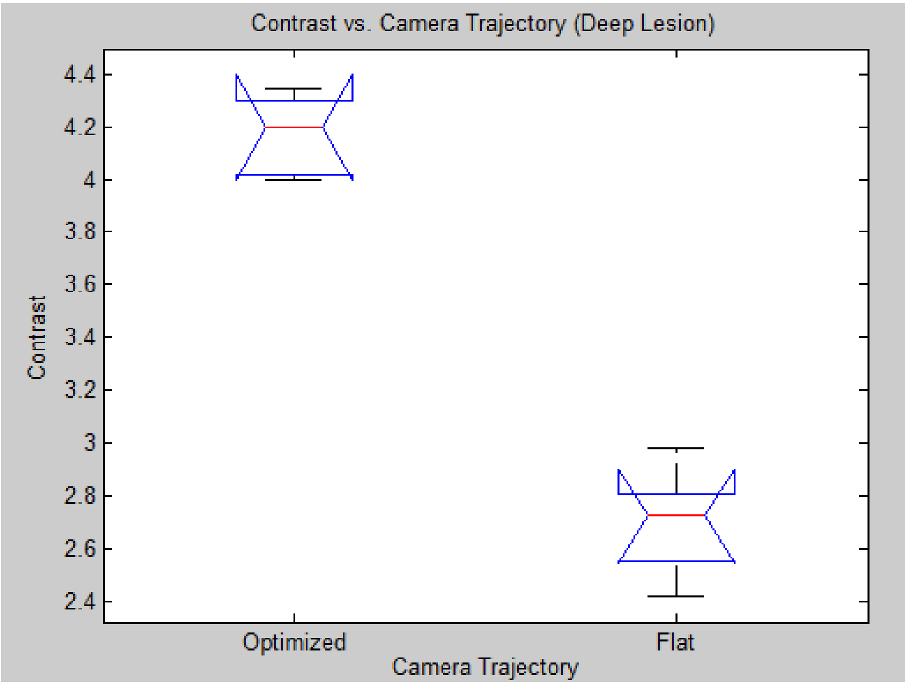

Figure 3-10: Box and whiskers plot comparing contrast (deep lesion)

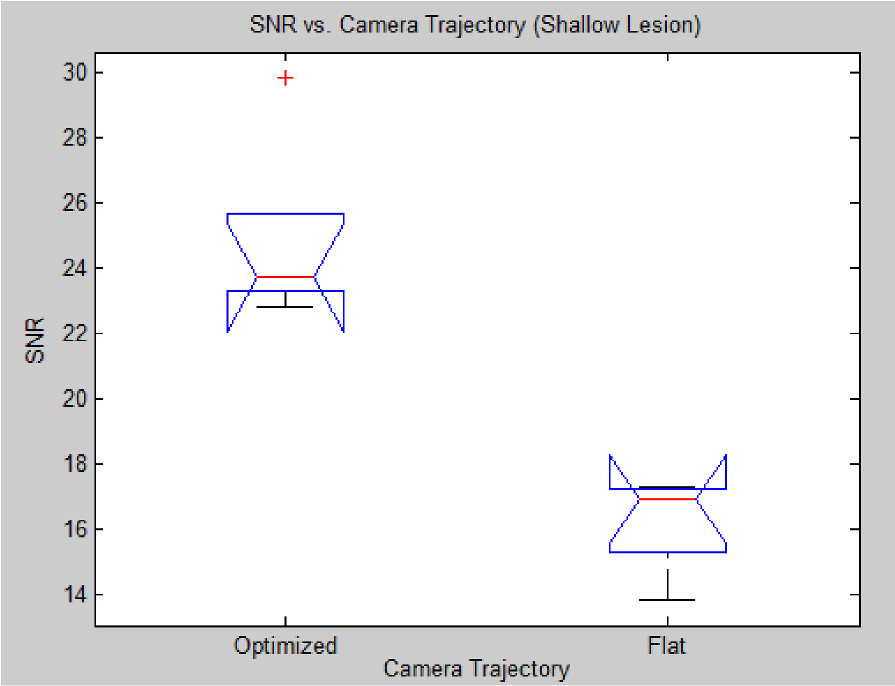

Figure 3-11: Box and whiskers plot comparing SNR (shallow lesion)

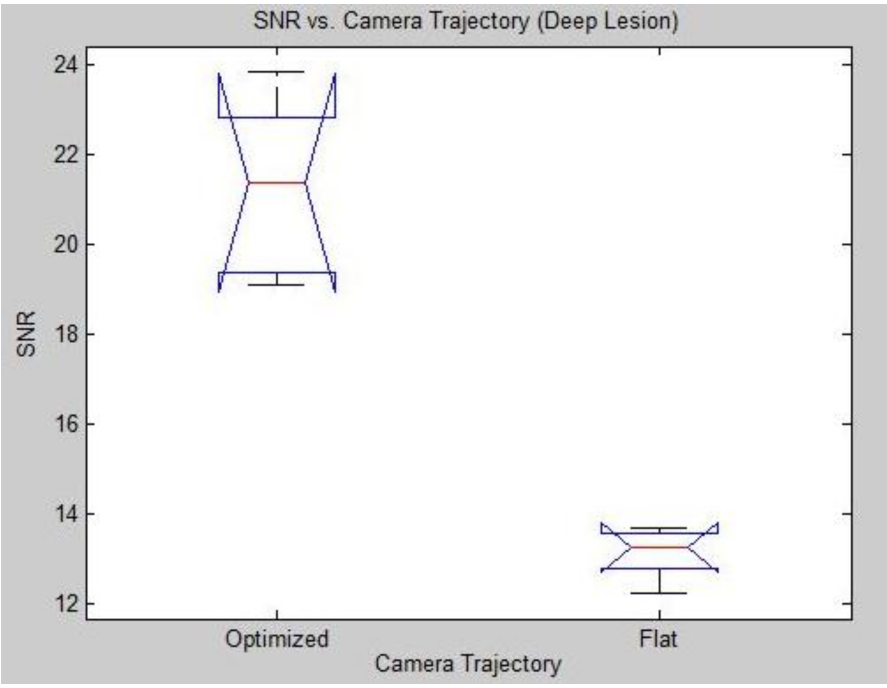

Figure 3-12: Box and whiskers plot comparing SNR (deep lesion)

Note: Box and whiskers plot nomenclature. Red central line denotes median data point, top black line denotes maximum data point, bottom black line denotes minimum data point, top blue line denotes 75th percentile (calculated using the quantile function & linear interpolation), bottom blue line denotes 25th percentile (also calculated using the quantile function and linear interpolation), and red + sign indicates outliers

CHAPTER 4

PROTOTYPE EVALUATION AND REDESIGN

Having assessed the validity of the optimized breast immobilization device experimentally using a gelatin breast phantom, we recognized the importance of evaluating the prototype in a research setting with real human breasts. As such, we integrated the prototype into the DMT gantry and recruited two women with very different breast sizes to participate in an investigative study aimed at understanding how well the prototype works to compress the breast. The strengths and weaknesses of the optimized device were revealed as a result of this study, ultimately driving future alternative design recommendations. The volunteers were not exposed to radiation during this investigation, as the goal of the study was to evaluate the prototype's ability to fully compress the breast, irrespective of size, shape, and elasticity.

4.1 Optimized Breast Immobilization Device Design Limitations

A pregnancy belly cast kit (Figure 4-1) was used to evaluate the effectiveness of the optimized breast immobilization device in terms of its ability to compress breasts of varying sizes. Though slightly unorthodox, this kit allowed us to create a mold of the breast during compression. First, the gantry arm was positioned at approximately +40° so that compression could be applied from the medial side of the breast to the lateral side of the breast at an oblique angle (MLO view). The MLO view was used to acquire projection data during the pilot DMT study.

Figure 4-1: Pregnancy belly cast kit

After positioning the gantry arm, we applied wet plaster from the belly cast kit to the breast of interest. A radiation technologist then positioned the breast inside the optimized breast immobilization device and applied compressive force using the mechanical crank system. The plaster dried into a mold of the compressed breast as shown in figure 4-2.

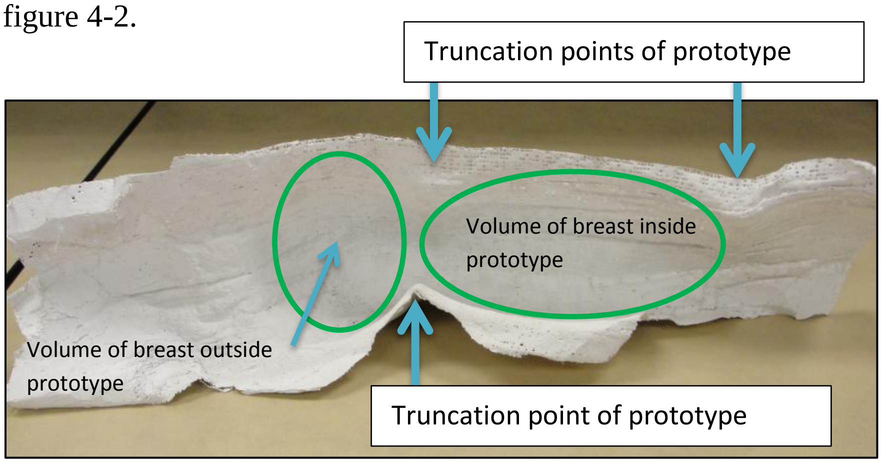

Figure 4-2: Mold of breast compressed with optimized immobilization device

While one of the participants in this study had a smaller breast size, equating to a 34A bra size, the other had a larger breast size, equating to a 32D bra size. Though these breast sizes differ significantly, the results of the study were qualitatively similar for both volunteers. Each mold showed that a certain percentage of breast tissue was not being compressed by the optimized breast immobilization device. The radiation technologist was able to position the breasts such that the pectoral muscle was held securely in place; however, the medial breast tissue was compromised. As evident in Figure 4-2, the prototype pinched the medial tissue, segmenting it into two distinct fractions, causing notable pain and discomfort. Simply put, the optimized breast immobilization device is not wide enough to accommodate all of the breast tissue, even for relatively small breast sizes.

4.2 Support System Limitations

Unfortunately, the support system that integrates the optimized breast immobilization device into the DMT gantry is not without design flaws as well. Delrin, a very strong though highly-attenuating polymer, was the material originally chosen for the side pieces of the support structure. However, we modified the design, and instead suggested the use of carbon-fiber. Carbon-fiber, also well known for its strength, is significantly less radio-opaque than Delrin. As such, we were hoping that it would not be as visible in the acquired x-ray projection images. Disappointingly, the rigid carbon-fiber supports were very obvious in the projection images, at different locations across the angular range employed. The carbon-fiber could potentially obscure small lesions or micro-calcifications, tiny speckles that can sometimes appear in a structural image and are, at times, indicative of disease presence. The support structures themselves would be very difficult to correct out of the x-ray image, and as such, alternative attachment methods were considered.

4.3 Optimized Breast Immobilization Device Alternative Design

An area analysis was completed to justify our experimental observations and help quantify a wider, more inclusive prototype to avoid "pinching" during future clinical trial studies. Recalling equation (22), we were able to calculate the total area associated with the truncated optimized breast immobilization device.

$$A_2 = 4 * \left[\frac{ab}{2}\sin^{-1}\left(\frac{w}{2a}\right) + \frac{bw}{4}\left(\sqrt{1-\frac{w^2}{4a^2}}\right) - \left(\Delta * \left(\frac{w}{2}\right)\right)\right]$$

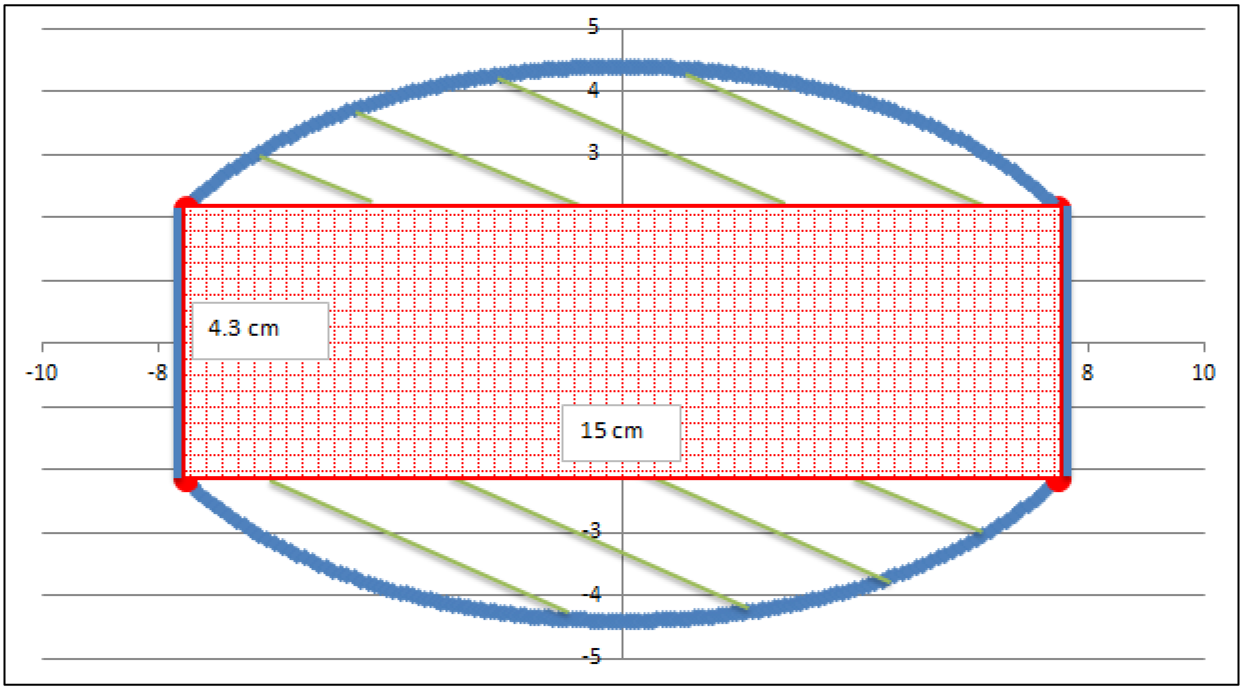

Figure 4-3: Cross-sectional area of truncated optimized breast immobilization device

A_2, the area enclosed by the blue lines in Figure 4-3, equates to 112.5 cm^2. Upon further consideration of Figure 4-3, we determined A_3, the area of the red checkered rectangle region and A_1, the area of the two regions defined by the green diagonal lines. A_3 = 64.6 cm^2, while A_1 = A_2-A_3 = 48 cm^2. The value of A_1 defines the cross-sectional area of a breast that is compressed such that the truncation points of the compression paddle touch the truncation points of the breast support, assuming that there is visible contact between breast tissue at the chest wall and each point defining the edge of the optimized breast immobilization device.

Recalling equation (6), the area of an ellipse characterized by our 1100 mL gelatin breast phantom was determined as follows:

$$A_4 = \pi * a * b = \pi * 8.6 * 4.4 = 118.9\ cm^2 \qquad (6)$$

Clearly, the value of A_1 is significantly less than the value of A_4 (48 cm^2 < 118.9 cm^2). Though the separation distance between the truncation points of the curved compression paddle and those of the breast support is dictated by both the volume and elasticity of the breast tissue, these area comparison results verify that we cannot expect to contain all of the tissue associated with a large breast within the constraints of the current optimized breast immobilization device.

These insights substantiate the need to propose a wider version of the original design, with the understanding that the recommended alternative *must* have an area (defined by the green diagonal line region) greater than or equal to A_4, while still maintaining the same semi-major to semi-minor axis ratio (a/b) as the prototype. The a/b ratio associated with the prototype is equal to 1.95. We decided to use the width of the current flat paddle (9.5 inches) as the starting point for determining the new truncated width of the adapted design, as it successfully immobilized even the largest breasts that were observed during the pilot DMT study. If the total truncated width (w_{scaled}) of the suggested alternative were to equal 9.5 inches (24.13 cm), instead of 5.9 inches, then $w_{scaled}/2$ would equal 4.75 inches or 12.065 cm. Prior to calculating the semi-major and semi-minor axes that correspond to w_{scaled}=9.5 inches=24.13 cm, the ratio of $w/2$ (the half-width of the original prototype) to the semi-major axis of the original design had to be computed. This ratio is equal to 0.87. The semi-major axis of the scaled design is then determined by dividing $w_{scaled}/2$ by 0.87. The new semi-major axis (a_{scaled}) is equal to 5.45 inches or 13.85 cm. The new semi-minor axis (b_{scaled}) can then be determined by dividing a_{scaled} by 1.95. The new semi-minor axis (b_{scaled}) is equal to 2.79 inches or 7.08 cm.

The area associated with the truncated alternative design, $A_{2\text{scaled}}$, is then calculated as previously shown using equation (22). $A_{2\text{scaled}}$=291.46 cm^2. In keeping with Figure 4-3, $A_{3\text{scaled}}$, the new area of the red-checkered region, equals 167.36 cm^2. Finally, $A_{1\text{scaled}}$, the new area defined by the green diagonal lines, is equal to 124.09 cm^2. Clearly, the value of $A_{1\text{scaled}}$ is slightly greater than A_4, the area of an ellipse defined by the 1100 mL gelatin breast phantom. In addition, $a_{\text{scaled}}/b_{\text{scaled}} = a/b$=1.95. Having met the suggested criterion, it appears that the scaled version of the prototype should successfully enclose all of the tissue when the cross-sectional area of the compressed breast is equal to that of the 1100 mL gelatin breast phantom, even if the truncation points of the scaled device are touching. The overall dimensions of the scaled prototype are 7.75 inches long x 9.50 inches wide x 1.78 inches high. A detailed drawing of the enlarged version of the optimized breast immobilization device is included in Appendix F.

The scaled version of the optimized breast immobilization device is designed to comfortably compress and immobilize rather large breasts; however, the ability to accomplish this task greatly depends on the elasticity of the tissue itself. Breast tissue that is very elastic has a low Young's modulus, while breast tissue that is not very elastic, has a much higher Young's modulus. Should a relatively large breast have a correspondingly low Young's modulus, it may prove difficult to immobilize, as we may experience a "zero force scenario" where the truncation points of the scaled device are touching without forcefully compressing or immobilizing the breast tissue. This scenario, in conjunction with the need to immobilize a wide range of breast sizes, motivated us to design yet another prototype with a total truncated width larger than that of the original design, yet smaller than that of the scaled alternative. The width of the mid-size design was chosen to be 7.50 inches or 19.05 cm. The aforementioned scaling ratios were again used to determine the semi-major and semi-minor axes of the mid-size design. The corresponding semi-major axis, a_{mid}, is equal to 4.30 inches or 10.93 cm, while the corresponding semi-minor axis, b_{mid}, is equal to 2.20 inches or 5.59 cm. The overall dimensions of the mid-size device are 7.75 inches long x 7.50 inches wide x 1.50 inches high. A detailed drawing is included in Appendix F.

4.4 Support System Alternative Design

A multitude of structural support system design alternatives were discussed as the project progressed. One alternative given serious consideration was an adaptation of the current support structure design, illustrated in Figure 2-11. The support system limitations outlined in section 4.2 emphasize the importance of maintaining a uniform, unobstructed background image, especially with respect to the location of the breast within a given projection view. As a result, our first inclination was to modify the current structure by cutting off the carbon-fiber side pieces such that they extend approximately one third of the way down the stabilizing lips of the immobilization device from the anterior end. This alteration would improve upon the current design and ensure that the carbon-fiber component parts would

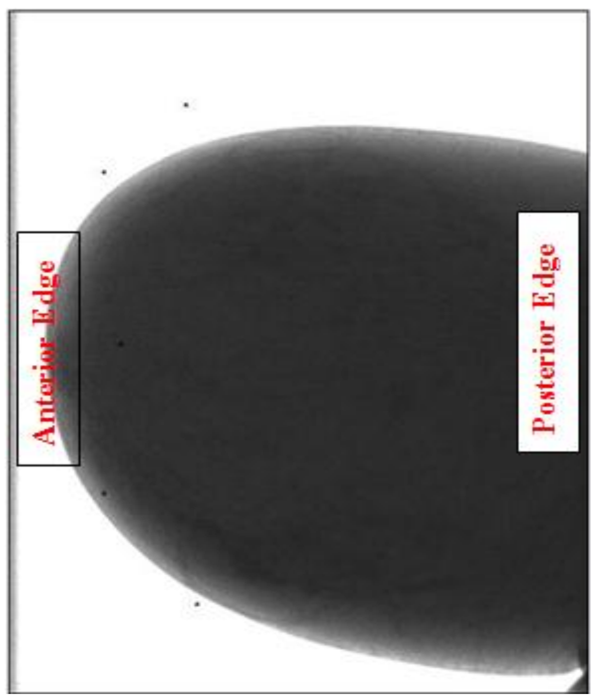

Figure 4-4: Example acquired image of a large breast

only appear at the anterior edge of the resulting image. On average, the breasts imaged thus far as part of the pilot DMT study occupied 55% of the total length of the image in the posterior to anterior direction. Figure 4-4 illustrates that a select few extended almost the entire length of the image in the posterior to anterior direction. As a result, this design alternative was ultimately abandoned in favor of a much cleaner approach.

Of the approaches considered, the design presented in Figure 4-5 was favored for two distinct reasons. First, all of the component parts are positioned outside of the field of view. Thus, any small lesions or micro-calcifications that may be present will not be obscured by the side supports. Second, the design is easily integrated into the lead screw crank system structure that was previously developed to assimilate the original prototype. The grey component part shown in Figure 4-5 is made of aluminum, while the green component part is made of

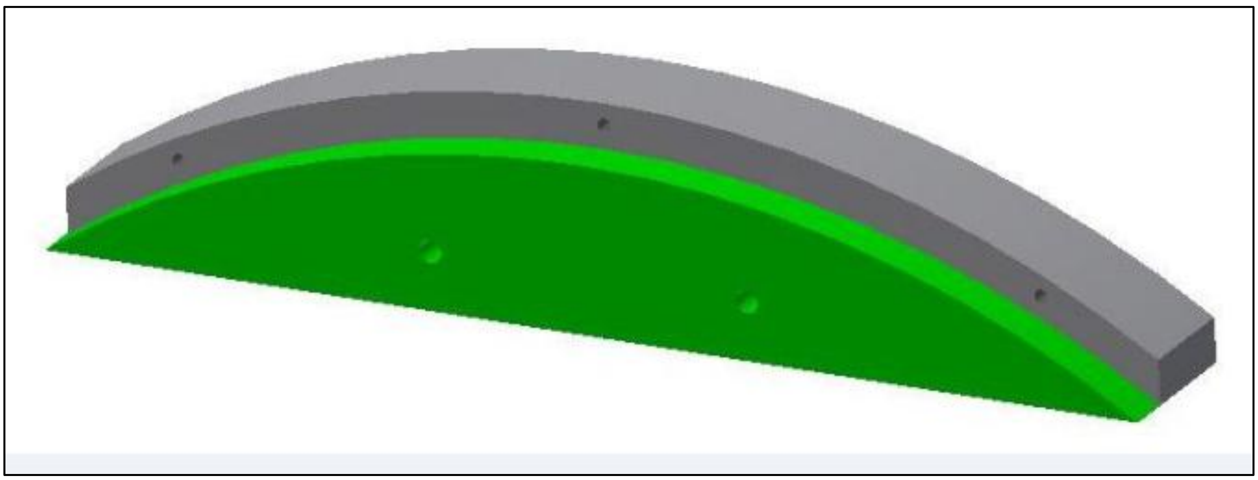

Figure 4-5: Redesigned support system structure

polycarbonate. The aluminum piece is ultimately affixed to the linear bearings that translate the immobilization device up and down in the z-direction. The polycarbonate piece is epoxied along the arc to the underside of the breast immobilization device and subsequently screwed into its aluminum counterpart. For added security, the breast immobilization device is also fastened to the aluminum piece with nylon screws as was shown in Figure 2-11. Three support system structures will be tailor-made for each of the aforementioned prototype designs to ensure both efficiency and functionality. Detailed drawings for the mid-size support structure, as well as the large support structure, are included in Appendix F.

CHAPTER 5

DMT SCANNER OPTIMIZATION

Though the curved nature of the optimized breast immobilization device permits wide angle acquisition, a number of hardware assembly restrictions, specific to the DMT scanner, hinder our ability to obtain projection views at wide angles. These limitations must be overcome to realistically attain the image quality improvements experimentally determined in Chapter 3. As such, a number of hardware component parts will need to be modified or replaced to accomplish the technical goals set forth at the onset of the project. For example, the aluminum arm shown in Figure 5-1 will need to be modified, as will its counterpart, which is mirrored about the z-axis of the DMT scanner. In addition, the x-ray detector supports shown in Figure 5-2 will need to be completely redesigned and ultimately replaced. These hardware adjustments are discussed in detail in the sections to follow, as are the motivating factors that compelled us to invoke change.

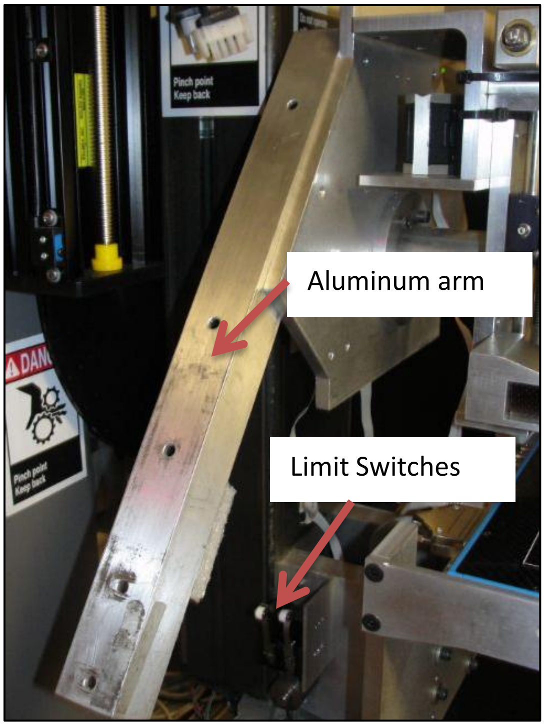

Figure 5-1: Photograph of aluminum arm

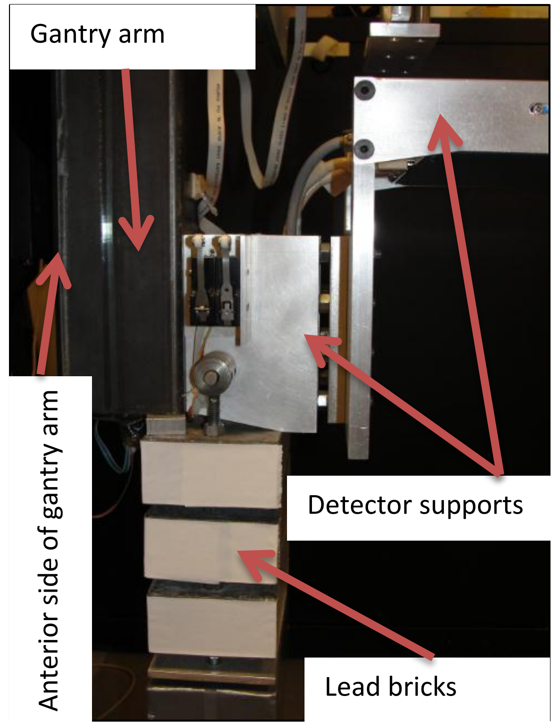

Figure 5-2: Photograph of X-ray detector housing

5.1 Aluminum Arm Deficiencies

The aluminum arm depicted in Figure 5-1 serves two primary purposes. First, it provides a place for the patient to rest her hand during the scan. Prior to positioning the breast, the radiation technologist places the patient's arm (corresponding to the breast of interest) in the "up position," resting her hand towards the top of the aluminum piece. Doing so permits easy access to the pectoral muscle and ensures that it will remain securely in place once compressed. Second, the aluminum arm serves as an attachment point for the aluminum stomach guard that shields the patient's stomach from moving parts (such as the x-ray detector) when the machine is in motion. Unfortunately, when the optimized breast immobilization device is integrated into the DMT scanner, these aluminum piece parts only allow the gantry arm to rotate +/- 36° away from the direction of compression. Should the rotation angle exceed +/-36°, the aluminum arms will collide with the limit switches attached to the x-ray detector housing, which serve as a safety mechanism to prevent over-rotation. The angle range dictated by the aluminum arms is significantly larger than the angle range used during the pilot DMT study. However, it proves undesirable when considering the angle range (+/-67.5°) employed experimentally.

5.2 Aluminum Arm Modifications

In order to permit wide angle acquisition, the aluminum arms will need to be cut off 10.125 inches from the top, so that as the DMT scanner rotates, the lowest point of the aluminum arm clears the horizontal plane tangent to the top of the x-ray detector housing. From a functional standpoint, this retrofit still provides the patient with a resting place for her hand; however, it eliminates the aluminum arm's ability to serve as an attachment point for the stomach guard. Consequently, the stomach guard will need to be modified accordingly. In addition, the limit switches will need to be moved to an appropriate location once an acquisition angle range has been solidified. These systematic modifications, though critical to the success of the optimized breast immobilization device, will ultimately be implemented as "future work" in keeping with the concluding remarks of Chapter 6.

5.3 X-ray Detector Support Deficiencies

The x-ray detector support, shown in Figure 5-2, attaches the x-ray detector to the DMT gantry arm. When the optimized breast immobilization device is used to compress the breast and the aluminum arms are retrofitted as previously suggested, the x-ray detector, in theory, should be free to rotate about the breast. However, because the

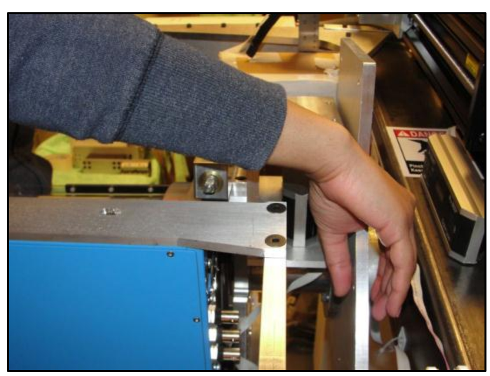

Figure 5-3: Photograph of x-ray detector & patient arm collision

patient's arm is placed in the "up position," as illustrated in Figure 5-3, the x-ray detector will eventually collide with it, preventing both the x-ray and gamma ray detectors from obtaining wide angle projection views at positive angles if the right breast is compressed, and at negative angles if the left breast is compressed. As such, we then had to consider the possibility of acquiring both XBT and MBIT projection images across an asymmetrical angle range. Though we chose to rotate the DMT scanner symmetrically about the AOR during the pilot DMT studies and the gelatin breast phantom experiments, nothing precludes us from considering an asymmetrical angle range as we move forward with the progression of the design and begin to look towards patient accrual.

The maximum attainable XBT acquisition angle (in one direction) will be dictated by the point at which the x-ray detector collides with the patient's arm; while, the maximum attainable XBT acquisition angle (in the opposite direction) will be dictated by the point at which the patient's arm begins to appear in the projection image. The total XBT and MBIT acquisition angle ranges are driven by the ergonomics of the DMT scanner in relation to patient positioning. The total MBIT acquisition angle range will differ from that of x-ray breast tomosynthesis, as the x-ray detector is not needed to acquire gamma ray projection images. Therefore, after the XBT projection views are acquired, the x-ray detector can be moved out of the way to permit wide angle MBIT acquisition.

5.3 X-ray Detector Support Modifications

Two different approaches were explored to accomplish wide angle MBIT acquisition. Initially, we considered removing the x-ray detector from the DMT gantry upon completion of the x-ray portion of the scan. This approach was ultimately abandoned for three reasons. First, it would be difficult to accomplish in a timely manner. Second, it would prove problematic in terms of accessibility, as the patient is standing (or sitting) directly in front of the x-ray detector, thus restricting access to it. Third, it would be very difficult to ensure that the x-ray detector was repositioned in the exact same place with each successive patient.

As a result, we chose to redesign the x-ray detector support such that the entire subassembly, including the x-ray detector itself, can be rotated 90° from its initial position parallel to the floor, to an alternative position, parallel to the DMT gantry arm. Two, low-profile mounted ball bearings, manufactured by Turner Mounted Bearings (model number UCTB-201-8), will serve as the axis-of-rotation for the subassembly. These ball bearings will be mirrored about the DMT gantry arm and mounted to identical aluminum plates on opposite sides of the scanner. They will also be fitted with aluminum cylinders that will be welded to the aluminum side arms of the x-ray detector. Though similar in size to their predecessors, these side arms will extend further in the posterior-to-anterior direction such that they intersect the axis-of-rotation dictated by the position of the ball bearings. The side arms, and by association the x-ray detector, will also be held securely in place by two close-fitting aluminum blocks wedged between the end of their respective anterior edges and the aluminum plates that will be mounted on opposite sides of the scanner. These aluminum blocks will ensure that the x-ray detector is returned to the exact same position with each successive scan. The subassembly has been built per the drawings presented in Appendix G; however, it will be integrated into the DMT scanner as “future work” in conjunction with the retrofits discussed in Section 5.2.

In order to accomplish the x-ray detector support modifications, the lead brick weights that hang from it, as shown in Figure 5-2, will have to be relocated. These lead bricks serve as a counterbalance to the x-ray tube, which weighs 82 pounds. By moving these bricks and attaching them from the anterior side of the gantry arm, we can ensure that they continue to offset the weight of the x-ray tube and clear the plane of the x-ray detector when it parallels the gantry arm, having been hinged down 90°. The subassembly that has been designed to accomplish this task consists of two aluminum piece parts, the smaller of which will attach directly to the anterior side of the gantry arm, the larger of which will anchor the weights. Much like the x-ray detector housing, the subassembly has been built per the drawings in Appendix G; however, it too will be integrated into the DMT scanner as “future work.”

CHAPTER 6

SUMMARY, CONCLUSIONS, AND FUTURE DIRECTION

6.1 Summary

The overall goal of this project was to develop an innovative breast immobilization device that can be integrated into the DMT scanner to improve image quality as well as patient comfort. We hypothesized that MBIT image quality could be improved by reducing the radial distance between the gamma camera and the breast at large viewing angles away from the zero degree view. More specifically, we predicted that the image contrast and signal-to-noise ratio (SNR) would improve as the radial distance was reduced. We also hypothesized that compressing the breast in a more natural configuration would increase the level of patient comfort during a scan.

Preliminary experimental studies showed that the optimized breast immobilization device that we created is capable of improving both image contrast and signal-to-noise ratio (SNR) as compared to standard, flat paddle compression. Notable improvement was realized, independent of lesion depth. The "shallow" lesion contrast improved from 3.6 to 5.0, an increase of 41%, while the "deep" lesion contrast improved from 2.7 to 4.2, an increase of 35%. The "shallow" lesion SNR improved from 16.2 to 24.8, an increase of 53%, while the "deep" lesion SNR improved from 13.1 to 21.3, an increase of 38%.

A prototype was built and integrated into the DMT scanner. The prototype is comprised of an elliptical compression paddle and breast support, both of which are vacuum formed from 0.125 inch thick polycarbonate. The overall dimensions of the device are 7.75 inches long x 5.91 inches wide x 1.26 inches high. Rigidity was added into the design by including a 0.375 inch high lip along the perimeter edge of both component parts. The prototype's ability to securely and comfortably compress a breast was evaluated using a body cast molding kit, which demonstrated that the device was not wide enough to accommodate the medial breast tissue, pinching it into two well-defined segments. Accordingly, we are in the process of fabricating similar immobilization devices with a range of sizes to be evaluated for their ability to comfortably accommodate a broad range of breast sizes, while still providing improved image contrast and SNR.

6.2 Conclusions

In conclusion, the optimized breast immobilization device, when sized appropriately to accommodate all of the breast tissue, allows for wide-angle acquisition, improved image quality and patient comfort. The total angular range employed for both XBT and MBIT will be determined based on DMT scanner system modifications and patient positioning. Actual image quality enhancement will need to be evaluated during future clinical trial case studies, once the angular range (specific to each modality) has been solidified. Moreover, patient comfort will also need to be assessed as we begin to look towards accruing human subjects for impending clinical trial studies.

6.3 Future Direction

Initial evaluation of the optimized breast immobilization device has proven encouraging; however, future assessment is necessary to further quantify improvement both from a technical and non-technical standpoint. As indicated in chapter 5, a number of DMT system modifications will need to be implemented prior to accruing patients, so as to assess the validity of the design using real human breasts. These system modifications include, retrofitting the aluminum arm that attaches to the DMT gantry, relocating the lead brick weights that counter-balance the x-ray tube, integrating the redesigned x-ray detector support mechanism into the DMT gantry, and designing and building a new stomach guard. In addition, the XBT and MBIT acquisition angle ranges will need to be solidified so that the limit switches can be properly moved such that they prevent unsafe over-rotation, but permit wide-angle acquisition. Once these adjustments have been made to the DMT system, we can begin accruing patients and acquiring data to corroborate our preliminary findings and authenticate the use of the optimized breast immobilization device.

APPENDIX A

(Elliptical coordinates of optimized immobilization device)

a= 3.385826772 in

b= 1.732283465 in

Green highlight cells represent truncation points

θ (°)	θ (radians)	r(in)	x (in)	y (in)	x (cm)	y (cm)
1	0.017453293	3.3844	3.383858023	0.059065461	8.594999378	0.150026272
2	0.034906585	3.3800	3.377967547	0.117961226	8.580037569	0.299621514
3	0.052359878	3.3728	3.368202285	0.176520002	8.555233804	0.448360805
4	0.06981317	3.3628	3.354639259	0.234579229	8.520783719	0.595831241
5	0.087266463	3.3501	3.337383808	0.291983249	8.476954871	0.741637452
6	0.104719755	3.3348	3.316567226	0.348585262	8.424080754	0.885406565
7	0.122173048	3.3171	3.292343921	0.404249003	8.362553559	1.026792467
8	0.13962634	3.2970	3.264888183	0.45885011	8.292815985	1.165479281
9	0.157079633	3.2747	3.234390718	0.512277164	8.215352423	1.301183996
10	0.174532925	3.2504	3.20105505	0.564432372	8.130679827	1.433658225
11	0.191986218	3.2243	3.165093932	0.615231937	8.039338587	1.56268912
12	0.20943951	3.1966	3.126725857	0.664606097	7.941883676	1.688099487
13	0.226892803	3.1674	3.086171772	0.712498894	7.838876301	1.809747192
14	0.244346095	3.1368	3.043652065	0.758867691	7.730876244	1.927523934
15	0.261799388	3.1052	2.999383874	0.803682487	7.61843504	2.041353517
16	0.27925268	3.0726	2.95357876	0.846925081	7.502090052	2.151189706
17	0.296705973	3.0392	2.906440749	0.888588111	7.382359503	2.257013802
18	0.314159265	3.0053	2.858164748	0.928674022	7.259738459	2.358832015
19	0.331612558	2.9708	2.808935324	0.967193996	7.134695722	2.45667275
20	0.34906585	2.9360	2.758925817	1.004166876	7.007671576	2.550583865
21	0.366519143	2.9010	2.708297762	1.039618107	6.879076317	2.640629992
22	0.383972435	2.8659	2.657200578	1.073578721	6.749289469	2.726889951
23	0.401425728	2.8308	2.605771495	1.106084376	6.618659598	2.809454316
24	0.41887902	2.7958	2.554135676	1.137174469	6.487504618	2.888423152
25	0.436332313	2.7611	2.502406504	1.166891317	6.356112521	2.963903945
26	0.453785606	2.7266	2.450685992	1.195279423	6.224742421	3.036009734
27	0.471238898	2.6925	2.399065294	1.222384822	6.093625846	3.104857448
28	0.488692191	2.6589	2.347625281	1.248254504	5.962968214	3.17056644
29	0.506145483	2.6256	2.296437174	1.272935912	5.832950422	3.233257216
30	0.523598776	2.5930	2.24556319	1.296476512	5.703730503	3.293050341
31	0.541052068	2.5608	2.19505721	1.318923434	5.575445314	3.350065523
32	0.558505361	2.5293	2.144965436	1.340323162	5.448212208	3.404420831
33	0.575958653	2.4984	2.095327038	1.360721289	5.322130677	3.456232073
34	0.593411946	2.4681	2.046174779	1.380162315	5.197283939	3.505612281

35	0.610865238	2.4385	1.997535611	1.398689492	5.073740451	3.552671311
36	0.628318531	2.4096	1.949431237	1.416344699	4.951555343	3.597515537
37	0.645771823	2.3814	1.901878648	1.433168358	4.830771765	3.640247629
38	0.663225116	2.3539	1.854890606	1.449199369	4.711422139	3.680966398
39	0.680678408	2.3271	1.808476113	1.46447508	4.593529326	3.719766704
40	0.698131701	2.3010	1.762640823	1.479031264	4.477107689	3.756739411
41	0.715584993	2.2756	1.717387434	1.49290212	4.362164082	3.791971385
42	0.733038286	2.2509	1.672716039	1.506120286	4.248698738	3.825545527
43	0.750491578	2.2269	1.628624444	1.518716864	4.136706089	3.857540834
44	0.767944871	2.2036	1.585108463	1.530721449	4.026175495	3.888032481
45	0.785398163	2.1809	1.542162172	1.542162172	3.917091917	3.917091917
46	0.802851456	2.1590	1.499778152	1.55306574	3.809436506	3.944786981
47	0.820304748	2.1378	1.457947695	1.563457489	3.703187145	3.971182021
48	0.837758041	2.1172	1.416660992	1.573361427	3.59831892	3.996338025
49	0.855211333	2.0972	1.375907305	1.582800295	3.494804555	4.02031275
50	0.872664626	2.0779	1.335675112	1.591795613	3.392614784	4.043160857
51	0.890117919	2.0593	1.29595224	1.600367736	3.291718689	4.064934049
52	0.907571211	2.0413	1.256725982	1.608535905	3.192083995	4.085681198
53	0.925024504	2.0238	1.217983202	1.616318301	3.093677333	4.105448484
54	0.942477796	2.0070	1.17971042	1.623732093	2.996464466	4.124279516
55	0.959931089	1.9908	1.141893894	1.630793489	2.900410492	4.142215463
56	0.977384381	1.9752	1.104519691	1.637517783	2.805480016	4.159295169
57	0.994837674	1.9601	1.067573741	1.6439194	2.711637303	4.175555277
58	1.012290966	1.9457	1.031041892	1.650011941	2.618846407	4.191030331
59	1.029744259	1.9317	0.994909955	1.655808225	2.527071285	4.20575289
60	1.047197551	1.9183	0.959163737	1.661320326	2.436275893	4.219753627
61	1.064650844	1.9055	0.92378908	1.666559616	2.346424263	4.233061425
62	1.082104136	1.8931	0.888771881	1.671536799	2.257480579	4.24570347
63	1.099557429	1.8813	0.85409812	1.676261943	2.169409225	4.257705336
64	1.117010721	1.8700	0.819753873	1.680744516	2.082174838	4.26909107
65	1.134464014	1.8592	0.785725332	1.684993412	1.995742344	4.279883268
66	1.151917306	1.8489	0.751998812	1.689016986	1.910076983	4.290103146
67	1.169370599	1.8390	0.718560764	1.692823075	1.82514434	4.299770611
68	1.186823891	1.8296	0.685397777	1.696419027	1.740910353	4.308904327
69	1.204277184	1.8207	0.652496586	1.699811721	1.657341328	4.31752177
70	1.221730476	1.8123	0.619844073	1.703007594	1.574403945	4.325639289
71	1.239183769	1.8043	0.587427267	1.70601266	1.492065259	4.333272156
72	1.256637061	1.7968	0.555233345	1.708832527	1.410292697	4.340434617
73	1.274090354	1.7897	0.523249628	1.711472417	1.329054056	4.347139938
74	1.291543646	1.7830	0.491463579	1.713937183	1.24831749	4.353400446
75	1.308996939	1.7768	0.459862798	1.716231326	1.168051506	4.359227567

76	1.326450232	1.7710	0.428435018	1.718359003	1.088224947	4.364631868
77	1.343903524	1.7656	0.397168101	1.720324049	1.008806977	4.369623084
78	1.361356817	1.7606	0.366050028	1.722129982	0.92976707	4.374210155
79	1.378810109	1.7560	0.335068893	1.723780019	0.851074988	4.378401247
80	1.396263402	1.7519	0.304212899	1.725277081	0.772700762	4.382203786
81	1.413716694	1.7481	0.273470346	1.726623809	0.694614678	4.385624475
82	1.431169987	1.7448	0.242829626	1.727822566	0.616787249	4.388669317
83	1.448623279	1.7419	0.212279213	1.728875447	0.5391892	4.391343635
84	1.466076572	1.7393	0.181807655	1.729784286	0.461791443	4.393652087
85	1.483529864	1.7372	0.151403565	1.730550662	0.384565054	4.395598683
86	1.500983157	1.7354	0.121055612	1.731175902	0.307481254	4.397186791
87	1.518436449	1.7340	0.090752512	1.731661086	0.23051138	4.398419158
88	1.535889742	1.7331	0.060483019	1.73200705	0.153626868	4.399297907
89	1.553343034	1.7325	0.030235915	1.732214391	0.076799223	4.399824552
90	1.570796327	1.7323	1.06115E-16	1.732283465	2.69533E-16	4.4
91	1.588249619	1.7325	-0.030235915	1.732214391	-0.076799223	4.399824552
92	1.605702912	1.7331	-0.060483019	1.73200705	-0.153626868	4.399297907
93	1.623156204	1.7340	-0.090752512	1.731661086	-0.23051138	4.398419158
94	1.640609497	1.7354	-0.121055612	1.731175902	-0.307481254	4.397186791
95	1.658062789	1.7372	-0.151403565	1.730550662	-0.384565054	4.395598683
96	1.675516082	1.7393	-0.181807655	1.729784286	-0.461791443	4.393652087
97	1.692969374	1.7419	-0.212279213	1.728875447	-0.5391892	4.391343635
98	1.710422667	1.7448	-0.242829626	1.727822566	-0.616787249	4.388669317
99	1.727875959	1.7481	-0.273470346	1.726623809	-0.694614678	4.385624475
100	1.745329252	1.7519	-0.304212899	1.725277081	-0.772700762	4.382203786
101	1.762782545	1.7560	-0.335068893	1.723780019	-0.851074988	4.378401247
102	1.780235837	1.7606	-0.366050028	1.722129982	-0.92976707	4.374210155
103	1.79768913	1.7656	-0.397168101	1.720324049	-1.008806977	4.369623084
104	1.815142422	1.7710	-0.428435018	1.718359003	-1.088224947	4.364631868
105	1.832595715	1.7768	-0.459862798	1.716231326	-1.168051506	4.359227567
106	1.850049007	1.7830	-0.491463579	1.713937183	-1.24831749	4.353400446
107	1.8675023	1.7897	-0.523249628	1.711472417	-1.329054056	4.347139938
108	1.884955592	1.7968	-0.555233345	1.708832527	-1.410292697	4.340434617
109	1.902408885	1.8043	-0.587427267	1.70601266	-1.492065259	4.333272156
110	1.919862177	1.8123	-0.619844073	1.703007594	-1.574403945	4.325639289
111	1.93731547	1.8207	-0.652496586	1.699811721	-1.657341328	4.31752177
112	1.954768762	1.8296	-0.685397777	1.696419027	-1.740910353	4.308904327
113	1.972222055	1.8390	-0.718560764	1.692823075	-1.82514434	4.299770611
114	1.989675347	1.8489	-0.751998812	1.689016986	-1.910076983	4.290103146
115	2.00712864	1.8592	-0.785725332	1.684993412	-1.995742344	4.279883268
116	2.024581932	1.8700	-0.819753873	1.680744516	-2.082174838	4.26909107

117	2.042035225	1.8813	-0.85409812	1.676261943	-2.169409225	4.257705336
118	2.059488517	1.8931	-0.888771881	1.671536799	-2.257480579	4.24570347
119	2.07694181	1.9055	-0.92378908	1.666559616	-2.346424263	4.233061425
120	2.094395102	1.9183	-0.959163737	1.661320326	-2.436275893	4.219753627
121	2.111848395	1.9317	-0.994909955	1.655808225	-2.527071285	4.20575289
122	2.129301687	1.9457	-1.031041892	1.650011941	-2.618846407	4.191030331
123	2.14675498	1.9601	-1.067573741	1.6439194	-2.711637303	4.175555277
124	2.164208272	1.9752	-1.104519691	1.637517783	-2.805480016	4.159295169
125	2.181661565	1.9908	-1.141893894	1.630793489	-2.900410492	4.142215463
126	2.199114858	2.0070	-1.17971042	1.623732093	-2.996464466	4.124279516
127	2.21656815	2.0238	-1.217983202	1.616318301	-3.093677333	4.105448484
128	2.234021443	2.0413	-1.256725982	1.608535905	-3.192083995	4.085681198
129	2.251474735	2.0593	-1.29595224	1.600367736	-3.291718689	4.064934049
130	2.268928028	2.0779	-1.335675112	1.591795613	-3.392614784	4.043160857
131	2.28638132	2.0972	-1.375907305	1.582800295	-3.494804555	4.02031275
132	2.303834613	2.1172	-1.416660992	1.573361427	-3.59831892	3.996338025
133	2.321287905	2.1378	-1.457947695	1.563457489	-3.703187145	3.971182021
134	2.338741198	2.1590	-1.499778152	1.55306574	-3.809436506	3.944786981
135	2.35619449	2.1809	-1.542162172	1.542162172	-3.917091917	3.917091917
136	2.373647783	2.2036	-1.585108463	1.530721449	-4.026175495	3.888032481
137	2.391101075	2.2269	-1.628624444	1.518716864	-4.136706089	3.857540834
138	2.408554368	2.2509	-1.672716039	1.506120286	-4.248698738	3.825545527
139	2.42600766	2.2756	-1.717387434	1.49290212	-4.362164082	3.791971385
140	2.443460953	2.3010	-1.762640823	1.479031264	-4.477107689	3.756739411
141	2.460914245	2.3271	-1.808476113	1.46447508	-4.593529326	3.719766704
142	2.478367538	2.3539	-1.854890606	1.449199369	-4.711422139	3.680966398
143	2.49582083	2.3814	-1.901878648	1.433168358	-4.830771765	3.640247629
144	2.513274123	2.4096	-1.949431237	1.416344699	-4.951555343	3.597515537
145	2.530727415	2.4385	-1.997535611	1.398689492	-5.073740451	3.552671311
146	2.548180708	2.4681	-2.046174779	1.380162315	-5.197283939	3.505612281
147	2.565634	2.4984	-2.095327038	1.360721289	-5.322130677	3.456232073
148	2.583087293	2.5293	-2.144965436	1.340323162	-5.448212208	3.404420831
149	2.600540585	2.5608	-2.19505721	1.318923434	-5.575445314	3.350065523
150	2.617993878	2.5930	-2.24556319	1.296476512	-5.703730503	3.293050341
151	2.635447171	2.6256	-2.296437174	1.272935912	-5.832950422	3.233257216
152	2.652900463	2.6589	-2.347625281	1.248254504	-5.962968214	3.17056644
153	2.670353756	2.6925	-2.399065294	1.222384822	-6.093625846	3.104857448
154	2.687807048	2.7266	-2.450685992	1.195279423	-6.224742421	3.036009734
155	2.705260341	2.7611	-2.502406504	1.166891317	-6.356112521	2.963903945
156	2.722713633	2.7958	-2.554135676	1.137174469	-6.487504618	2.888423152
157	2.740166926	2.8308	-2.605771495	1.106084376	-6.618659598	2.809454316

158	2.757620218	2.8659	-2.657200578	1.073578721	-6.749289469	2.726889951
159	2.775073511	2.9010	-2.708297762	1.039618107	-6.879076317	2.640629992
160	2.792526803	2.9360	-2.758925817	1.004166876	-7.007671576	2.550583865
161	2.809980096	2.9708	-2.808935324	0.967193996	-7.134695722	2.45667275
162	2.827433388	3.0053	-2.858164748	0.928674022	-7.259738459	2.358832015
163	2.844886681	3.0392	-2.906440749	0.888588111	-7.382359503	2.257013802
164	2.862339973	3.0726	-2.95357876	0.846925081	-7.502090052	2.151189706
165	2.879793266	3.1052	-2.999383874	0.803682487	-7.61843504	2.041353517
166	2.897246558	3.1368	-3.043652065	0.758867691	-7.730876244	1.927523934
167	2.914699851	3.1674	-3.086171772	0.712498894	-7.838876301	1.809747192
168	2.932153143	3.1966	-3.126725857	0.664606097	-7.941883676	1.688099487
169	2.949606436	3.2243	-3.165093932	0.615231937	-8.039338587	1.56268912
170	2.967059728	3.2504	-3.20105505	0.564432372	-8.130679827	1.433658225
171	2.984513021	3.2747	-3.234390718	0.512277164	-8.215352423	1.301183996
172	3.001966313	3.2970	-3.264888183	0.45885011	-8.292815985	1.165479281
173	3.019419606	3.3171	-3.292343921	0.404249003	-8.362553559	1.026792467
174	3.036872898	3.3348	-3.316567226	0.348585262	-8.424080754	0.885406565
175	3.054326191	3.3501	-3.337383808	0.291983249	-8.476954871	0.741637452
176	3.071779484	3.3628	-3.354639259	0.234579229	-8.520783719	0.595831241
177	3.089232776	3.3728	-3.368202285	0.176520002	-8.555233804	0.448360805
178	3.106686069	3.3800	-3.377967547	0.117961226	-8.580037569	0.299621514
179	3.124139361	3.3844	-3.383858023	0.059065461	-8.594999378	0.150026272
180	3.141592654	3.3858	-3.385826772	4.14814E-16	-8.6	1.05363E-15
181	3.159045946	3.3844	-3.383858023	-0.059065461	-8.594999378	-0.150026272
182	3.176499239	3.3800	-3.377967547	-0.117961226	-8.580037569	-0.299621514
183	3.193952531	3.3728	-3.368202285	-0.176520002	-8.555233804	-0.448360805
184	3.211405824	3.3628	-3.354639259	-0.234579229	-8.520783719	-0.595831241
185	3.228859116	3.3501	-3.337383808	-0.291983249	-8.476954871	-0.741637452
186	3.246312409	3.3348	-3.316567226	-0.348585262	-8.424080754	-0.885406565
187	3.263765701	3.3171	-3.292343921	-0.404249003	-8.362553559	-1.026792467
188	3.281218994	3.2970	-3.264888183	-0.45885011	-8.292815985	-1.165479281
189	3.298672286	3.2747	-3.234390718	-0.512277164	-8.215352423	-1.301183996
190	3.316125579	3.2504	-3.20105505	-0.564432372	-8.130679827	-1.433658225
191	3.333578871	3.2243	-3.165093932	-0.615231937	-8.039338587	-1.56268912
192	3.351032164	3.1966	-3.126725857	-0.664606097	-7.941883676	-1.688099487
193	3.368485456	3.1674	-3.086171772	-0.712498894	-7.838876301	-1.809747192
194	3.385938749	3.1368	-3.043652065	-0.758867691	-7.730876244	-1.927523934
195	3.403392041	3.1052	-2.999383874	-0.803682487	-7.61843504	-2.041353517
196	3.420845334	3.0726	-2.95357876	-0.846925081	-7.502090052	-2.151189706
197	3.438298626	3.0392	-2.906440749	-0.888588111	-7.382359503	-2.257013802
198	3.455751919	3.0053	-2.858164748	-0.928674022	-7.259738459	-2.358832015

199	3.473205211	2.9708	-2.808935324	-0.967193996	-7.134695722	-2.45667275
200	3.490658504	2.9360	-2.758925817	-1.004166876	-7.007671576	-2.550583865
201	3.508111797	2.9010	-2.708297762	-1.039618107	-6.879076317	-2.640629992
202	3.525565089	2.8659	-2.657200578	-1.073578721	-6.749289469	-2.726889951
203	3.543018382	2.8308	-2.605771495	-1.106084376	-6.618659598	-2.809454316
204	3.560471674	2.7958	-2.554135676	-1.137174469	-6.487504618	-2.888423152
205	3.577924967	2.7611	-2.502406504	-1.166891317	-6.356112521	-2.963903945
206	3.595378259	2.7266	-2.450685992	-1.195279423	-6.224742421	-3.036009734
207	3.612831552	2.6925	-2.399065294	-1.222384822	-6.093625846	-3.104857448
208	3.630284844	2.6589	-2.347625281	-1.248254504	-5.962968214	-3.17056644
209	3.647738137	2.6256	-2.296437174	-1.272935912	-5.832950422	-3.233257216
210	3.665191429	2.5930	-2.24556319	-1.296476512	-5.703730503	-3.293050341
211	3.682644722	2.5608	-2.19505721	-1.318923434	-5.575445314	-3.350065523
212	3.700098014	2.5293	-2.144965436	-1.340323162	-5.448212208	-3.404420831
213	3.717551307	2.4984	-2.095327038	-1.360721289	-5.322130677	-3.456232073
214	3.735004599	2.4681	-2.046174779	-1.380162315	-5.197283939	-3.505612281
215	3.752457892	2.4385	-1.997535611	-1.398689492	-5.073740451	-3.552671311
216	3.769911184	2.4096	-1.949431237	-1.416344699	-4.951555343	-3.597515537
217	3.787364477	2.3814	-1.901878648	-1.433168358	-4.830771765	-3.640247629
218	3.804817769	2.3539	-1.854890606	-1.449199369	-4.711422139	-3.680966398
219	3.822271062	2.3271	-1.808476113	-1.46447508	-4.593529326	-3.719766704
220	3.839724354	2.3010	-1.762640823	-1.479031264	-4.477107689	-3.756739411
221	3.857177647	2.2756	-1.717387434	-1.49290212	-4.362164082	-3.791971385
222	3.874630939	2.2509	-1.672716039	-1.506120286	-4.248698738	-3.825545527
223	3.892084232	2.2269	-1.628624444	-1.518716864	-4.136706089	-3.857540834
224	3.909537524	2.2036	-1.585108463	-1.530721449	-4.026175495	-3.888032481
225	3.926990817	2.1809	-1.542162172	-1.542162172	-3.917091917	-3.917091917
226	3.94444411	2.1590	-1.499778152	-1.55306574	-3.809436506	-3.944786981
227	3.961897402	2.1378	-1.457947695	-1.563457489	-3.703187145	-3.971182021
228	3.979350695	2.1172	-1.416660992	-1.573361427	-3.59831892	-3.996338025
229	3.996803987	2.0972	-1.375907305	-1.582800295	-3.494804555	-4.02031275
230	4.01425728	2.0779	-1.335675112	-1.591795613	-3.392614784	-4.043160857
231	4.031710572	2.0593	-1.29595224	-1.600367736	-3.291718689	-4.064934049
232	4.049163865	2.0413	-1.256725982	-1.608535905	-3.192083995	-4.085681198
233	4.066617157	2.0238	-1.217983202	-1.616318301	-3.093677333	-4.105448484
234	4.08407045	2.0070	-1.17971042	-1.623732093	-2.996464466	-4.124279516
235	4.101523742	1.9908	-1.141893894	-1.630793489	-2.900410492	-4.142215463
236	4.118977035	1.9752	-1.104519691	-1.637517783	-2.805480016	-4.159295169
237	4.136430327	1.9601	-1.067573741	-1.6439194	-2.711637303	-4.175555277
238	4.15388362	1.9457	-1.031041892	-1.650011941	-2.618846407	-4.191030331
239	4.171336912	1.9317	-0.994909955	-1.655808225	-2.527071285	-4.20575289

240	4.188790205	1.9183	-0.959163737	-1.661320326	-2.436275893	-4.219753627
241	4.206243497	1.9055	-0.92378908	-1.666559616	-2.346424263	-4.233061425
242	4.22369679	1.8931	-0.888771881	-1.671536799	-2.257480579	-4.24570347
243	4.241150082	1.8813	-0.85409812	-1.676261943	-2.169409225	-4.257705336
244	4.258603375	1.8700	-0.819753873	-1.680744516	-2.082174838	-4.26909107
245	4.276056667	1.8592	-0.785725332	-1.684993412	-1.995742344	-4.279883268
246	4.29350996	1.8489	-0.751998812	-1.689016986	-1.910076983	-4.290103146
247	4.310963252	1.8390	-0.718560764	-1.692823075	-1.82514434	-4.299770611
248	4.328416545	1.8296	-0.685397777	-1.696419027	-1.740910353	-4.308904327
249	4.345869837	1.8207	-0.652496586	-1.699811721	-1.657341328	-4.31752177
250	4.36332313	1.8123	-0.619844073	-1.703007594	-1.574403945	-4.325639289
251	4.380776423	1.8043	-0.587427267	-1.70601266	-1.492065259	-4.333272156
252	4.398229715	1.7968	-0.555233345	-1.708832527	-1.410292697	-4.340434617
253	4.415683008	1.7897	-0.523249628	-1.711472417	-1.329054056	-4.347139938
254	4.4331363	1.7830	-0.491463579	-1.713937183	-1.24831749	-4.353400446
255	4.450589593	1.7768	-0.459862798	-1.716231326	-1.168051506	-4.359227567
256	4.468042885	1.7710	-0.428435018	-1.718359003	-1.088224947	-4.364631868
257	4.485496178	1.7656	-0.397168101	-1.720324049	-1.008806977	-4.369623084
258	4.50294947	1.7606	-0.366050028	-1.722129982	-0.92976707	-4.374210155
259	4.520402763	1.7560	-0.335068893	-1.723780019	-0.851074988	-4.378401247
260	4.537856055	1.7519	-0.304212899	-1.725277081	-0.772700762	-4.382203786
261	4.555309348	1.7481	-0.273470346	-1.726623809	-0.694614678	-4.385624475
262	4.57276264	1.7448	-0.242829626	-1.727822566	-0.616787249	-4.388669317
263	4.590215933	1.7419	-0.212279213	-1.728875447	-0.5391892	-4.391343635
264	4.607669225	1.7393	-0.181807655	-1.729784286	-0.461791443	-4.393652087
265	4.625122518	1.7372	-0.151403565	-1.730550662	-0.384565054	-4.395598683
266	4.64257581	1.7354	-0.121055612	-1.731175902	-0.307481254	-4.397186791
267	4.660029103	1.7340	-0.090752512	-1.731661086	-0.23051138	-4.398419158
268	4.677482395	1.7331	-0.060483019	-1.73200705	-0.153626868	-4.399297907
269	4.694935688	1.7325	-0.030235915	-1.732214391	-0.076799223	-4.399824552
270	4.71238898	1.7323	-3.18346E-16	-1.732283465	-8.08598E-16	-4.4
271	4.729842273	1.7325	0.030235915	-1.732214391	0.076799223	-4.399824552
272	4.747295565	1.7331	0.060483019	-1.73200705	0.153626868	-4.399297907
273	4.764748858	1.7340	0.090752512	-1.731661086	0.23051138	-4.398419158
274	4.78220215	1.7354	0.121055612	-1.731175902	0.307481254	-4.397186791
275	4.799655443	1.7372	0.151403565	-1.730550662	0.384565054	-4.395598683
276	4.817108736	1.7393	0.181807655	-1.729784286	0.461791443	-4.393652087
277	4.834562028	1.7419	0.212279213	-1.728875447	0.5391892	-4.391343635
278	4.852015321	1.7448	0.242829626	-1.727822566	0.616787249	-4.388669317
279	4.869468613	1.7481	0.273470346	-1.726623809	0.694614678	-4.385624475
280	4.886921906	1.7519	0.304212899	-1.725277081	0.772700762	-4.382203786

281	4.904375198	1.7560	0.335068893	-1.723780019	0.851074988	-4.378401247
282	4.921828491	1.7606	0.366050028	-1.722129982	0.92976707	-4.374210155
283	4.939281783	1.7656	0.397168101	-1.720324049	1.008806977	-4.369623084
284	4.956735076	1.7710	0.428435018	-1.718359003	1.088224947	-4.364631868
285	4.974188368	1.7768	0.459862798	-1.716231326	1.168051506	-4.359227567
286	4.991641661	1.7830	0.491463579	-1.713937183	1.24831749	-4.353400446
287	5.009094953	1.7897	0.523249628	-1.711472417	1.329054056	-4.347139938
288	5.026548246	1.7968	0.555233345	-1.708832527	1.410292697	-4.340434617
289	5.044001538	1.8043	0.587427267	-1.70601266	1.492065259	-4.333272156
290	5.061454831	1.8123	0.619844073	-1.703007594	1.574403945	-4.325639289
291	5.078908123	1.8207	0.652496586	-1.699811721	1.657341328	-4.31752177
292	5.096361416	1.8296	0.685397777	-1.696419027	1.740910353	-4.308904327
293	5.113814708	1.8390	0.718560764	-1.692823075	1.82514434	-4.299770611
294	5.131268001	1.8489	0.751998812	-1.689016986	1.910076983	-4.290103146
295	5.148721293	1.8592	0.785725332	-1.684993412	1.995742344	-4.279883268
296	5.166174586	1.8700	0.819753873	-1.680744516	2.082174838	-4.26909107
297	5.183627878	1.8813	0.85409812	-1.676261943	2.169409225	-4.257705336
298	5.201081171	1.8931	0.888771881	-1.671536799	2.257480579	-4.24570347
299	5.218534463	1.9055	0.92378908	-1.666559616	2.346424263	-4.233061425
300	5.235987756	1.9183	0.959163737	-1.661320326	2.436275893	-4.219753627
301	5.253441049	1.9317	0.994909955	-1.655808225	2.527071285	-4.20575289
302	5.270894341	1.9457	1.031041892	-1.650011941	2.618846407	-4.191030331
303	5.288347634	1.9601	1.067573741	-1.6439194	2.711637303	-4.175555277
304	5.305800926	1.9752	1.104519691	-1.637517783	2.805480016	-4.159295169
305	5.323254219	1.9908	1.141893894	-1.630793489	2.900410492	-4.142215463
306	5.340707511	2.0070	1.17971042	-1.623732093	2.996464466	-4.124279516
307	5.358160804	2.0238	1.217983202	-1.616318301	3.093677333	-4.105448484
308	5.375614096	2.0413	1.256725982	-1.608535905	3.192083995	-4.085681198
309	5.393067389	2.0593	1.29595224	-1.600367736	3.291718689	-4.064934049
310	5.410520681	2.0779	1.335675112	-1.591795613	3.392614784	-4.043160857
311	5.427973974	2.0972	1.375907305	-1.582800295	3.494804555	-4.02031275
312	5.445427266	2.1172	1.416660992	-1.573361427	3.59831892	-3.996338025
313	5.462880559	2.1378	1.457947695	-1.563457489	3.703187145	-3.971182021
314	5.480333851	2.1590	1.499778152	-1.55306574	3.809436506	-3.944786981
315	5.497787144	2.1809	1.542162172	-1.542162172	3.917091917	-3.917091917
316	5.515240436	2.2036	1.585108463	-1.530721449	4.026175495	-3.888032481
317	5.532693729	2.2269	1.628624444	-1.518716864	4.136706089	-3.857540834
318	5.550147021	2.2509	1.672716039	-1.506120286	4.248698738	-3.825545527
319	5.567600314	2.2756	1.717387434	-1.49290212	4.362164082	-3.791971385
320	5.585053606	2.3010	1.762640823	-1.479031264	4.477107689	-3.756739411
321	5.602506899	2.3271	1.808476113	-1.46447508	4.593529326	-3.719766704

322	5.619960191	2.3539	1.854890606	-1.449199369	4.711422139	-3.680966398
323	5.637413484	2.3814	1.901878648	-1.433168358	4.830771765	-3.640247629
324	5.654866776	2.4096	1.949431237	-1.416344699	4.951555343	-3.597515537
325	5.672320069	2.4385	1.997535611	-1.398689492	5.073740451	-3.552671311
326	5.689773362	2.4681	2.046174779	-1.380162315	5.197283939	-3.505612281
327	5.707226654	2.4984	2.095327038	-1.360721289	5.322130677	-3.456232073
328	5.724679947	2.5293	2.144965436	-1.340323162	5.448212208	-3.404420831
329	5.742133239	2.5608	2.19505721	-1.318923434	5.575445314	-3.350065523
330	5.759586532	2.5930	2.24556319	-1.296476512	5.703730503	-3.293050341
331	5.777039824	2.6256	2.296437174	-1.272935912	5.832950422	-3.233257216
332	5.794493117	2.6589	2.347625281	-1.248254504	5.962968214	-3.17056644
333	5.811946409	2.6925	2.399065294	-1.222384822	6.093625846	-3.104857448
334	5.829399702	2.7266	2.450685992	-1.195279423	6.224742421	-3.036009734
335	5.846852994	2.7611	2.502406504	-1.166891317	6.356112521	-2.963903945
336	5.864306287	2.7958	2.554135676	-1.137174469	6.487504618	-2.888423152
337	5.881759579	2.8308	2.605771495	-1.106084376	6.618659598	-2.809454316
338	5.899212872	2.8659	2.657200578	-1.073578721	6.749289469	-2.726889951
339	5.916666164	2.9010	2.708297762	-1.039618107	6.879076317	-2.640629992
340	5.934119457	2.9360	2.758925817	-1.004166876	7.007671576	-2.550583865
341	5.951572749	2.9708	2.808935324	-0.967193996	7.134695722	-2.45667275
342	5.969026042	3.0053	2.858164748	-0.928674022	7.259738459	-2.358832015
343	5.986479334	3.0392	2.906440749	-0.888588111	7.382359503	-2.257013802
344	6.003932627	3.0726	2.95357876	-0.846925081	7.502090052	-2.151189706
345	6.021385919	3.1052	2.999383874	-0.803682487	7.61843504	-2.041353517
346	6.038839212	3.1368	3.043652065	-0.758867691	7.730876244	-1.927523934
347	6.056292504	3.1674	3.086171772	-0.712498894	7.838876301	-1.809747192
348	6.073745797	3.1966	3.126725857	-0.664606097	7.941883676	-1.688099487
349	6.091199089	3.2243	3.165093932	-0.615231937	8.039338587	-1.56268912
350	6.108652382	3.2504	3.20105505	-0.564432372	8.130679827	-1.433658225
351	6.126105675	3.2747	3.234390718	-0.512277164	8.215352423	-1.301183996
352	6.143558967	3.2970	3.264888183	-0.45885011	8.292815985	-1.165479281
353	6.16101226	3.3171	3.292343921	-0.404249003	8.362553559	-1.026792467
354	6.178465552	3.3348	3.316567226	-0.348585262	8.424080754	-0.885406565
355	6.195918845	3.3501	3.337383808	-0.291983249	8.476954871	-0.741637452
356	6.213372137	3.3628	3.354639259	-0.234579229	8.520783719	-0.595831241
357	6.23082543	3.3728	3.368202285	-0.176520002	8.555233804	-0.448360805
358	6.248278722	3.3800	3.377967547	-0.117961226	8.580037569	-0.299621514
359	6.265732015	3.3844	3.383858023	-0.059065461	8.594999378	-0.150026272
360	6.283185307	3.3858	3.385826772	-8.29628E-16	8.6	-2.10726E-15

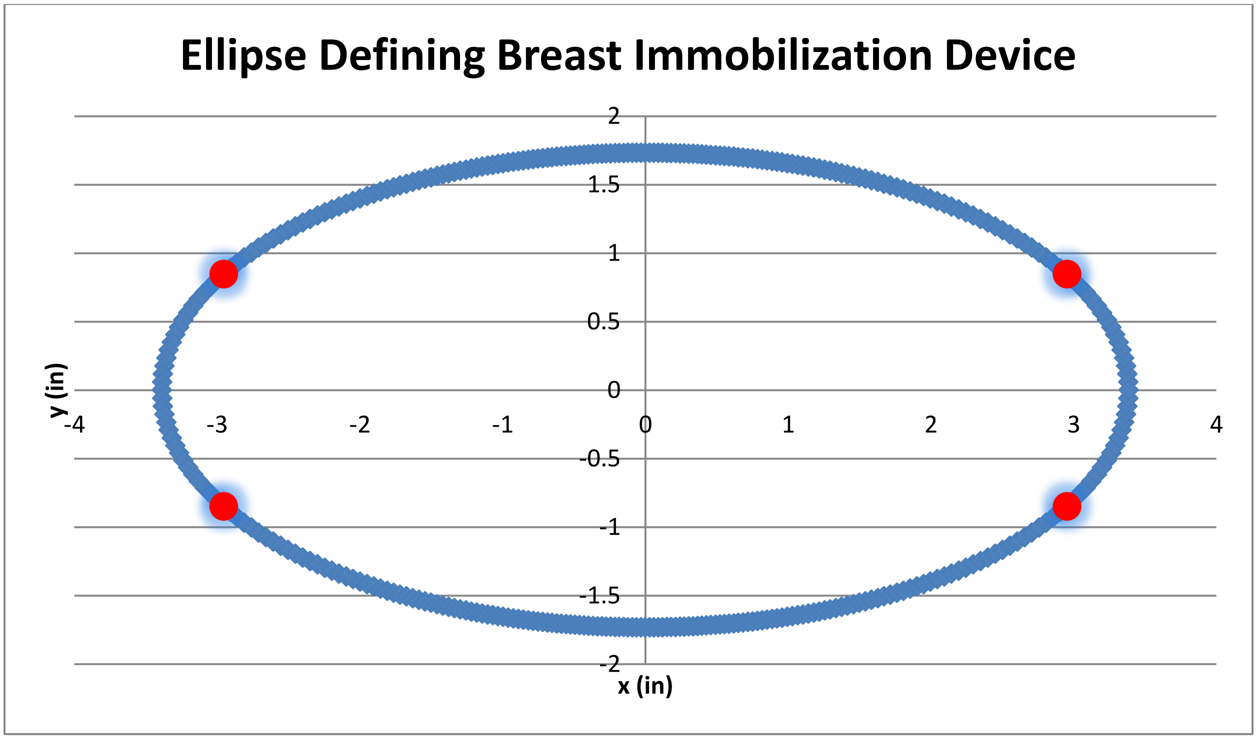

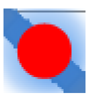 Truncation Point Locations

APPENDIX B

(Optimized immobilization device truncation point calculations)

a (1100 mL breast volume) (cm)	b (1100 mL breast volume) (cm)	b (840 mL breast volume) (cm)	∆ (distance compression paddle moves from original elliptical location) (cm)
8.6	4.4	4.25	0.15

w (cm)	**w/2 (cm)**	**A_2 (cm^2)**
0	0	0
0.25	0.125	2.124922535
0.5	0.25	4.249380217
0.75	0.375	6.372907901
1	0.5	8.495039849
1.25	0.625	10.61530943
1.5	0.75	12.73324884
1.75	0.875	14.84838877
2	1	16.96025809
2.25	1.125	19.0683836
2.5	1.25	21.17228961
2.75	1.375	23.27149769
3	1.5	25.3655263
3.25	1.625	27.45389043
3.5	1.75	29.53610125
3.75	1.875	31.61166575
4	2	33.68008631
4.25	2.125	35.74086032
4.5	2.25	37.79347978
4.75	2.375	39.83743078
5	2.5	41.87219311
5.25	2.625	43.89723972
5.5	2.75	45.9120362
5.75	2.875	47.91604024
6	3	49.90870104
6.25	3.125	51.88945868
6.5	3.25	53.85774346
6.75	3.375	55.81297517
7	3.5	57.75456232
7.25	3.625	59.68190136

7.5	3.75	61.59437573
7.75	3.875	63.49135494
8	4	65.37219351
8.25	4.125	67.23622982
8.5	4.25	69.08278493
8.75	4.375	70.91116115
9	4.5	72.72064063
9.25	4.625	74.51048368
9.5	4.75	76.27992696
9.75	4.875	78.02818155
10	5	79.75443064
10.25	5.125	81.45782711
10.5	5.25	83.13749074
10.75	5.375	84.79250508
11	5.5	86.42191389
11.25	5.625	88.02471714
11.5	5.75	89.59986645
11.75	5.875	91.14625973
12	6	92.66273518
12.25	6.125	94.1480641
12.5	6.25	95.60094266
12.75	6.375	97.01998201
13	6.5	98.40369661
13.25	6.625	99.75049013
13.5	6.75	101.0586383
13.75	6.875	102.326268
14	7	103.5513307
14.25	7.125	104.7315692
14.5	7.25	105.864475
14.75	7.375	106.9472315
15	7.5	107.9766377

APPENDIX C

(Optimized Breast Immobilization Device & Support Drawings)

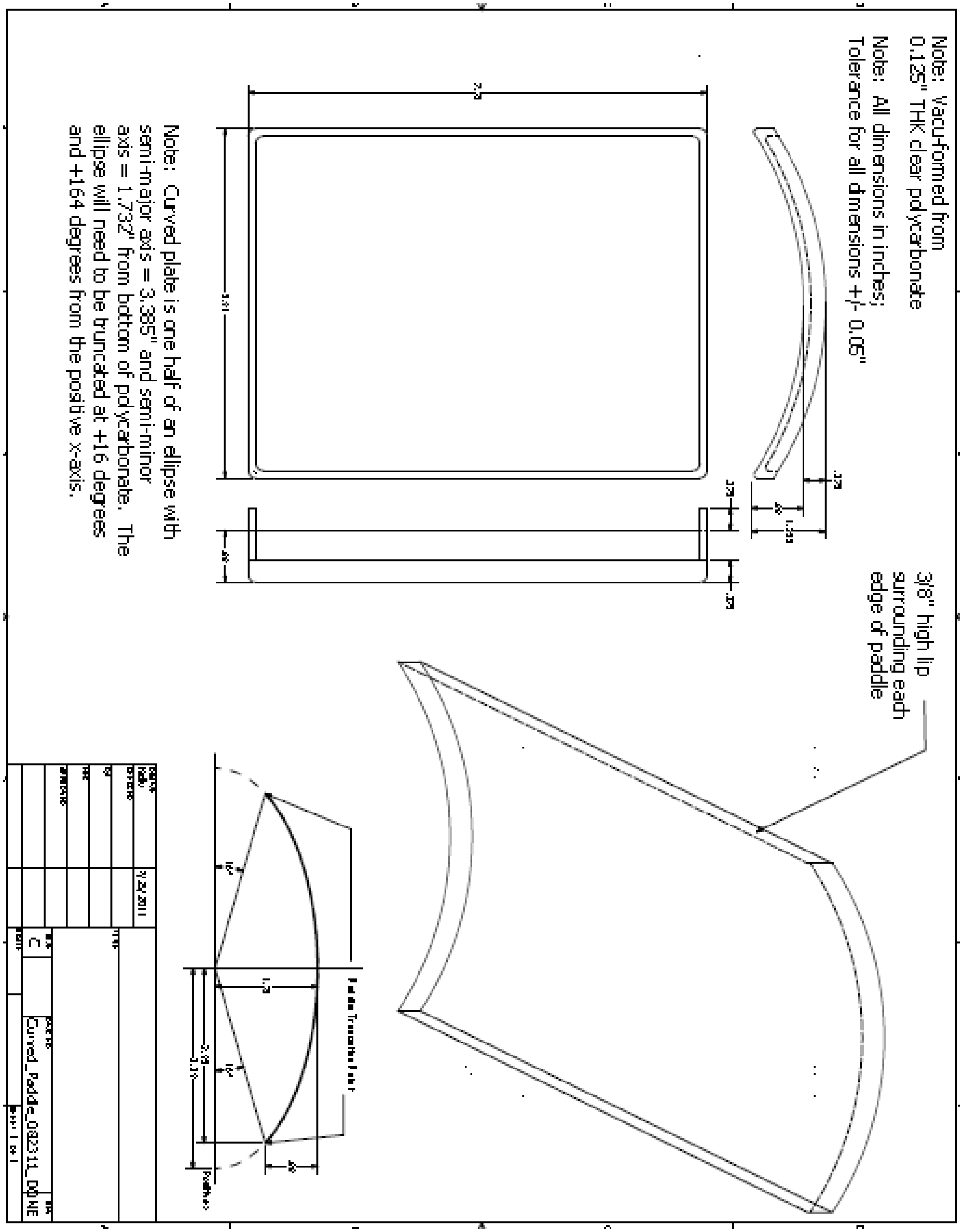

Breast Immobilization Device Support System

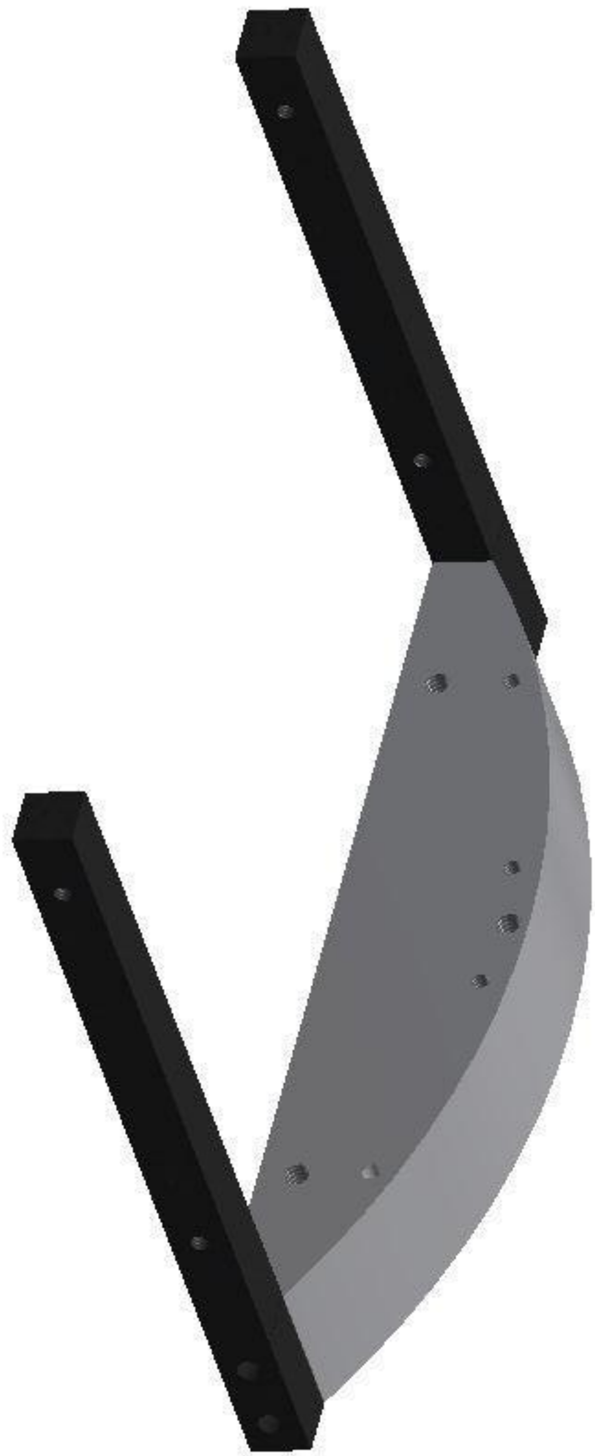

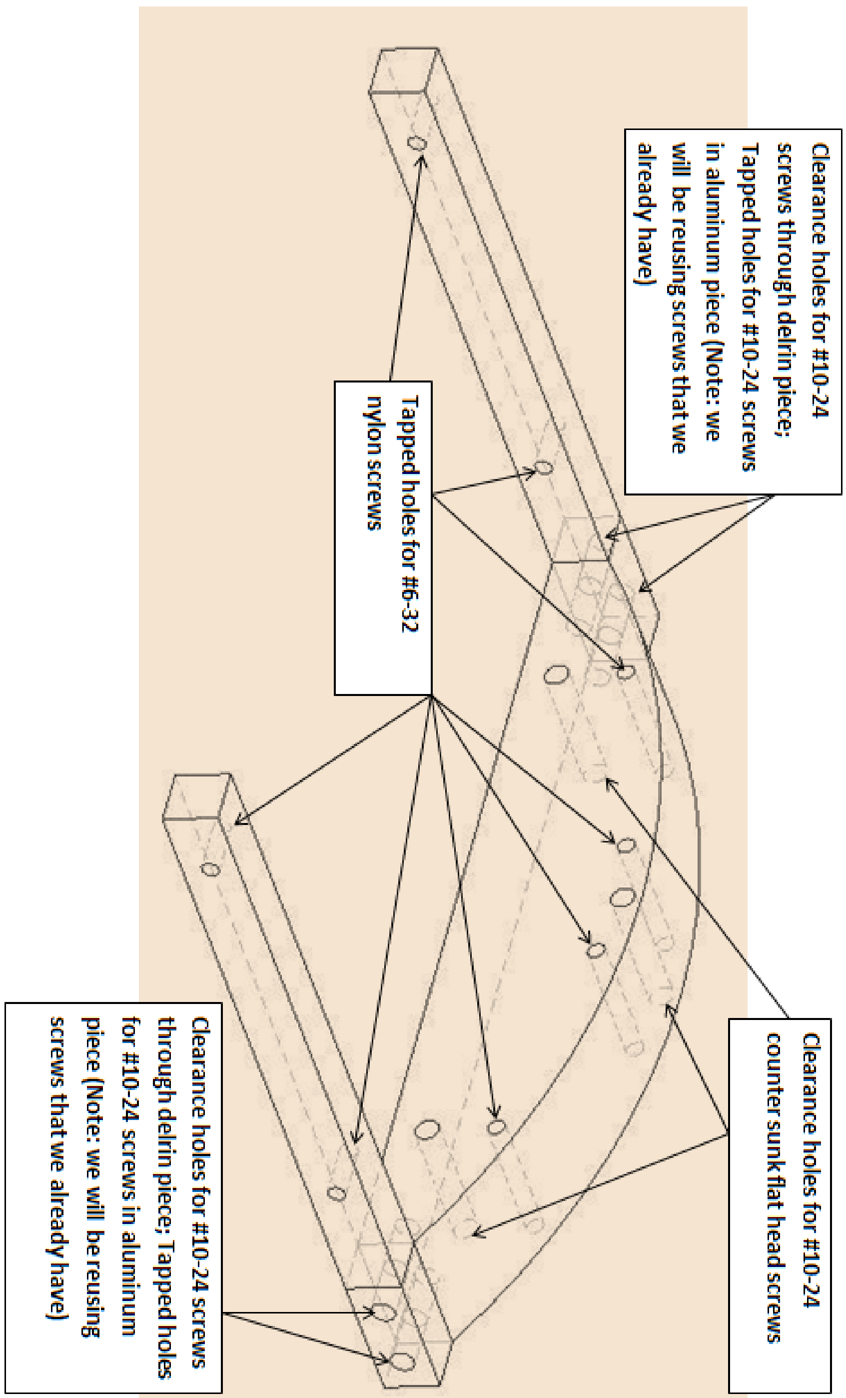
Clearance holes for #10-24 screws through delrin piece; Tapped holes for #10-24 screws in aluminum piece (Note: we will be reusing screws that we already have)
Tapped holes for #6-32 nylon screws
Clearance holes for #10-24 counter sunk flat head screws
Clearance holes for #10-24 screws through delrin piece; Tapped holes for #10-24 screws in aluminum piece (Note: we will be reusing screws that we already have)

FRONT VIEW

Note: All dimensions in inches

Tolerance for all dimensions: +/-0.05”

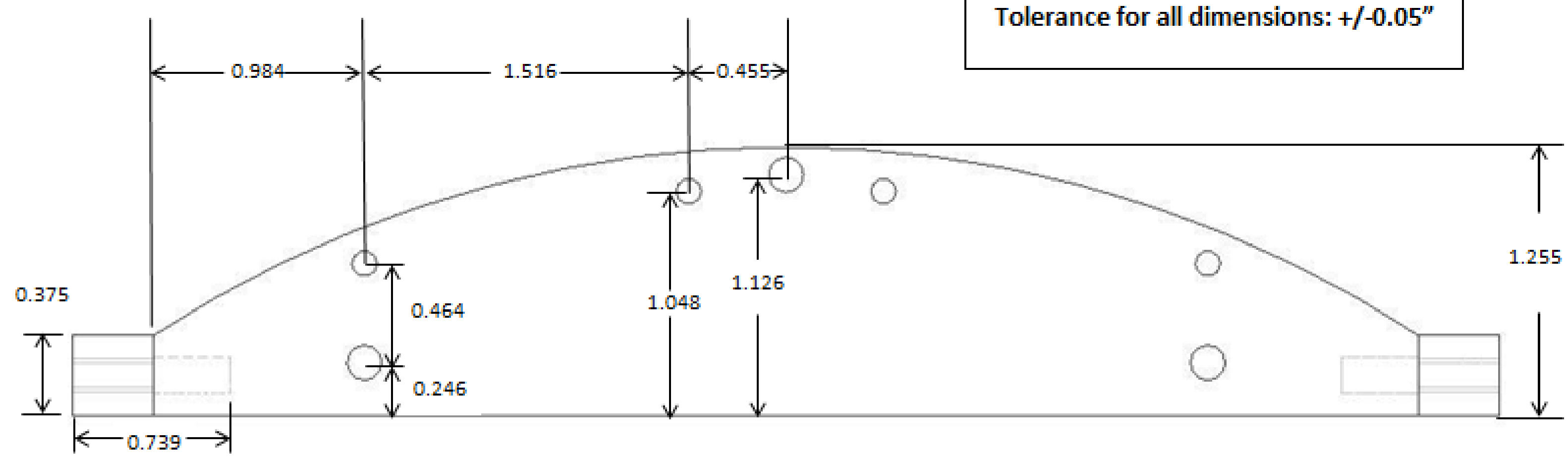

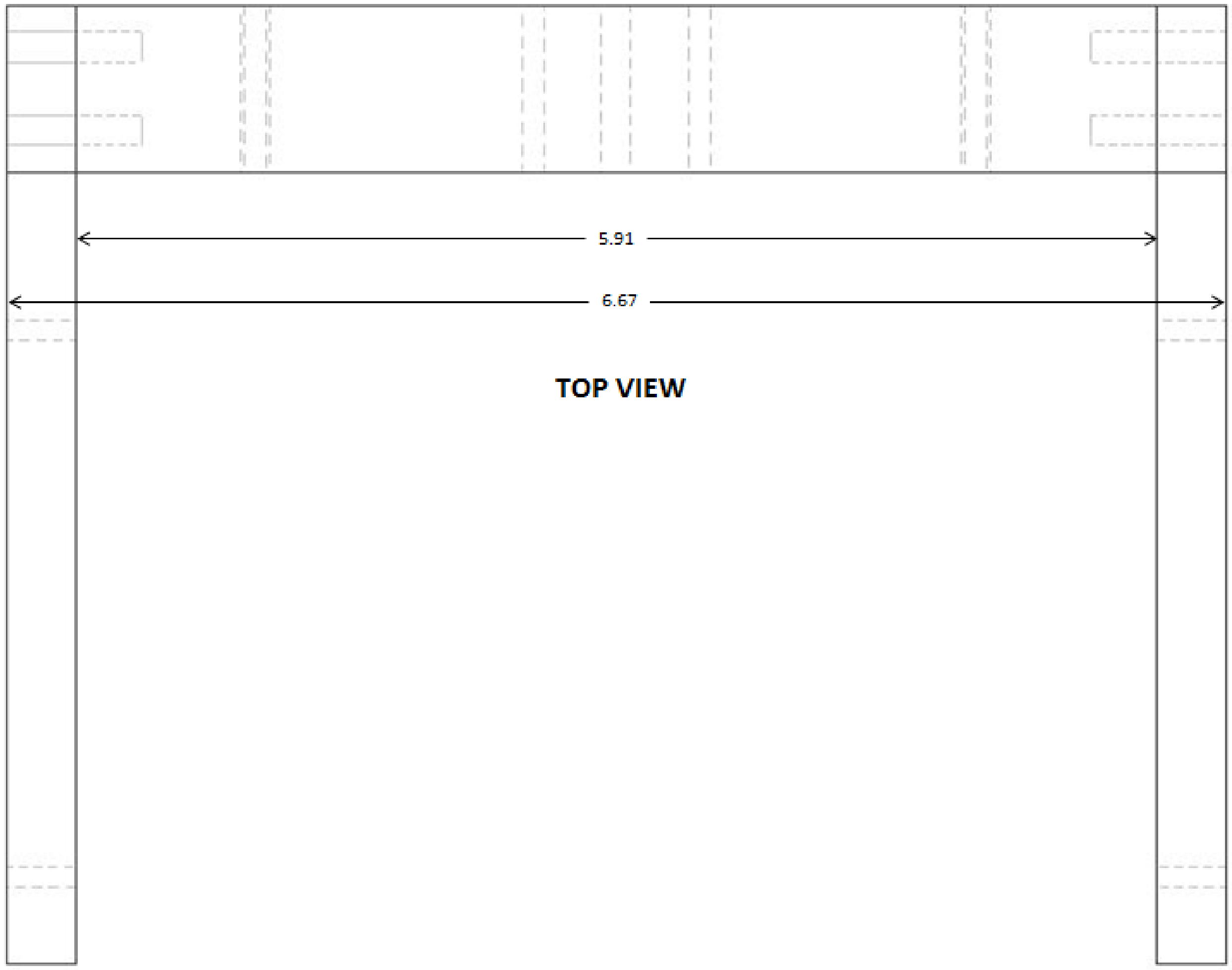

TOP VIEW

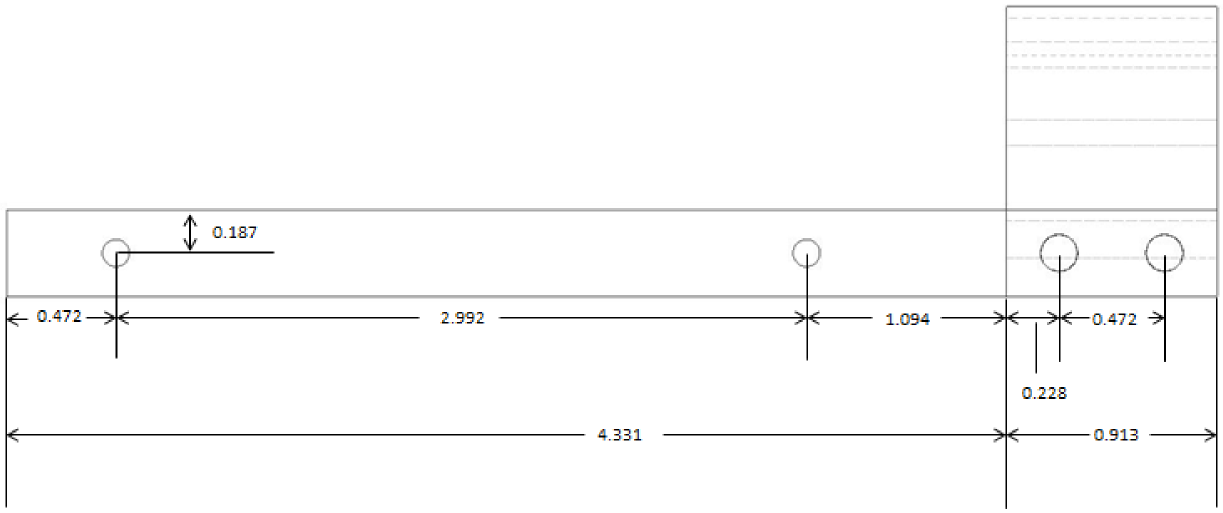

SIDE VIEW

APPENDIX D

(Trajectory Calculations)

"Flat Paddle" Trajectory Calculations

a=	12.065	cm	x1	Used 1/2 the width of the flat compression paddle used during the pilot DMT study
b=	6.23125	cm	y1	Used 1/2 the avg. compressed breast thickness observed during the pilot study & added 1/2 the thickness of the breast support and compression paddle combined.

θ (°)	θ (radians)	m	mo	x2	y2
0	0	0	0	0	6.23125
6	0.104719755	-0.1051	9.514364	0.77959946	7.417393393
12	0.20943951	-0.21256	4.70463	1.78877588	8.415528866
18	0.314159265	-0.32492	3.077684	2.983423408	9.182033108
24	0.41887902	-0.44523	2.246037	4.311330214	9.683406205
30	0.523598776	-0.57735	1.732051	5.714460399	9.897735748
36	0.628318531	-0.72654	1.376382	7.13149044	9.815654508
42	0.733038286	-0.9004	1.110613	8.500489326	9.440749827
48	0.837758041	-1.11061	0.900404	9.761625235	8.78940684
54	0.942477796	-1.37638	0.726543	10.85978048	7.890092361
60	1.047197551	-1.73205	0.57735	11.7469604	6.782110748
66	1.151917306	-2.24604	0.445229	12.38439098	5.513886114
72	1.256637061	-3.07768	0.32492	12.74421345	4.140845961
78	1.361356817	-4.70463	0.212557	12.81070183	2.722998733
84	1.466076572	-9.51436	0.105104	12.58095026	1.322311156
90	1.570796327	-1.6E+16	6.13E-17	12.065	7.39071E-16
96	1.675516082	9.514364	-0.1051	-12.58095026	1.322311156
102	1.780235837	4.70463	-0.21256	-12.81070183	2.722998733
108	1.884955592	3.077684	-0.32492	-12.74421345	4.140845961
114	1.989675347	2.246037	-0.44523	-12.38439098	5.513886114
120	2.094395102	1.732051	-0.57735	-11.7469604	6.782110748
126	2.199114858	1.376382	-0.72654	-10.85978048	7.890092361
132	2.303834613	1.110613	-0.9004	-9.761625235	8.78940684
138	2.408554368	0.900404	-1.11061	-8.500489326	9.440749827

144	2.513274123	0.726543	-1.37638	-7.13149044	9.815654508
150	2.617993878	0.57735	-1.73205	-5.714460399	9.897735748
156	2.722713633	0.445229	-2.24604	-4.311330214	9.683406205
162	2.827433388	0.32492	-3.07768	-2.983423408	9.182033108
168	2.932153143	0.212557	-4.70463	-1.78877588	8.415528866
174	3.036872898	0.105104	-9.51436	-0.77959946	7.417393393
180	3.141592654	1.23E-16	-8.2E+15	-7.63421E-16	6.23125
186	3.246312409	-0.1051	9.514364	-0.77959946	-7.417393393
192	3.351032164	-0.21256	4.70463	-1.78877588	-8.415528866
198	3.455751919	-0.32492	3.077684	-2.983423408	-9.182033108
204	3.560471674	-0.44523	2.246037	-4.311330214	-9.683406205
210	3.665191429	-0.57735	1.732051	-5.714460399	-9.897735748
216	3.769911184	-0.72654	1.376382	-7.13149044	-9.815654508
222	3.874630939	-0.9004	1.110613	-8.500489326	-9.440749827
228	3.979350695	-1.11061	0.900404	-9.761625235	-8.78940684
234	4.08407045	-1.37638	0.726543	-10.85978048	-7.890092361
240	4.188790205	-1.73205	0.57735	-11.7469604	-6.782110748
246	4.29350996	-2.24604	0.445229	-12.38439098	-5.513886114
252	4.398229715	-3.07768	0.32492	-12.74421345	-4.140845961
258	4.50294947	-4.70463	0.212557	-12.81070183	-2.722998733
264	4.607669225	-9.51436	0.105104	-12.58095026	-1.322311156
270	4.71238898	-5.4E+15	1.84E-16	-12.065	-2.21721E-15
276	4.817108736	9.514364	-0.1051	12.58095026	-1.322311156
282	4.921828491	4.70463	-0.21256	12.81070183	-2.722998733
288	5.026548246	3.077684	-0.32492	12.74421345	-4.140845961
294	5.131268001	2.246037	-0.44523	12.38439098	-5.513886114
300	5.235987756	1.732051	-0.57735	11.7469604	-6.782110748
306	5.340707511	1.376382	-0.72654	10.85978048	-7.890092361
312	5.445427266	1.110613	-0.9004	9.761625235	-8.78940684
318	5.550147021	0.900404	-1.11061	8.500489326	-9.440749827
324	5.654866776	0.726543	-1.37638	7.13149044	-9.815654508
330	5.759586532	0.57735	-1.73205	5.714460399	-9.897735748
336	5.864306287	0.445229	-2.24604	4.311330214	-9.683406205
342	5.969026042	0.32492	-3.07768	2.983423408	-9.182033108
348	6.073745797	0.212557	-4.70463	1.78877588	-8.415528866
354	6.178465552	0.105104	-9.51436	0.77959946	-7.417393393
360	6.283185307	2.45E-16	-4.1E+15	1.52684E-15	-6.23125

Optimized Breast Immobilization Device Trajectory Calculations:

a=	9.5525	cm	Used 1/2 the width of the 1100 mL gelatin breast phantom & added 3/8" to account for height of the lip of the optimized breast immobilization device
b=	5.3525	cm	Used 1/2 the thickness of the 1100 mL gelatin breast phantom & added 3/8" to account for height of the lip of the optimized breast immobilization device

θ (°)	Θ (radians)	m	mo	x1	y1	x2	y2
0	0	0	0	0	5.3525	0	5.3525
6	0.104719755	-0.1051	9.514364	-1.76112	5.260749581	-0.56613	5.386348147
12	0.20943951	-0.21256	4.70463	-3.38811	5.00451599	-1.16422	5.477218404
18	0.314159265	-0.32492	3.077684	-4.79191	4.630325188	-1.8184	5.596474257
24	0.41887902	-0.44523	2.246037	-5.9427	4.190635092	-2.54025	5.705501601
29	0.506145483	-0.55431	1.804048	-6.71809	3.805159438	-3.1925	5.759423456
30	0.523598776	-0.57735	1.732051	-6.85496	3.727730789	-3.32789	5.764080992
36	0.628318531	-0.72654	1.376382	-7.56426	3.268772694	-4.16778	5.73645934
42	0.733038286	-0.9004	1.110613	-8.11032	2.828001875	-5.03753	5.594748585
48	0.837758041	-1.11061	0.900404	-8.52855	2.410969295	-5.90889	5.32038993
54	0.942477796	-1.37638	0.726543	-8.84745	2.018172782	-6.75043	4.904473336
60	1.047197551	-1.73205	0.57735	-9.08874	1.647488685	-7.52994	4.347413204
66	1.151917306	-2.24604	0.445229	-9.26844	1.295593683	-8.21652	3.658231036
72	1.256637061	-3.07768	0.32492	-9.39802	0.958719347	-8.78235	2.853557241
78	1.361356817	-4.70463	0.212557	-9.48546	0.63301243	-9.20417	1.956405769
84	1.466076572	-9.51436	0.105104	-9.53598	0.314676773	-9.4645	0.994758812
90	1.570796327	-1.6E+16	6.13E-17	-9.5525	0	-9.5525	5.85162E-16
96	1.675516082	9.514364	-0.1051	-9.53598	-0.31467677	-9.4645	-0.994758812
102	1.780235837	4.70463	-0.21256	-9.48546	-0.63301243	-9.20417	-1.956405769
108	1.884955592	3.077684	-0.32492	-9.39802	-0.95871935	-8.78235	-2.853557241
114	1.989675347	2.246037	-0.44523	-9.26844	-1.29559368	-8.21652	-3.658231036
120	2.094395102	1.732051	-0.57735	-9.08874	-1.64748869	-7.52994	-4.347413204
126	2.199114858	1.376382	-0.72654	-8.84745	-2.01817278	-6.75043	-4.904473336
132	2.303834613	1.110613	-0.9004	-8.52855	-2.4109693	-5.90889	-5.32038993
138	2.408554368	0.900404	-1.11061	-8.11032	-2.82800188	-5.03753	-5.594748585
144	2.513274123	0.726543	-1.37638	-7.56426	-3.26877269	-4.16778	-5.73645934
150	2.617993878	0.57735	-1.73205	-6.85496	-3.72773079	-3.32789	-5.764080992

156	2.722713633	0.445229	-2.24604	-5.9427	-4.19063509	-2.54025	-5.705501601
162	2.827433388	0.32492	-3.07768	-4.79191	-4.63032519	-1.8184	-5.596474257
168	2.932153143	0.212557	-4.70463	-3.38811	-5.00451599	-1.16422	-5.477218404
174	3.036872898	0.105104	-9.51436	-1.76112	-5.26074958	-0.56613	-5.386348147
180	3.141592654	1.23E-16	-8.2E+15	-2.1E-15	-5.3525	-6.6E-16	-5.3525
186	3.246312409	-0.1051	9.514364	1.761119	-5.26074958	0.566128	-5.386348147
192	3.351032164	-0.21256	4.70463	3.388109	-5.00451599	1.164219	-5.477218404
198	3.455751919	-0.32492	3.077684	4.791906	-4.63032519	1.818405	-5.596474257
204	3.560471674	-0.44523	2.246037	5.942699	-4.19063509	2.540253	-5.705501601
211	3.682644722	-0.60086	1.664279	6.986181	-3.65044128	3.464758	-5.766325784
216	3.769911184	-0.72654	1.376382	7.564261	-3.26877269	4.167782	-5.73645934
222	3.874630939	-0.9004	1.110613	8.110318	-2.82800188	5.037534	-5.594748585
228	3.979350695	-1.11061	0.900404	8.528546	-2.4109693	5.908892	-5.32038993
234	4.08407045	-1.37638	0.726543	8.847449	-2.01817278	6.750428	-4.904473336
240	4.188790205	-1.73205	0.57735	9.088743	-1.64748869	7.529941	-4.347413204
246	4.29350996	-2.24604	0.445229	9.268435	-1.29559368	8.216521	-3.658231036
252	4.398229715	-3.07768	0.32492	9.398016	-0.95871935	8.782346	-2.853557241
258	4.50294947	-4.70463	0.212557	9.485461	-0.63301243	9.204165	-1.956405769
264	4.607669225	-9.51436	0.105104	9.535977	-0.31467677	9.464498	-0.994758812
270	4.71238898	-5.4E+15	1.84E-16	9.5525	0	9.5525	-1.75548E-15
276	4.817108736	9.514364	-0.1051	9.535977	0.314676773	9.464498	0.994758812
282	4.921828491	4.70463	-0.21256	9.485461	0.63301243	9.204165	1.956405769
288	5.026548246	3.077684	-0.32492	9.398016	0.958719347	8.782346	2.853557241
294	5.131268001	2.246037	-0.44523	9.268435	1.295593683	8.216521	3.658231036
300	5.235987756	1.732051	-0.57735	9.088743	1.647488685	7.529941	4.347413204
306	5.340707511	1.376382	-0.72654	8.847449	2.018172782	6.750428	4.904473336
312	5.445427266	1.110613	-0.9004	8.528546	2.410969295	5.908892	5.32038993
318	5.550147021	0.900404	-1.11061	8.110318	2.828001875	5.037534	5.594748585
324	5.654866776	0.726543	-1.37638	7.564261	3.268772694	4.167782	5.73645934
330	5.759586532	0.57735	-1.73205	6.854956	3.727730789	3.327894	5.764080992
336	5.864306287	0.445229	-2.24604	5.942699	4.190635092	2.540253	5.705501601
342	5.969026042	0.32492	-3.07768	4.791906	4.630325188	1.818405	5.596474257
348	6.073745797	0.212557	-4.70463	3.388109	5.00451599	1.164219	5.477218404
354	6.178465552	0.105104	-9.51436	1.761119	5.260749581	0.566128	5.386348147
360	6.283185307	2.45E-16	-4.1E+15	4.18E-15	5.3525	1.31E-15	5.3525

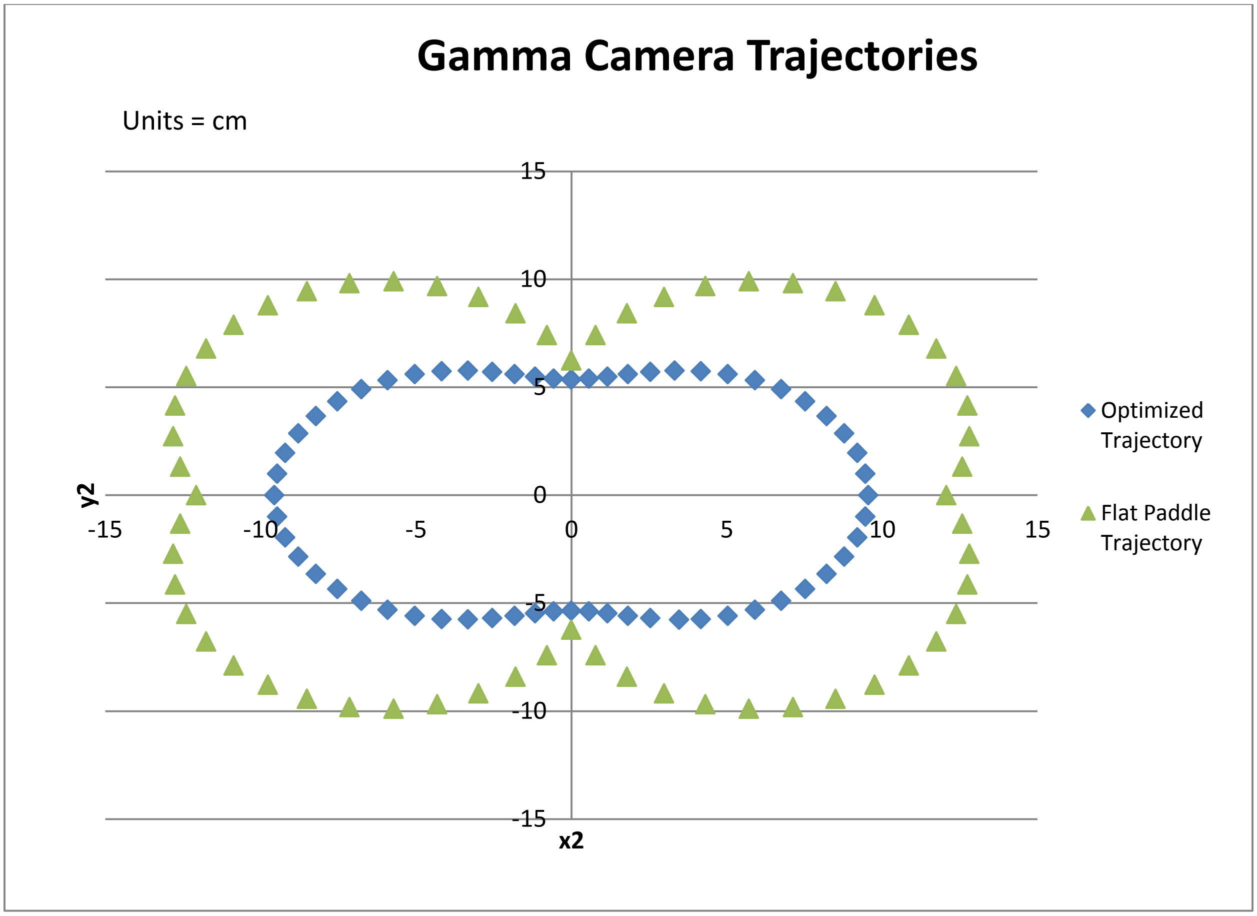
Gamma Camera Trajectories
Units = cm
15
10
5
0
-5
-10
-15
-15
-10
-5
0
5
10
15
y2
x2
Optimized Trajectory
Flat Paddle Trajectory

APPENDIX E

(Image Contrast & SNR Excel Files; Matlab Source code)

Trajectory: Optimized Breast Immobilization Device
800% magnification in Image J
Deep Lesion (5 cm)

Trial #	Lesion ROI Area	Lesion Mean Pixel Value	Lesion STD Pixel Value	BKG ROI Area	BKG Mean Pixel Value	BKG STD Pixel Value	Slice #	x-cord of top left corner of ROI (Lesion)	y-cord of top left corner of ROI (Lesion)	x-cord of top left corner of ROI (Bkg)	y-cord of top left corner of ROI (Bkg)	Contrast	SNR
1	16	54.685	9.821	600	10.229	1.975	42 of 94	33	25	44	5	4.346075	22.50937
2	16	54.917	8.226	600	10.395	1.867	42 of 94	33	25	44	5	4.283021	23.84681
3	16	52.459	9.813	600	10.093	1.982	42 of 94	33	25	44	5	4.197563	21.37538
4	16	50.748	13.678	600	10.106	2.128	42 of 94	33	25	44	5	4.021571	19.09868
5	16	49.508	10.54	600	9.911	2.034	42 of 94	33	25	44	5	3.995258	19.46755

Trajectory: Optimized Breast Immobilization Device
800% magnification in Image J
Shallow Lesion (2 cm)

Trial #	Lesion ROI Area	Lesion Mean Pixel Value	Lesion STD Pixel Value	BKG ROI Area	BKG Mean Pixel Value	BKG STD Pixel Value	Slice #	x-cord of top left corner of ROI (Lesion)	y-cord of top left corner of ROI (Lesion)	x-cord of top left corner of ROI (Bkg)	y-cord of top left corner of ROI (Bkg)	Contrast	SNR
1	16	71.533	15.911	600	10.769	2.037	54 of 94	65	22	23	7	5.642492	29.83014
2	16	69.131	15.64	600	11.029	2.473	54 of 94	65	22	23	7	5.268111	23.49454
3	16	66.24	17.803	600	10.735	2.286	54 of 94	65	22	23	7	5.17047	24.2804
4	16	58.901	13.568	600	10.703	2.032	54 of 94	65	22	23	7	4.503223	23.71949
5	16	59.075	18.506	600	10.848	2.114	54 of 94	65	22	23	7	4.445704	22.81315

Trajectory: "Flat Paddle"
800% magnification in Image J
Deep Lesion (5 cm)

Trial #	Lesion ROI Area	Lesion Mean Pixel Value	Lesion STD Pixel Value	BKG ROI Area	BKG Mean Pixel Value	BKG STD Pixel Value	Slice #	x-cord of top left corner of ROI (Lesion)	y-cord of top left corner of ROI (Lesion)	x-cord of top left corner of ROI (Bkg)	y-cord of top left corner of ROI (Bkg)	Contrast	SNR
1	16	41.22	6.906	600	10.357	2.285	42 of 94	33	33	44	13	2.979917	13.50678
2	16	38.882	7.615	600	10.369	2.2	42 of 94	33	33	44	13	2.749831	12.96045
3	16	37.002	7.889	600	9.941	1.974	42 of 94	33	33	44	13	2.722161	13.70871
4	16	32.179	7.683	600	9.411	1.859	42 of 94	33	33	44	13	2.419297	12.24744
5	16	33.485	6.601	600	9.304	1.825	42 of 94	33	33	44	13	2.59899	13.24986

Trajectory: "Flat Paddle"
800% magnification in Image J
Shallow Lesion (2 cm)

Trial #	Lesion ROI Area	Lesion Mean Pixel Value	Lesion STD Pixel Value	BKG ROI Area	BKG Mean Pixel Value	BKG STD Pixel Value	Slice #	x-cord of top left corner of ROI (Lesion)	y-cord of top left corner of ROI (Lesion)	x-cord of top left corner of ROI (Bkg)	y-cord of top left corner of ROI (Bkg)	Contrast	SNR
1	16	43.43	10.006	600	9.774	1.943	54 of 94	66	28	23	15	3.443421	17.32167
2	16	46.993	10.965	600	9.807	2.195	54 of 94	66	28	23	15	3.791781	16.94123
3	16	38.993	7.624	600	9.327	2.141	54 of 94	66	28	23	15	3.180658	13.85614
4	16	41.566	7.338	600	9.134	2.052	54 of 94	66	28	23	15	3.55069	15.80507
5	16	43.685	11.451	600	9.14	2.006	54 of 94	66	28	23	15	3.77954	17.22084

Matlab Source Code (Contrast Plots):

```
clear all
%%By Kelly Klanian
%% Contrast Plots
shallow=20;
deep=50;
cont_dp_ell=[4.346075, 4.283021, 4.197563, 4.021571, 3.995258];
cont_sh_ell=[5.642492, 5.268111, 5.17047, 4.503223, 4.445704];
cont_dp_flat=[2.979917, 2.749831, 2.722161, 2.419297, 2.59899];
cont_sh_flat=[3.443421, 3.791781, 3.180658, 3.55069, 3.77954];
a = mean(cont_sh_ell);
b = std(cont_sh_ell);
c = mean(cont_sh_flat);
d = std(cont_sh_flat);
e = mean(cont_dp_ell);
f = std(cont_dp_ell);
g = mean(cont_dp_flat);
h = std(cont_dp_flat);
figure(1);
errorbar(shallow,a,b,'go');
xlim([0 70]);
ylim([0 7]);
title('Contrast vs. Lesion Depth');
xlabel('Lesion Depth (mm)');
ylabel('Contrast');
hold on;
errorbar(shallow,c,d,'squarer');
hold on;
errorbar(deep, e,f,'go');
hold on;
errorbar(deep,g,h,'squarer');
legend('Optimized Device','Flat Device');

```

Matlab Source Code (SNR Plots):

```
%%
%SNR Plot
shallow=20;
deep=50;
SNR_sh_ell=[29.83014, 23.49454, 24.2804, 23.71949, 22.81315];
SNR_dp_ell=[22.50937, 23.84681, 21.37538, 19.09868, 19.46755];
SNR_sh_flat=[17.32167, 16.94123, 13.85614, 15.80507, 17.22084];
SNR_dp_flat=[13.50678, 12.96045, 13.70871, 12.24744, 13.24986];
i = mean(SNR_sh_ell);
j = std(SNR_sh_ell);
k = mean(SNR_sh_flat);
l = std(SNR_sh_flat);
m = mean(SNR_dp_ell);
n = std(SNR_dp_ell);
o = mean(SNR_dp_flat);
p = std(SNR_dp_flat);
figure(2);
errorbar(shallow,i,j,'co');
xlim([0 70]);
ylim([0 30]);
title('SNR vs. Lesion Depth');
xlabel('Lesion Depth (mm)');
ylabel('SNR');
hold on;
errorbar(shallow,k,l,'squarem');
hold on;
errorbar(deep,m,n,'co');
hold on;
errorbar(deep,o,p,'squarem');
legend('Optimized Device','Flat Device');
```

Matlab Source Code (Kruska-Wallis Testing):

```
%%
%By Kelly Klanian
%P-value Calculations (Kruskalwallis Test - nonparametric)
%Contrast, Shallow Lesion
contrast_sh = [5.642492, 5.268111, 5.17047, 4.503223, 4.445704, 3.443421, 3.791781, 3.180658, 3.55069, 3.77954];
compression = {'Optimized','Optimized','Optimized','Optimized','Optimized','Flat','Flat','Flat','Flat','Flat'};
p_sh_contrast = kruskalwallis(contrast_sh,compression)

%Contrast, Deep Lesion
contrast_dp = [4.346075, 4.283021, 4.197563, 4.021571, 3.995258, 2.979917, 2.749831, 2.722161, 2.419297, 2.59899];
compression = {'Optimized','Optimized','Optimized','Optimized','Optimized','Flat','Flat','Flat','Flat','Flat'};
p_dp_contrast = kruskalwallis(contrast_dp,compression)


%SNR, Shallow Lesion
SNR_sh = [29.83014, 23.49454, 24.2804, 23.71949, 22.81315, 17.32167, 16.94123, 13.85614, 15.80507, 17.22084];
compression = {'Optimized','Optimized','Optimized','Optimized','Optimized','Flat','Flat','Flat','Flat','Flat'};
p_sh_SNR = kruskalwallis(SNR_sh,compression)


%SNR, Deep Lesion
SNR_dp = [22.50937, 23.84681, 21.37538, 19.09868, 19.46755, 13.50678, 12.96045, 13.70871, 12.24744, 13.24986];
compression = {'Optimized','Optimized','Optimized','Optimized','Optimized','Flat','Flat','Flat','Flat','Flat'};
p_dp_SNR = kruskalwallis(SNR_dp,compression)
```

Matlab Source Code (QQ Plots):

```
%%
%By Kelly Klanian
%QQPlots to establish normality
cont_dp_ell=[4.346075, 4.283021, 4.197563, 4.021571, 3.995258];
cont_sh_ell=[5.642492, 5.268111, 5.17047, 4.503223, 4.445704];
cont_dp_flat=[2.979917, 2.749831, 2.722161, 2.419297, 2.59899];
cont_sh_flat=[3.443421, 3.791781, 3.180658, 3.55069, 3.77954];
SNR_sh_ell=[29.83014, 23.49454, 24.2804, 23.71949, 22.81315];
SNR_dp_ell=[22.50937, 23.84681, 21.37538, 19.09868, 19.46755];
SNR_sh_flat=[17.32167, 16.94123, 13.85614, 15.80507, 17.22084];
SNR_dp_flat=[13.50678, 12.96045, 13.70871, 12.24744, 13.24986];

figure(1);
qqplot(cont_dp_ell)
title('QQ Plot of Optimized Trajectory Deep Lesion Contrast vs Standard Normal');
figure(2);
qqplot(cont_sh_ell)
title('QQ Plot of Optimized Trajectory Shallow Lesion Contrast vs Standard Normal');
figure(3);
qqplot(cont_dp_flat)
title('QQ Plot of Flat Trajectory Deep Lesion Contrast vs Standard Normal');
figure(4);
qqplot(cont_sh_flat)
title('QQ Plot of Flat Trajectory Shallow Lesion Contrast vs Standard Normal');
figure(5);
qqplot(SNR_dp_ell)
title('QQ Plot of Optimized Trajectory Deep Lesion SNR vs Standard Normal');
figure(6);
qqplot(SNR_sh_ell)
title('QQ Plot of Optimized Trajectory Shallow Lesion SNR vs Standard Normal');
figure(7);
qqplot(SNR_dp_flat)
title('QQ Plot of Flat Trajectory Deep Lesion SNR vs Standard Normal');
figure(8);
qqplot(SNR_sh_flat)
title('QQ Plot of Flat Trajectory Shallow Lesion SNR vs Standard Normal');
```

QQ Plots:

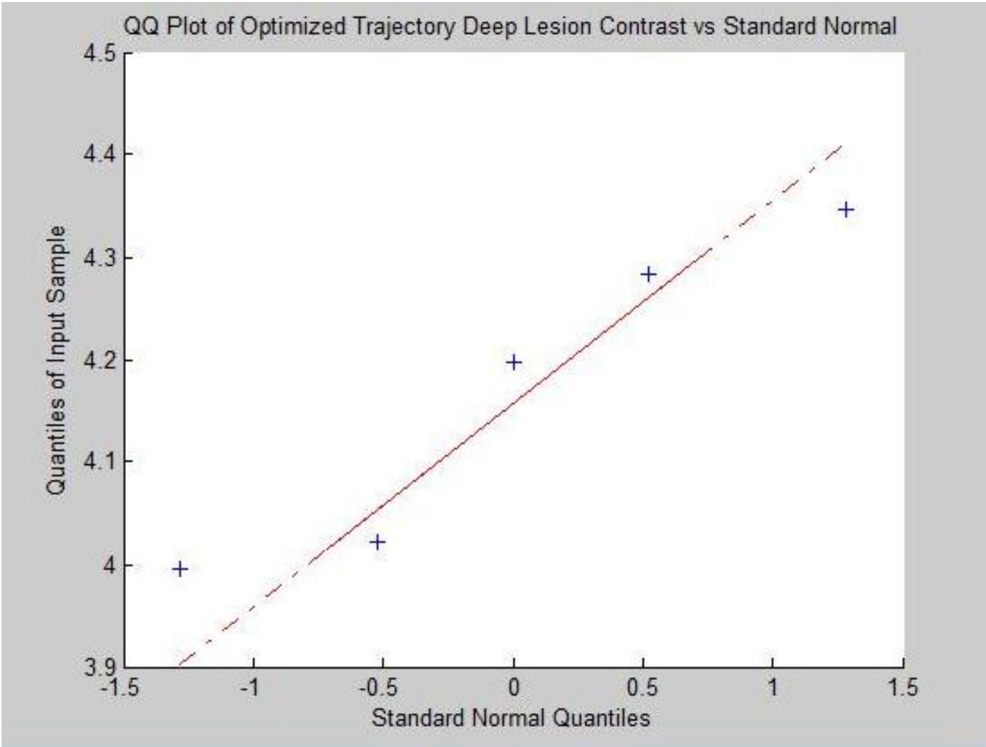

QQ Plot of Optimized Trajectory Deep Lesion Contrast vs Standard Normal
Quantiles of Input Sample
Standard Normal Quantiles
4.5
4.4
4.3
4.2
4.1
4
3.9
-1.5
-1
-0.5
0
0.5
1
1.5

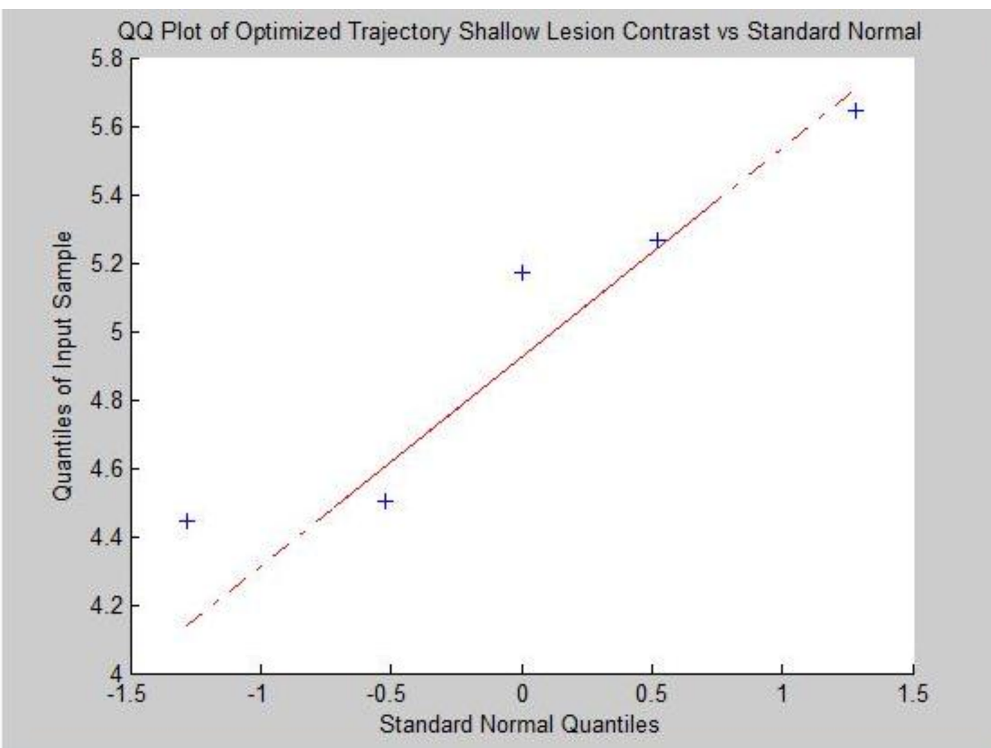

QQ Plot of Optimized Trajectory Shallow Lesion Contrast vs Standard Normal
Quantiles of Input Sample
Standard Normal Quantiles
5.8
5.6
5.4
5.2
5
4.8
4.6
4.4
4.2
4
-1.5
-1
-0.5
0
0.5
1
1.5

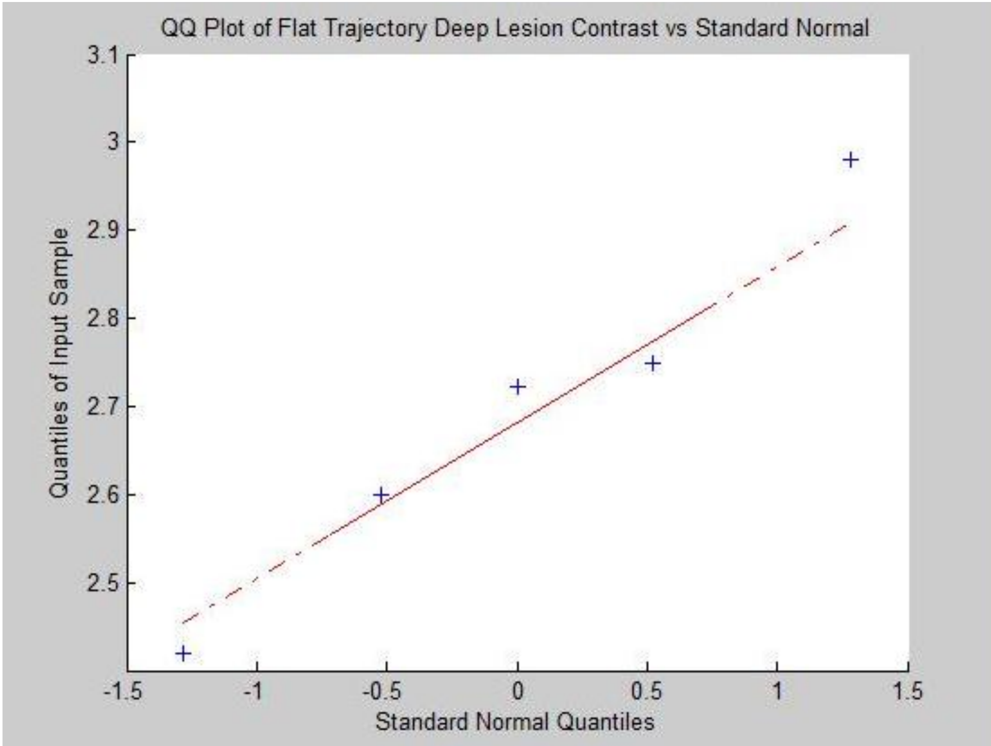

QQ Plot of Flat Trajectory Deep Lesion Contrast vs Standard Normal
Quantiles of Input Sample
Standard Normal Quantiles
3.1
3
2.9
2.8
2.7
2.6
2.5
-1.5
-1
-0.5
0
0.5
1
1.5

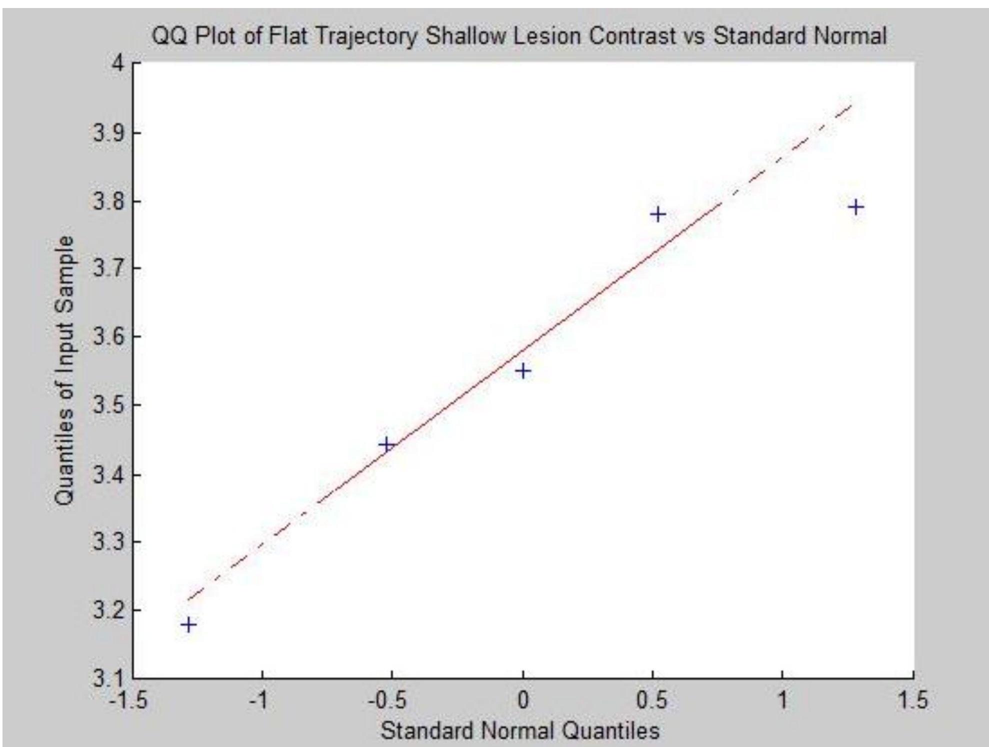

QQ Plot of Flat Trajectory Shallow Lesion Contrast vs Standard Normal
Quantiles of Input Sample
Standard Normal Quantiles
4
3.9
3.8
3.7
3.6
3.5
3.4
3.3
3.2
3.1
-1.5
-1
-0.5
0
0.5
1
1.5

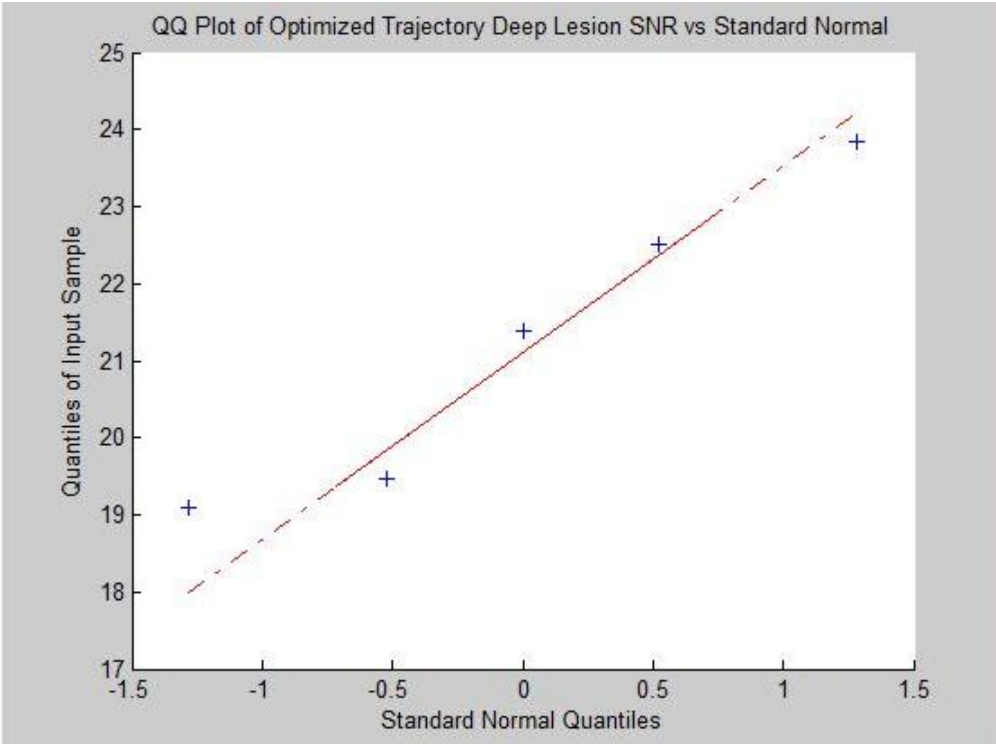
QQ Plot of Optimized Trajectory Deep Lesion SNR vs Standard Normal
Quantiles of Input Sample
Standard Normal Quantiles

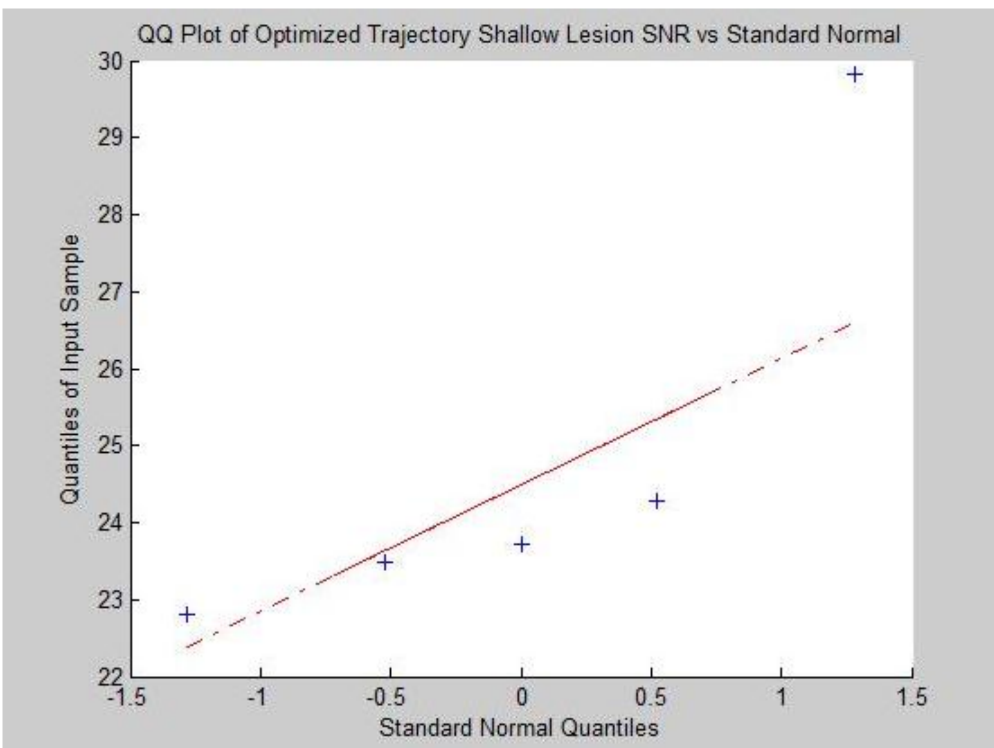
QQ Plot of Optimized Trajectory Shallow Lesion SNR vs Standard Normal
Quantiles of Input Sample
Standard Normal Quantiles

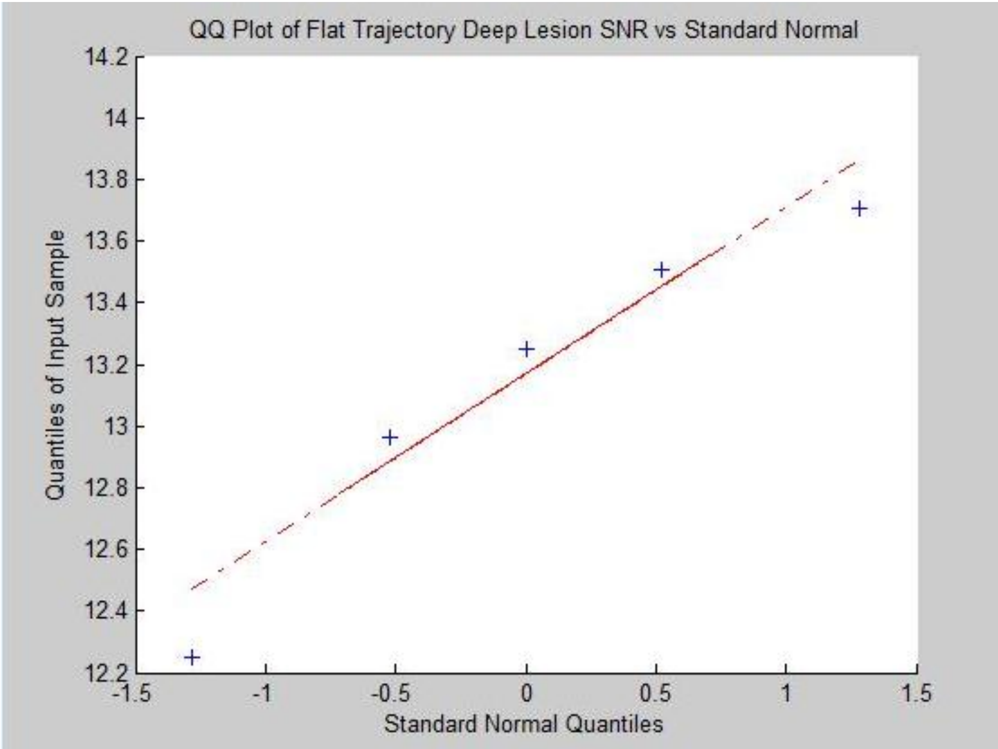
QQ Plot of Flat Trajectory Deep Lesion SNR vs Standard Normal
Quantiles of Input Sample
Standard Normal Quantiles
14.2
14
13.8
13.6
13.4
13.2
13
12.8
12.6
12.4
12.2
-1.5
-1
-0.5
0
0.5
1
1.5

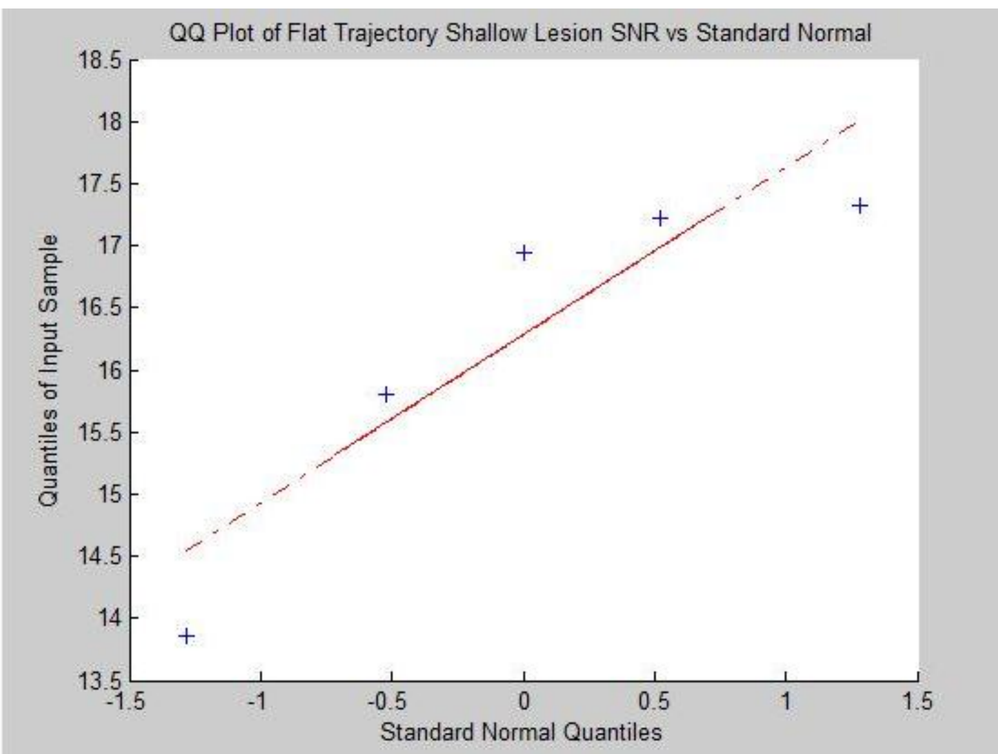
QQ Plot of Flat Trajectory Shallow Lesion SNR vs Standard Normal
Quantiles of Input Sample
Standard Normal Quantiles
18.5
18
17.5
17
16.5
16
15.5
15
14.5
14
13.5
-1.5
-1
-0.5
0
0.5
1
1.5

Calculated Variance:

Trajectory: Optimized Breast Immobilization Device						
800% magnification in Image J						
Deep Lesion (5 cm)						
Trial #	**Contrast**	**SNR**	**STD Contrast**	**STD SNR**	**Variance Contrast**	**Variance SNR**
1	4.346075	22.50937	0.155799	2.009352	0.024273	4.037497
2	4.283021	23.84681				
3	4.197563	21.37538				
4	4.021571	19.09868				
5	3.995258	19.46755				

Trajectory: Optimized Breast Immobilization Device						
800% magnification in Image J						
Shallow Lesion (2 cm)						
Trial #	**Contrast**	**SNR**	**STD Contrast**	**STD SNR**	**Variance Contrast**	**Variance SNR**
1	5.642492	29.83014	0.516621	2.845515	0.266898	8.096955
2	5.268111	23.49454				
3	5.17047	24.2804				
4	4.503223	23.71949				
5	4.445704	22.81315				

Trajectory: "Flat Paddle"						
800% magnification in Image J						
Deep Lesion (5 cm)						
Trial #	**Contrast**	**SNR**	**STD Contrast**	**STD SNR**	**Variance Contrast**	**Variance SNR**
1	2.979917	13.50678	0.206245	0.569821	0.042537	0.324696
2	2.749831	12.96045				
3	2.722161	13.70871				
4	2.419297	12.24744				
5	2.59899	13.24986				

Trajectory: "Flat Paddle"						
800% magnification in Image J						
Shallow Lesion (2 cm)						
Trial #	**Contrast**	**SNR**	**STD Contrast**	**STD SNR**	**Variance Contrast**	**Variance SNR**
1	3.443421	17.32167	0.254419	1.457319	0.064729	2.123777
2	3.791781	16.94123				
3	3.180658	13.85614				
4	3.55069	15.80507				
5	3.77954	17.22084				

APPENDIX F

(Large & Medium Scaled Optimized Immobilization Device & Support Drawings)

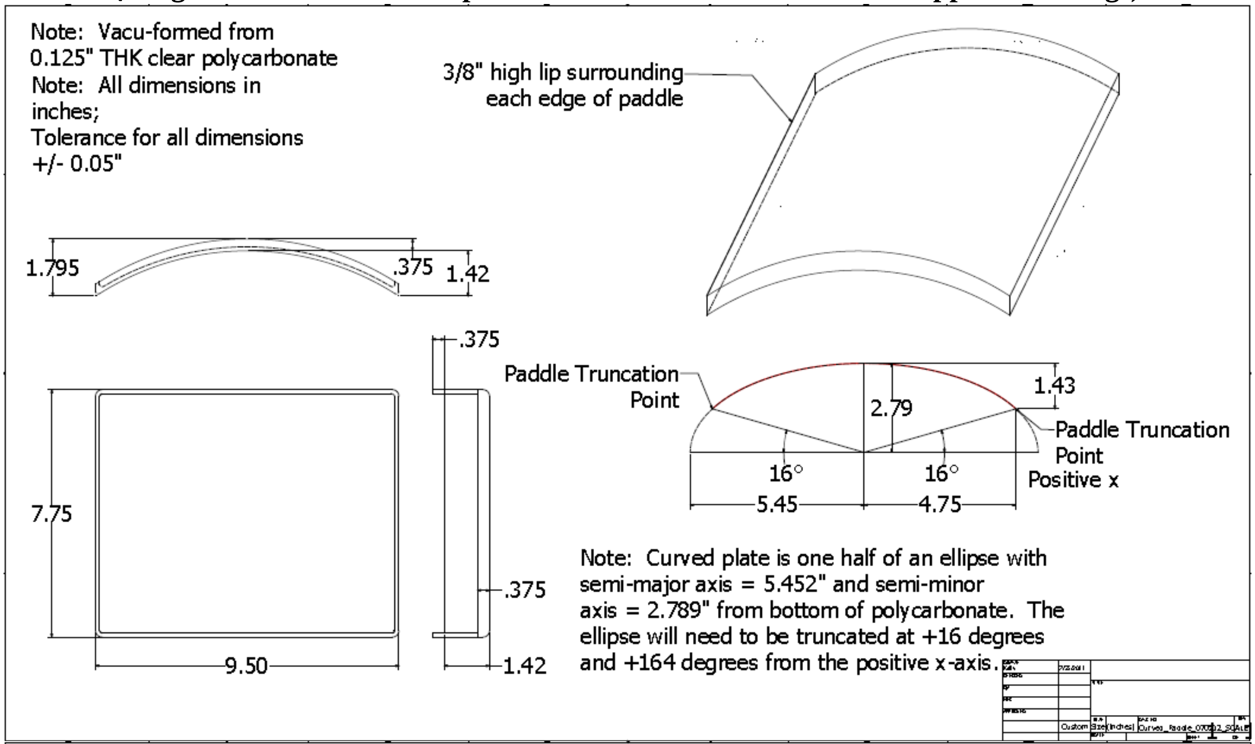

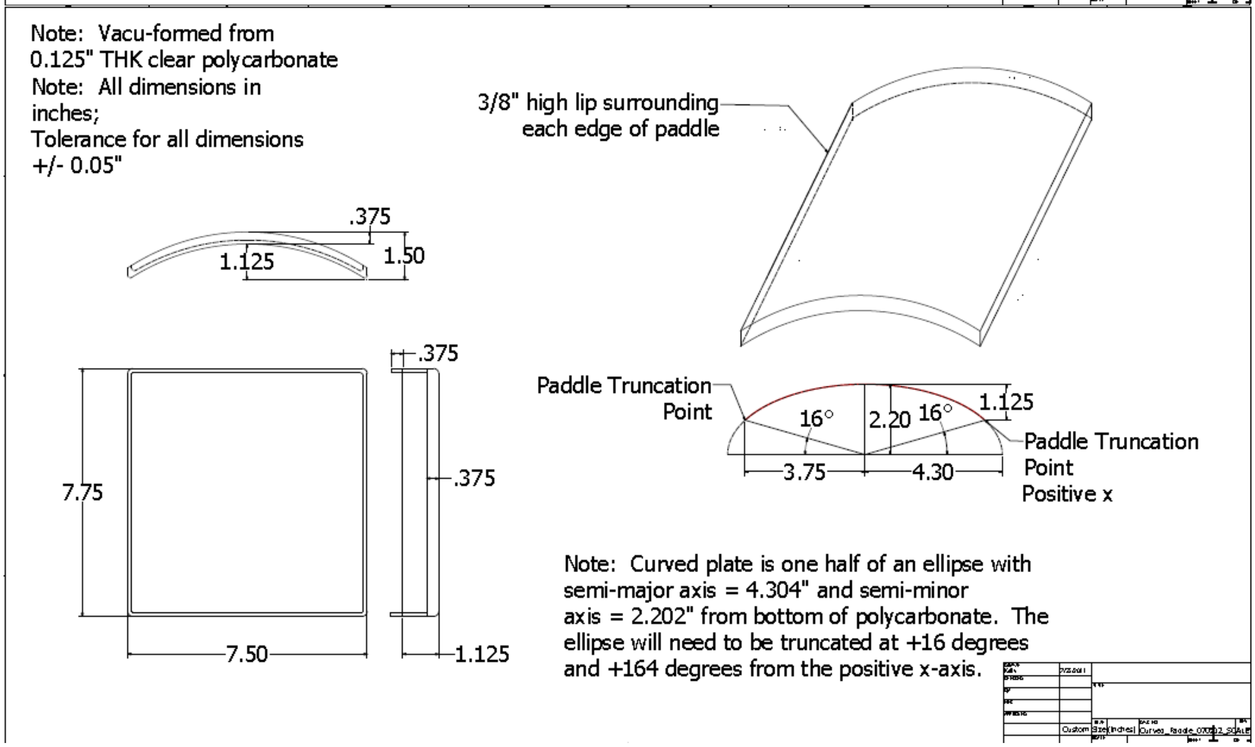

Breast Immobilization Device Support System Redesign (Large)

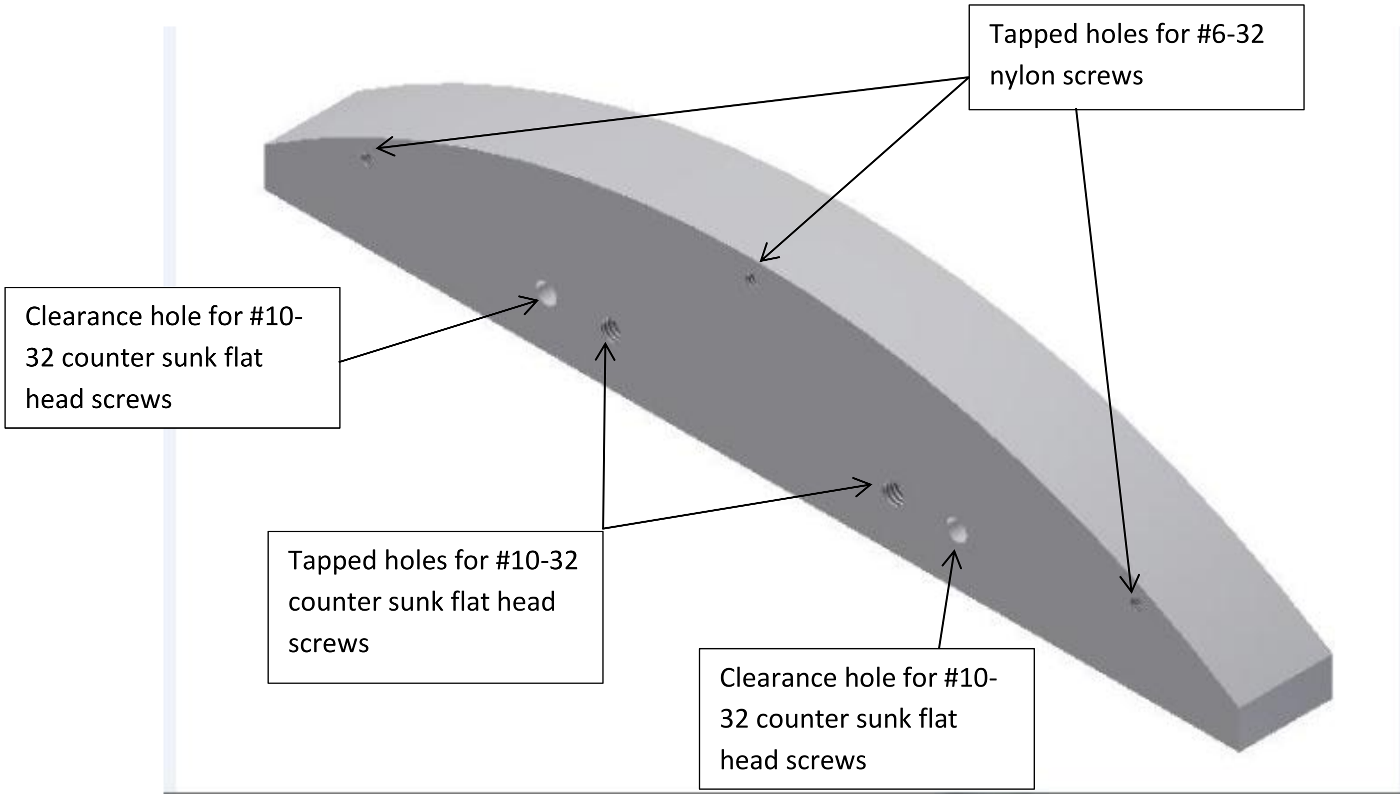

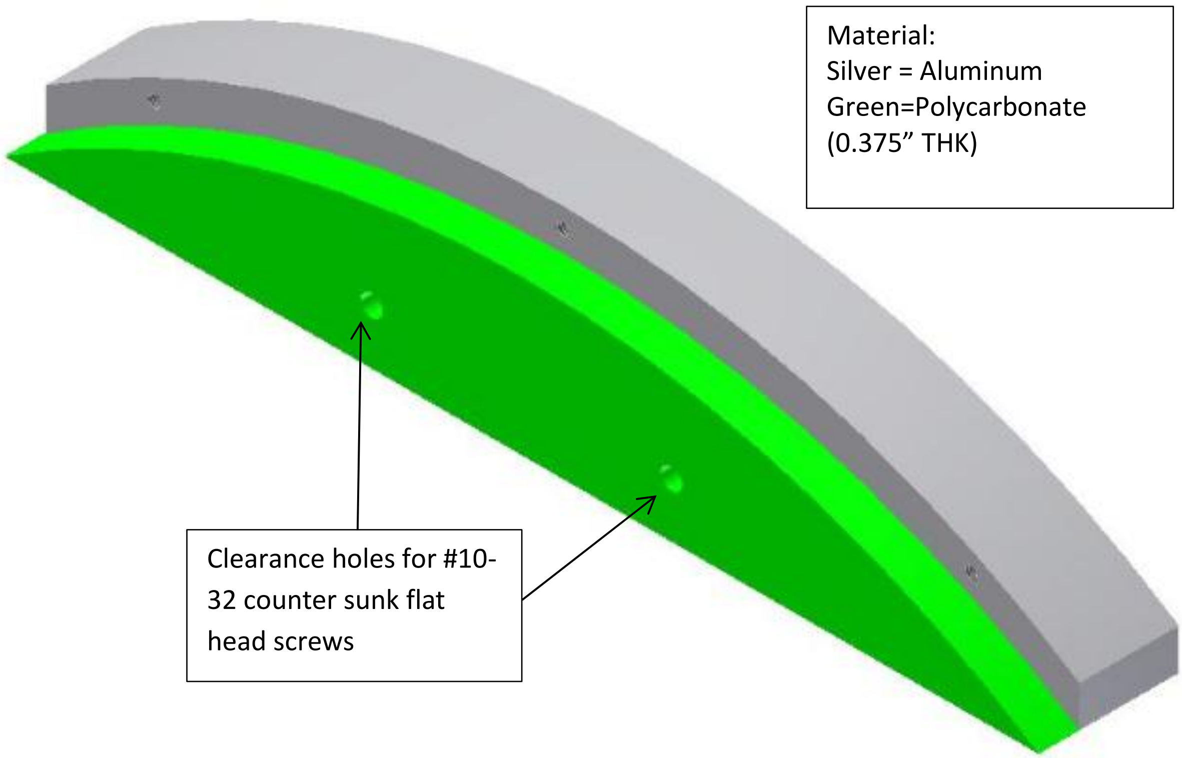
Material:
Silver = Aluminum
Green=Polycarbonate
(0.375” THK)
Clearance holes for #10-32 counter sunk flat head screws

FRONT VIEW – ALUMINUM PIECE

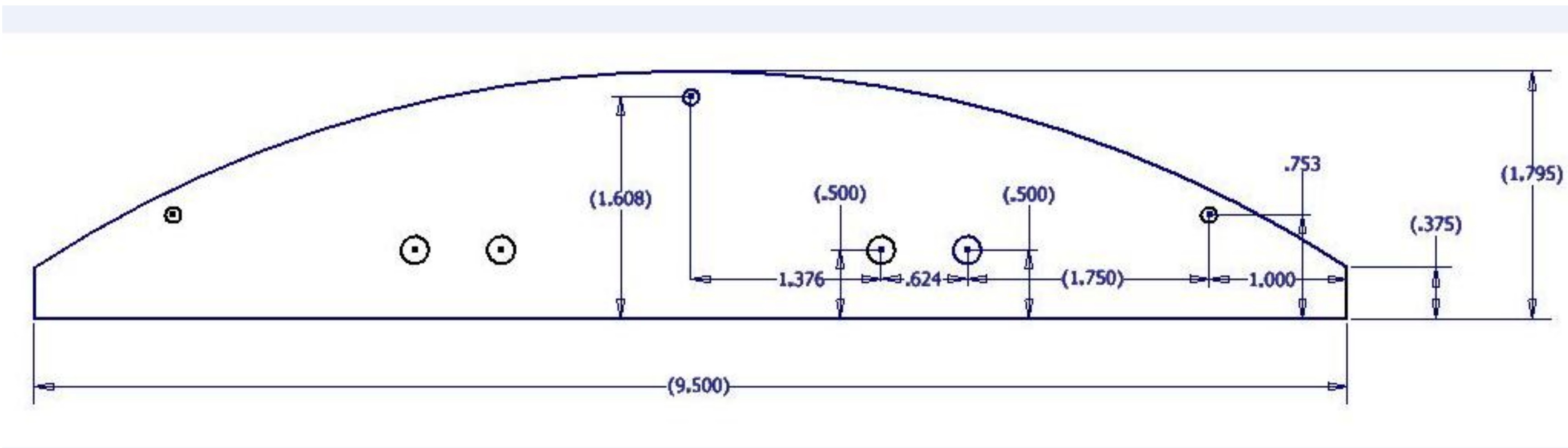

FRONT VIEW – POLYCARBONATE PIECE

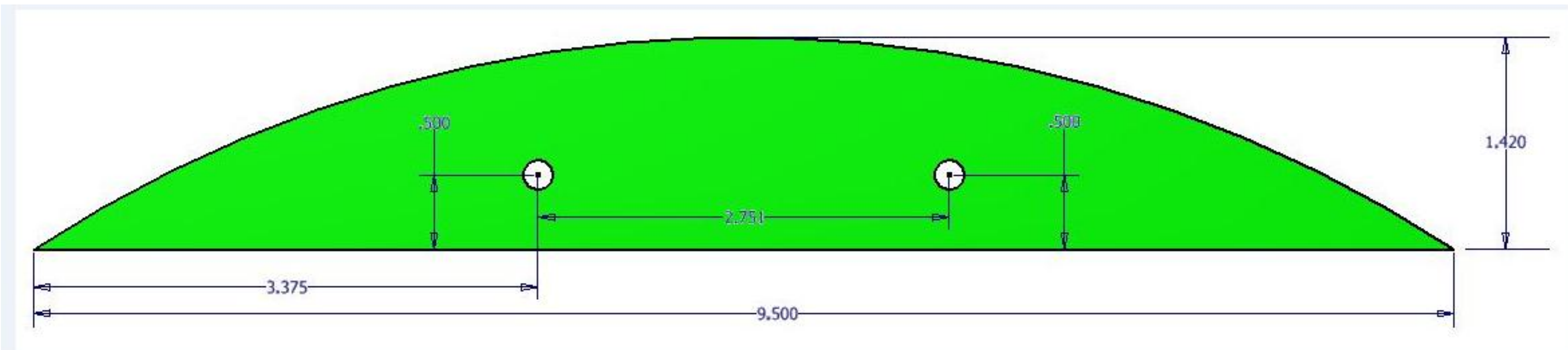

SIDE VIEW – BOTH ALUMINUM AND POLYCARBONATE PIECES

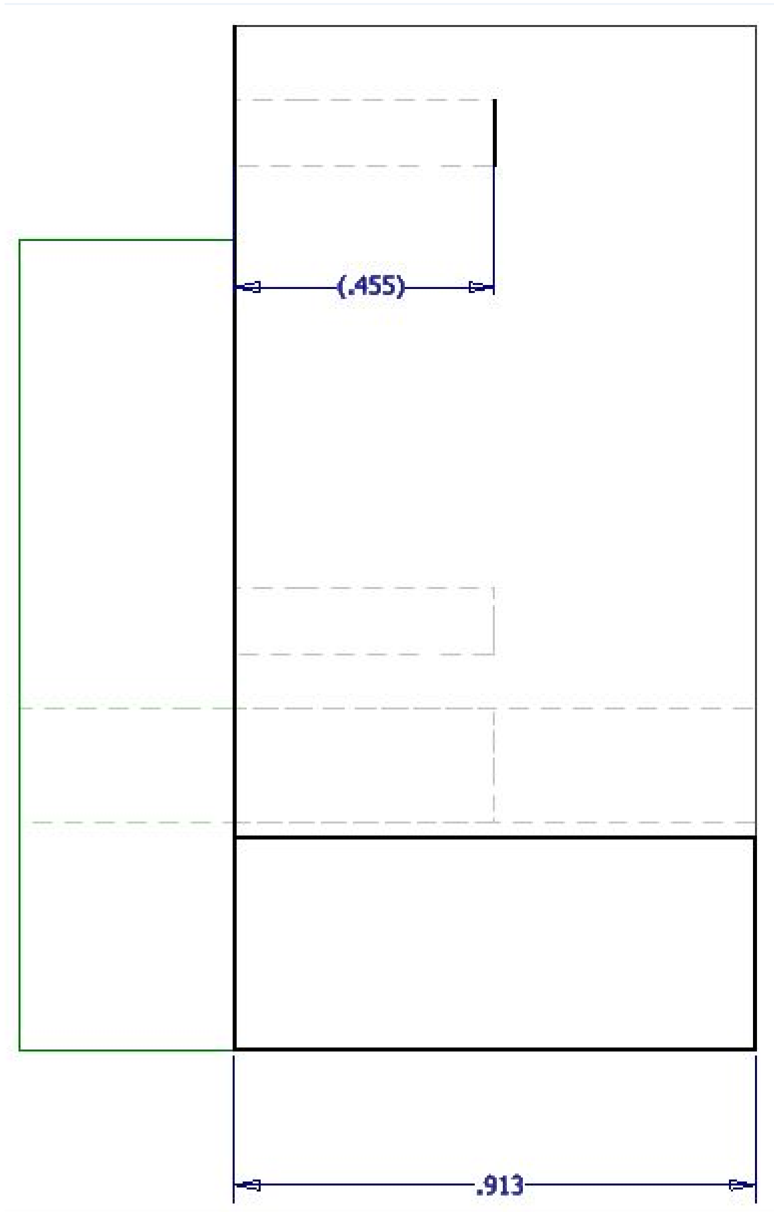

Breast Immobilization Device Support System Redesign (Medium)

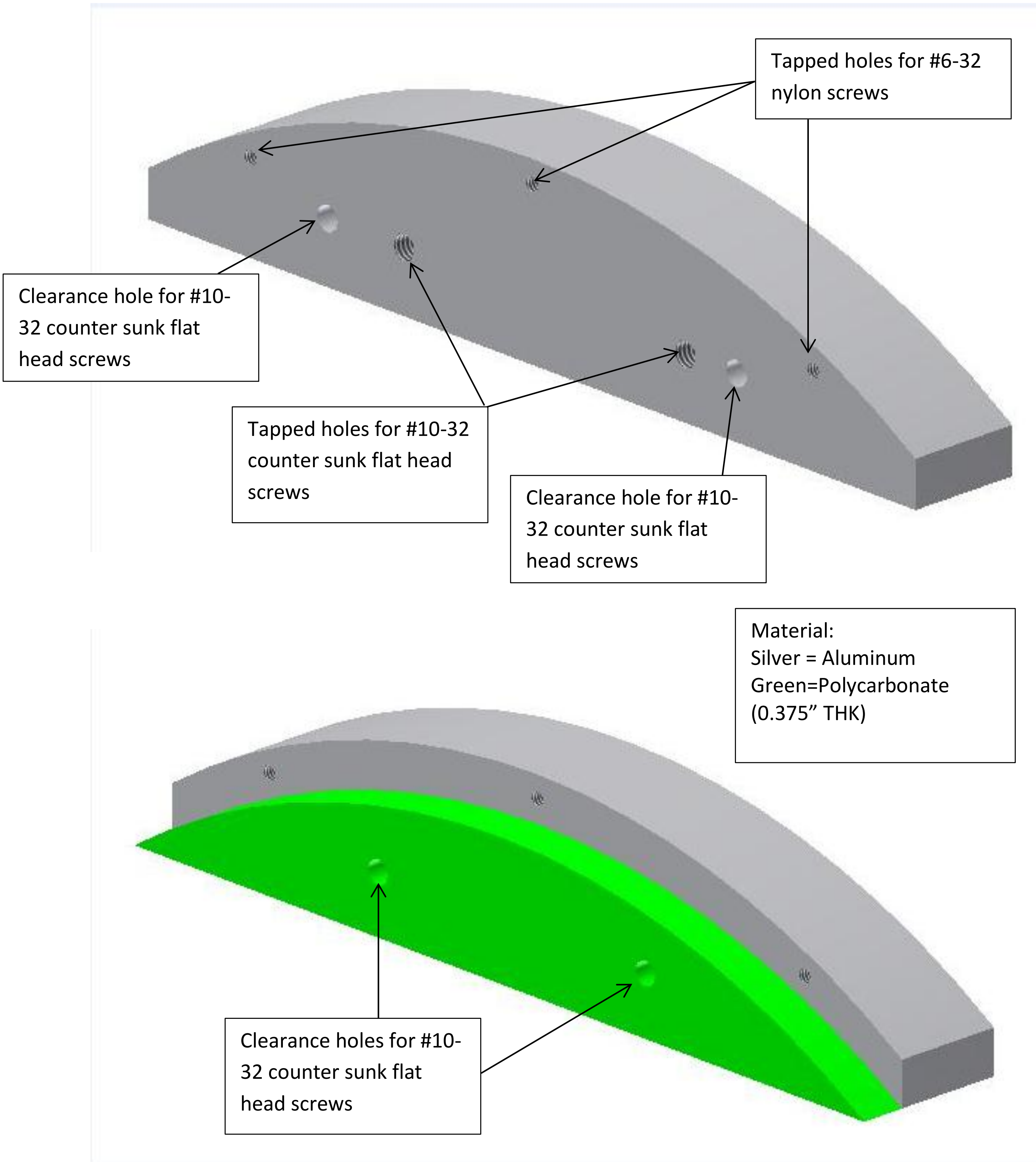

FRONT VIEW – ALUMINUM PIECE

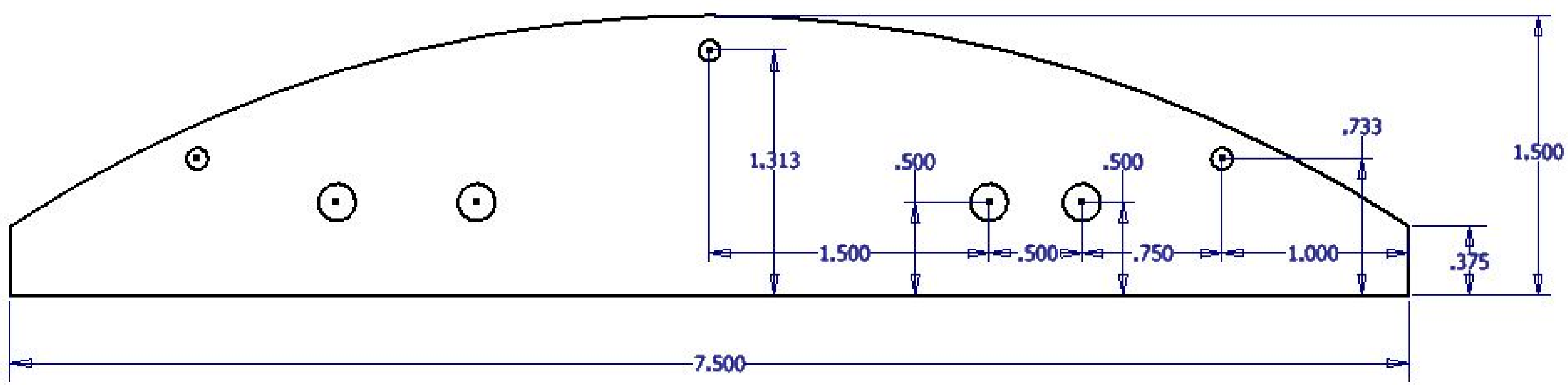

FRONT VIEW – POLYCARBONATE PIECE

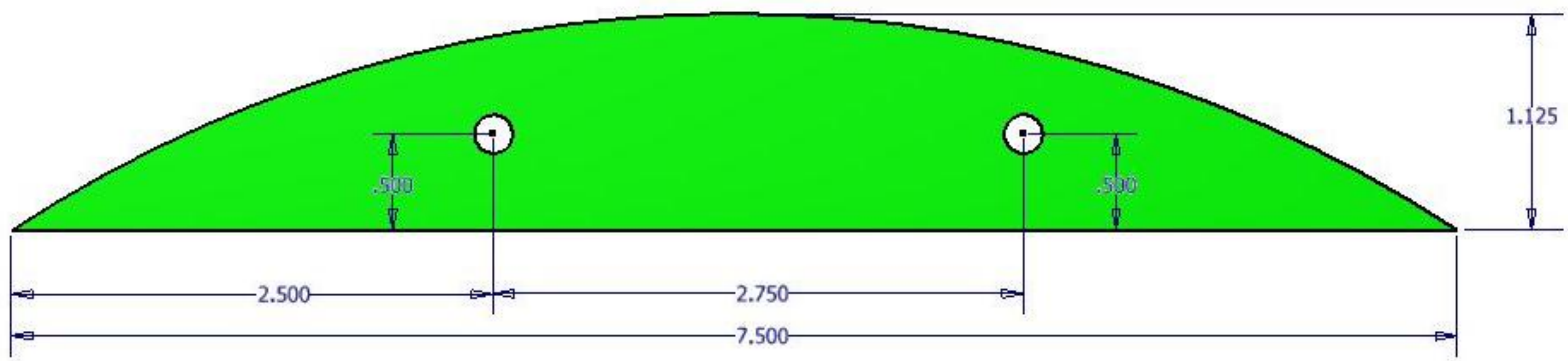

SIDE VIEW – BOTH ALUMINUM AND POLYCARBONATE PIECES

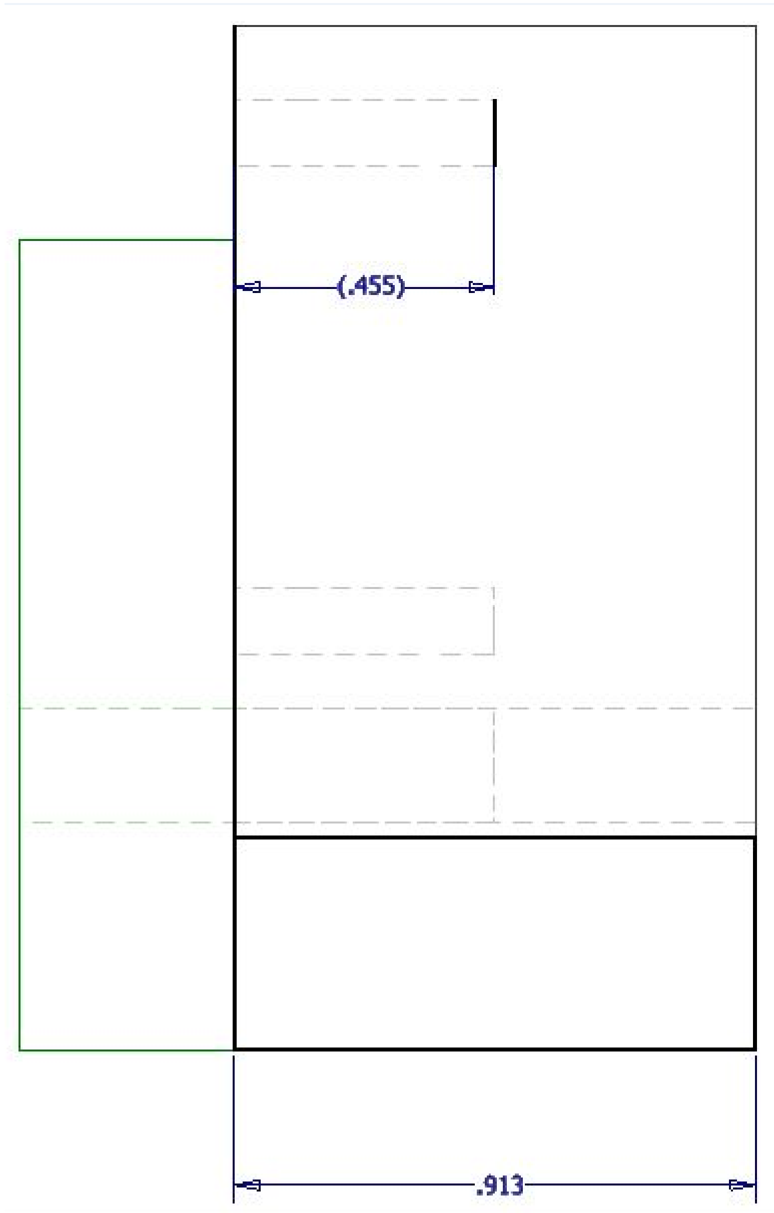

APPENDIX G

(X-ray detector hinge & lead brick weight subassembly drawings)

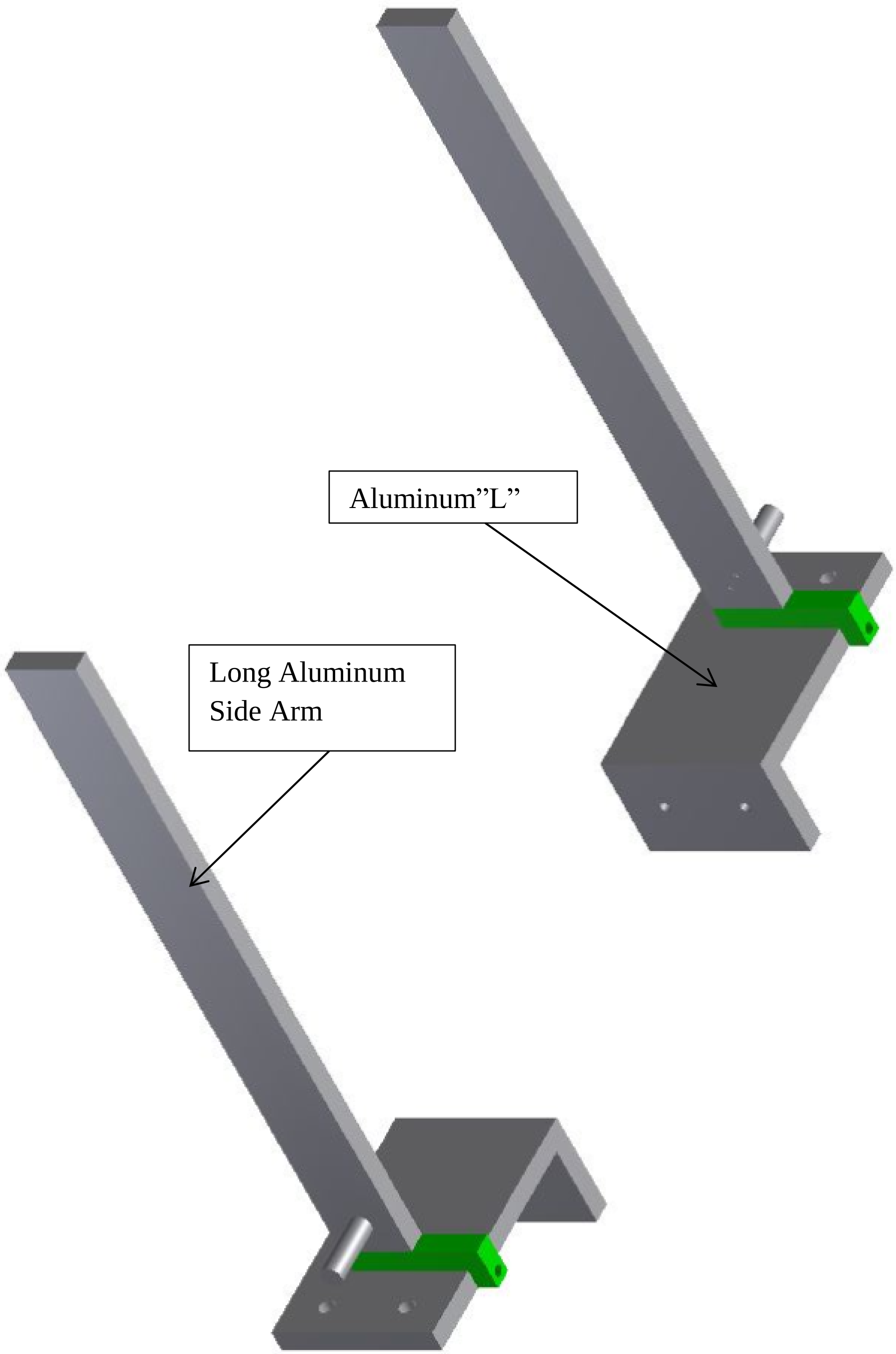

TOP VIEW – ALUMINUM “L” PIECE

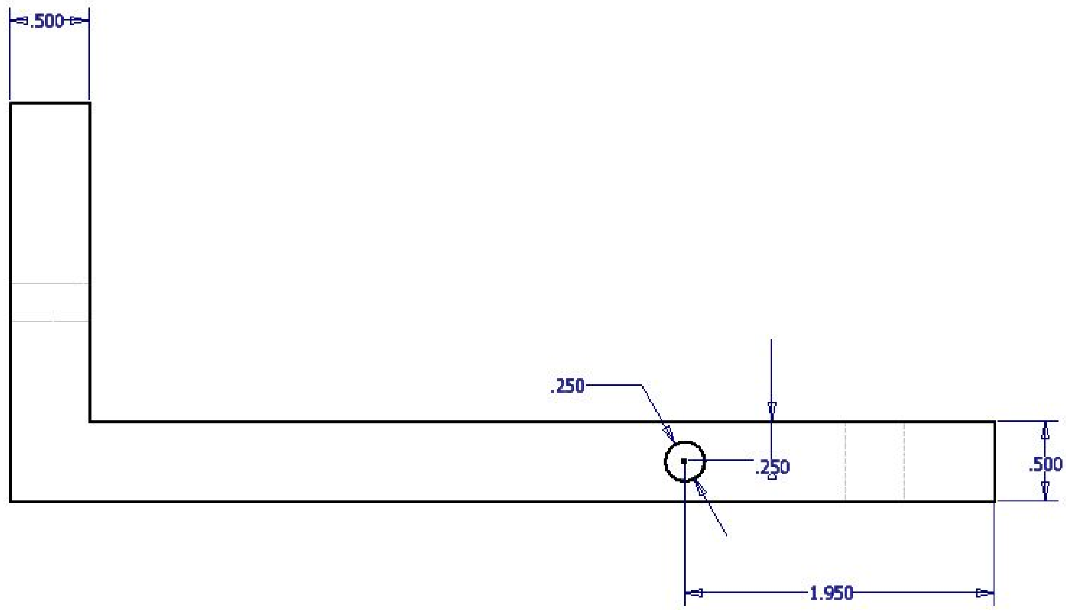

FRONT VIEW – ALUMINUM “L” PIECE

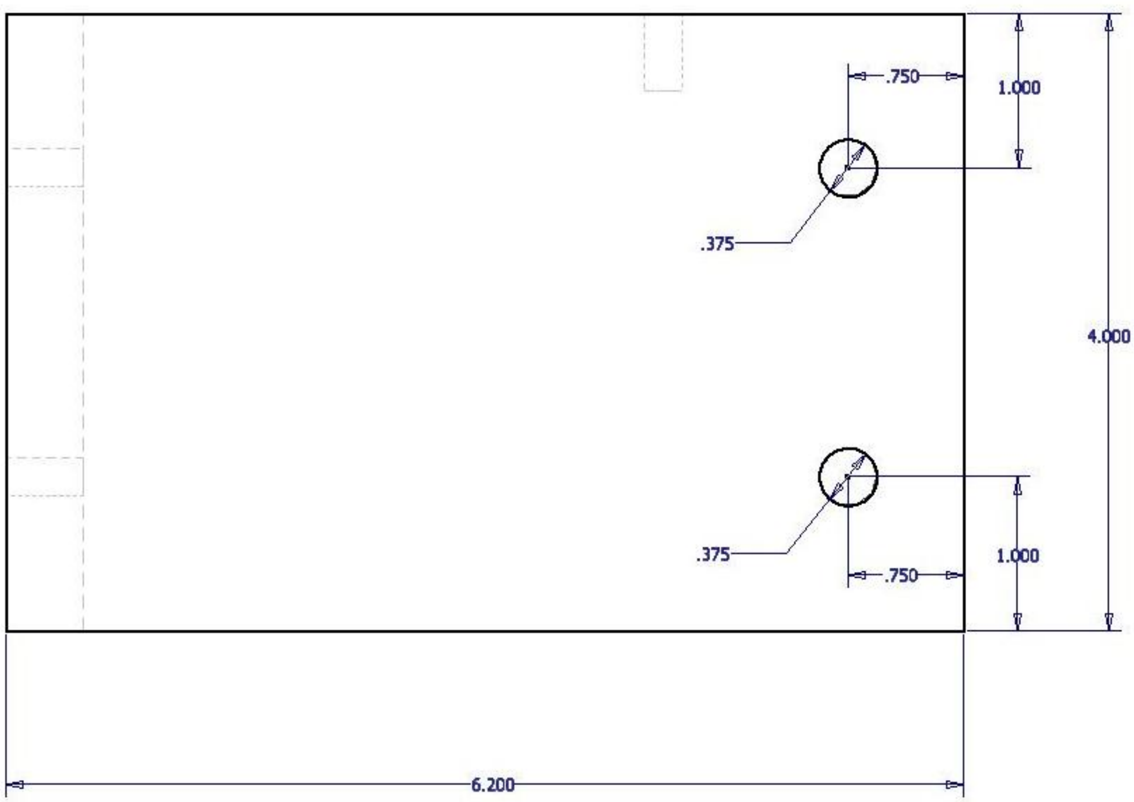

SIDE VIEW – ALUMINUM “L” PIECE

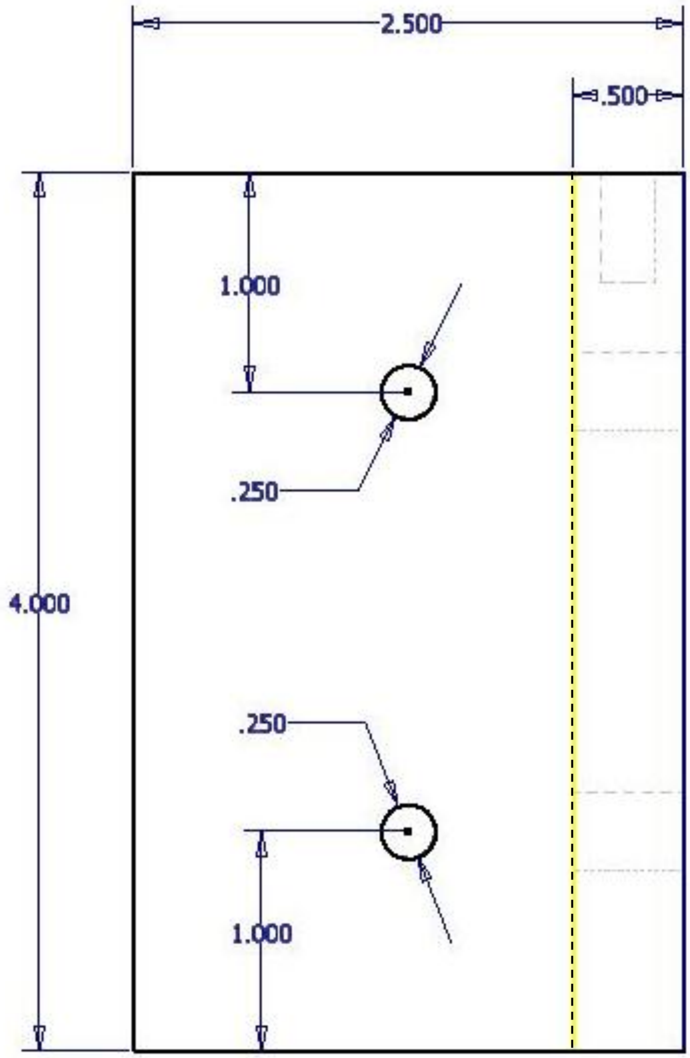

FRONT VIEW – LONG ALUMINUM SIDE ARM

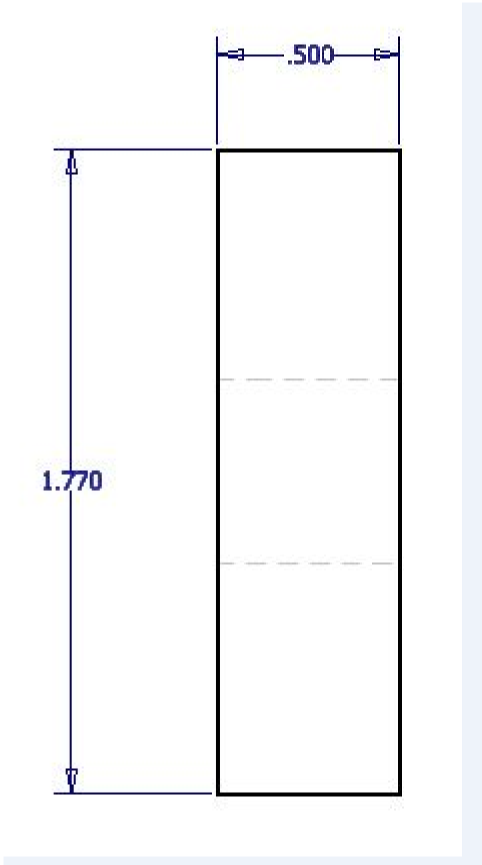

SIDE VIEW – LONG ALUMINUM SIDE ARM

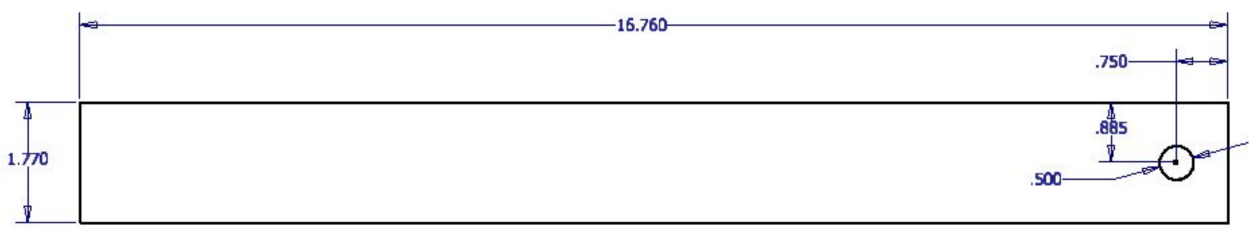

<u>Lead brick weight subassembly</u>

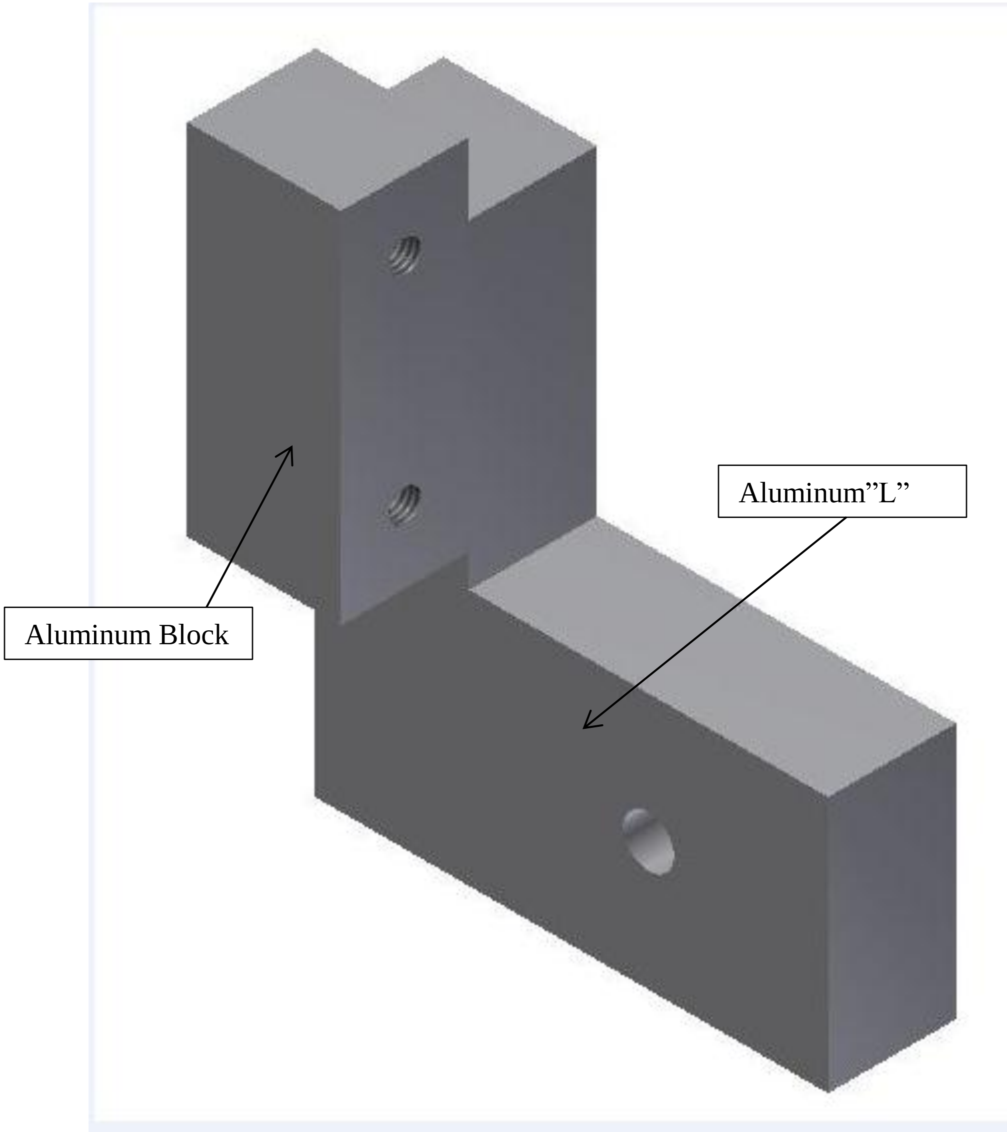
Aluminum"L"
Aluminum Block

FRONT VIEW – ALUMINUM “L” PIECE

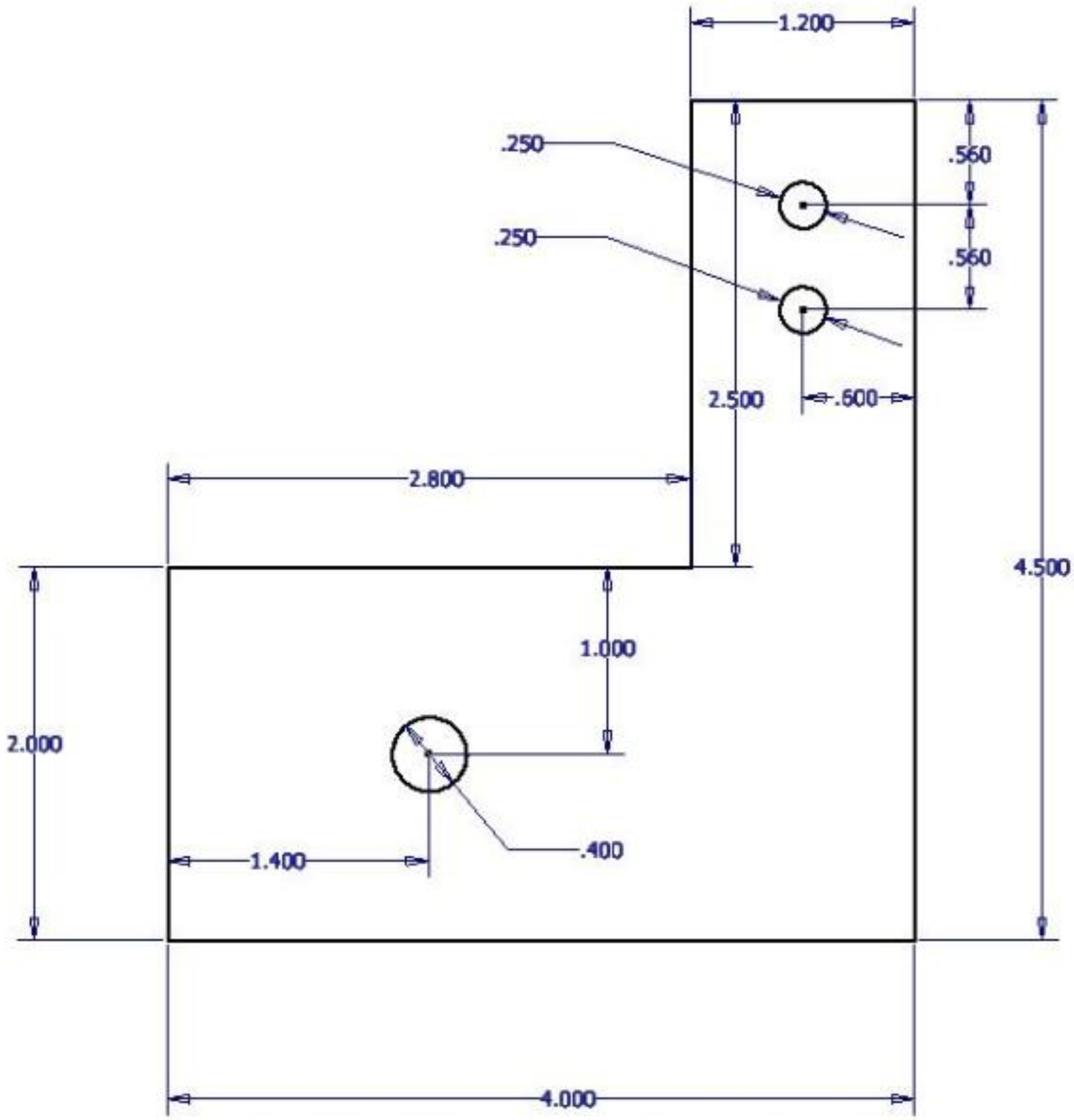

SIDE VIEW – ALUMINUM “L” PIECE

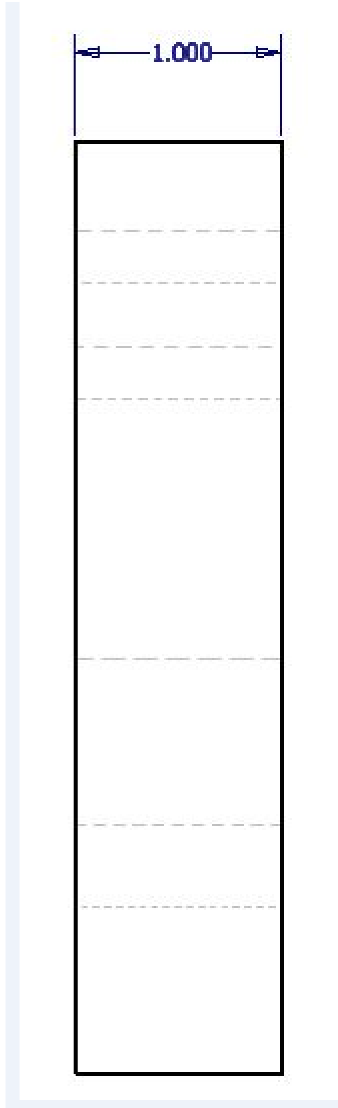

FRONT VIEW – ALUMINUM BLOCK

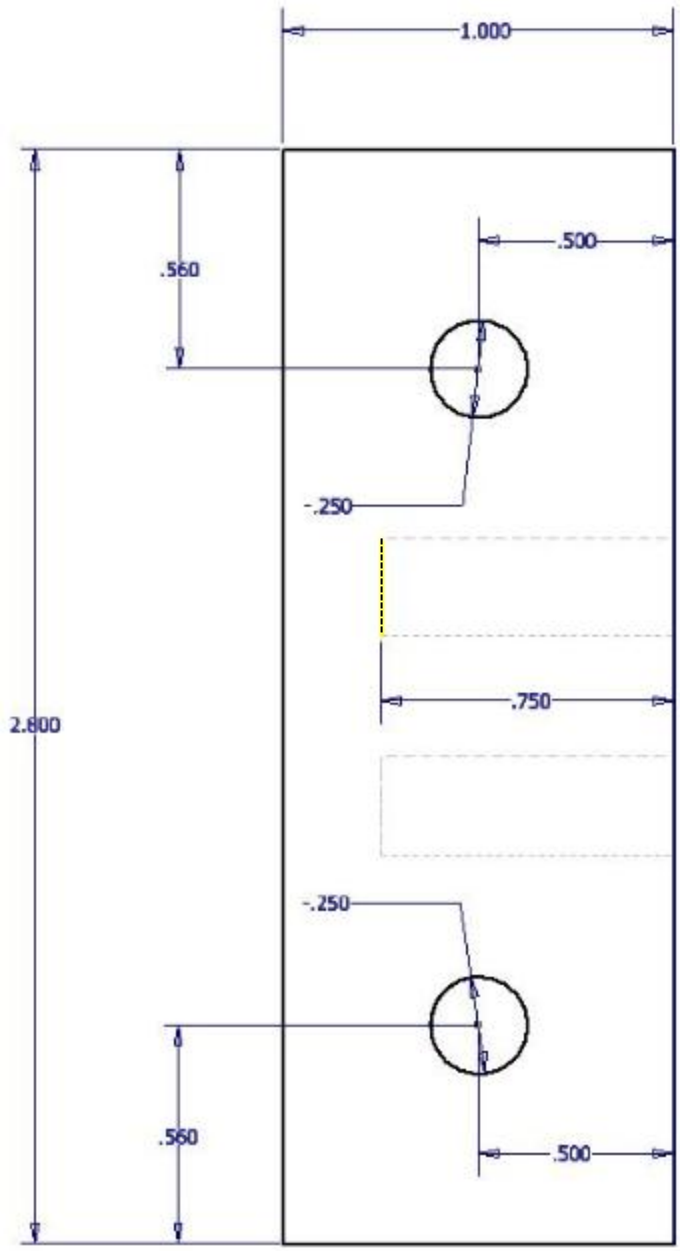

SIDE VIEW – ALUMINUM BLOCK

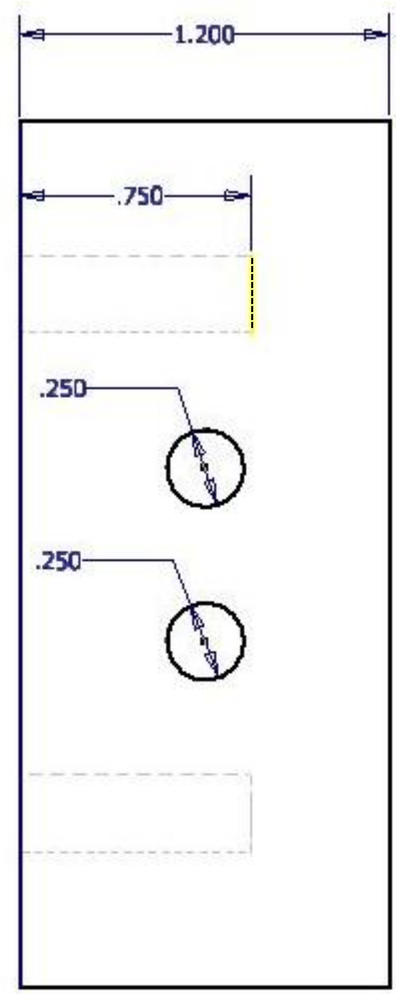

References

[1] Beaukbeuk (2009, March 13). Retrieved June 18, 2012 from http://en.wikipedia.org/wiki/File:Ameda_lactaline_personal_breast_pump.JPG#file

[2] Blumenthal, W., Cady, C., Lopez, M., Gray, G., & Idar, D. (2002). Influence of Temperature and Strain Rate on the Compressive Behavior of PMMA and Polycarbonate Polymers. *American Institute of Physics*, 620, 665-668. Retrieved from http://scitation.aip.org/getpdf/servlet/GetPDFServlet?filetype=pdf&id=APCPCS000620000001000665000001&idtype=cvips&doi=10.1063/1.1483626&prog=normal

[3] Boas, G (2005, January). IMAGING TECHOLOGIES: Diffuse Optical Imaging. Retrieved from http://www.nmr.mgh.harvard.edu/martinos/research/technologiesDOI.php

[4] Boedeker Plastics (2012). Polycarbonate Specifications. Retrieved from http://www.boedeker.com/polyc_p.htm

[5] Breastcancer.org (2012). American College of Radiology Supports Starting Mammograms at 40. Retrieved from http://www.breastcancer.org/symptoms/testing/new_research/20100105.jsp?gclid=CJDJm_WbqLACFQlN4AodxBuCXA

[6] Buitrago, Carlos (n.d.). Polycarbonate (PC). Retrieved from http://www.eng.buffalo.edu/Courses/ce435/PC_CB.pdf

[7] Cambridge University Engineering Dept (n.d.). Property Information: Young's Modulus and Specific Stiffness. Retrieved from http://www-materials.eng.cam.ac.uk/mpsite/properties/non-IE/stiffness.html

[8] Cedar-Sinai (2012). Breast MRI Procedure Information. Retrieved from http://www.cedars-sinai.edu/Patients/Programs-and-Services/Imaging-Center/Imaging-Procedures/MRI/Breast/

[9] Cedar-Sinai (2012). Breast Ultrasound. Retrieved from http://www.cedars-sinai.edu/Patients/Programs-and-Services/Imaging-Center/For-Patients/Exams-by-Procedure/Ultrasound/Breast-Ultrasound/

[10] Centers for Disease Control and Prevention (CDC). Breast Cancer Statistics. Retrieved from http://www.cdc.gov/cancer/breast/statistics/

[11] Champaign, Judy L., & Cederbom, Gunnar J. (2000, January). Advances in Breast Cancer Detection with Screening Mammography. Retrieved from http://www.ncbi.nlm.nih.gov/pmc/articles/PMC3117552/

[12] Dobbins, James T., & Godfrey, Devon J. (2003, September 16). Digital X-ray Tomosynthesis: Current State of the Art and Clinical Potential. *Physics in Medicine and Biology*, 48, R65-R106. Retrieved from http://iopscience.iop.org/0031-9155/48/19/R01

[13] Gong, Zongyi, Klanian, Kelly, Patel, Tushita, Sullivan, Olivia, & Williams, Mark (Manuscript Submitted to Medical Physics for Publication). Implementation and Evaluation of an Expectation Maximization Reconstruction Algorithm for Gamma Emission Breast Tomosynthesis.

[14] Ideal Pharmacy (2012). Mammography: Patient Teaching Aid. Retrieved from http://www.idealpharmacyla.com/index.php?id=24

[15] Imaginis Corporation (2008). How Does Nuclear Medicine Work? Retrieved from http://www.imaginis.com/nuclear-medicine/how-does-nuclear-medicine-work

[16] Judy, Patricia G. (2010). Dual Modality Surgical Guidance. (Doctoral dissertation).

[17] Kuhl, Christiane K., Schrading, Simone, Leutner, Claudia C., Morakkabati-Spitz, Nuschin, Wardelmann, Eva, Fimmers, Rolf, Kuhn, Walther, & Schild, Hans H. (2005, November 20). Mammography, Breast Ultrasound, and Magnetic Resonance Imaging for Surveillance of Women at High Familial Risk for Breast Cancer. *Journal of Clinical Oncology*, 23(33), 8469-8476. Retrieved from http://www.ncbi.nlm.nih.gov/pubmed/16293877

[18] Lee, Carol H., Dershaw, D., Kopans, Daniel, Evans, Phil, Monsees, Barbara, Monticciolo, Debra, Brenner, R., Bassett, Lawrence, Berg, Wendie, Feig, Stephen, Hendrick, Edward, Mendelson, Ellen, D'Orsi, Carl, Sickles, Edward, & Burhenne, Linda (2010, January 2). Breast Cancer Screening With Imaging: Recommendations from the Society of Breast Imaging and the ACR on the Use of Mammography, Breast MRI, Breast Ultrasound, and Other Technologies for the

Detection of Clinically Occult Breast Cancer. *Journal of the American College of Radiology*, 7(1), 18-27. Retrieved from http://www.sciencedirect.com/science/article/pii/S1546144009004803

[19] Machinist-materials.com. Comparison Table for Plastics. Retrieved from http://www.machinist-materials.com/comparison_table_for_plastics.htm

[20] Mariani, John J. (2000). 2nd Edition, Cracking the Boards: USMLE Step 2. *Google Books*, 91. Retrieved from http://books.google.com/books?id=NYAP52DQZsgC

[21] National Cancer Institute. SEER Training: Breast Anatomy. Retrieved from http://training.seer.cancer.gov/breast/anatomy/

[22] Pogue, Brian, Testorf, Markus, McBride, Troy, Osterberg, Ulf, & Paulsen, Keith (1997, December 22). Instrumentation and Design of a Frequency-domain Diffuse Optical Tomography Imager for Breast Cancer Detection. *Optics Express*, 1(13), 391-403. Retrieved from http://www.opticsinfobase.org/view_article.cfm?gotourl=http%3A%2F%2Fwww%2Eopticsinfobase%2Eorg%2FDirectPDFAccess%2F7B51B16D%2DC90F%2DC461%2D5C1CBFA9F3294D00%5F63220%2Foe%2D1%2D13%2D391%2Epdf%3Fda%3D1%26id%3D63220%26seq%3D0%26mobile%3Dno&org=

[23] Poplack, Steven P., Tosteson, Tor D., Kogel, Christine A., & Nagy, Helene M. (2007, April 19). Digital Breast Tomosynthesis: Initial Experience in 98 Women with Abnormal Digital Screening Mammography. *American Journal of Roentgenology*, 189(3), 616-623. Retrieved from http://www.ajronline.org/content/189/3/616.short

[24] Schaefer, Jacob, Stejskal, E., Perchak, Dennis, Skolnick, Jeffery, & Yaris, Robert (1995, March). Molecular Mechanism of the Ring-flip Process in Polycarbonate. *Macromolecules (ACS Publications*, 18(3), 368-373. Retrieved from http://pubs.acs.org/doi/abs/10.1021/ma00145a012

[25] Stanford University School of Medicine (2012). Patient Care: What is Nuclear Medicine? Retrieved from http://nuclearmedicine.stanford.edu/patient_care/

[26] Stony Brook University Physicians. Breast Cancer Center – Breast Lumps. Retrieved from http://www.stonybrookphysicians.com/center/breast-care-center-pi-breast-lumps.asp

[27] Susan G. Komen for the Cure (2012). Breast Cancer Statistics. Retrieved from http://ww5.komen.org/BreastCancer/Statistics.html

[28] The Engineering Toolbox (n.d.). Elastic Properties and Young Modulus for Some Materials. Retrieved from http://www.engineeringtoolbox.com/young-modulus-d_417.html

[29] The Mathworks, Inc. (1994-2012). ANOVA1. Retrieved from http://www.mathworks.com/help/toolbox/stats/anova1.html

[30] The Mathworks, Inc. (1984-2012). Kruskalwallis. Retrieved from http://www.mathworks.com/help/toolbox/stats/kruskalwallis.html

[31] Virginia Industrial Plastics Inc. (n.d.). Retrieved from http://www.vaplastic.com/Vacuum-Forming.html